1 **Design, Synthesis, and Unprecedented Interactions of Covalent Dipeptide-Based**

2 **Inhibitors of SARS-CoV-2 Main Protease and its Variants Displaying Potent Antiviral**

3 **Activity**

4 Philipp Flury,[a,≠] Nadine Krüger,[b,≠] Katharina Sylvester,[c] Julian Breidenbach,[c] Ghazl Al

5 Hamwi,[c] Jingxin Qiao,[d] Yan Chen,[d] Cheila Rocha,[e] Mateus Sá Magalhães Serafim,[f,g] Elany

6 Barbosa da Silva,[g] Stefan Pöhlmann,[e,h] Antti Poso,[a,i] Thales Kronenberger,[a,i,j] Katharina Rox,[k,l]

7 Anthony J. O'Donoghue,[g] Shengyong Yang,[d] Norbert Sträter,[m] Michael Gütschow,[c] Stefan A.

8 Laufer,[a] Christa E. Müller,[c] and Thanigaimalai Pillaiyar[a,*,]

9

10 [a]Institute of Pharmacy, Pharmaceutical/Medicinal Chemistry and Tübingen Center for

11 Academic Drug Discovery, Eberhard Karls University Tübingen, Auf der Morgenstelle 8,

12 72076 Tübingen, Germany

13 [b]Platform Infection Models, German Primate Center, Leibniz Institute for Primate Research

14 Göttingen, Kellnerweg 4, 37077 Göttingen, Germany

15 [c]PharmaCenter Bonn, Pharmaceutical Institute, Pharmaceutical & Medicinal Chemistry,

16 University of Bonn, An der Immenburg 4, 53121 Bonn, Germany

17 [d]Department of Biotherapy, Cancer Center and State Key Laboratory of Biotherapy, West

18 China Hospital, Sichuan University, Chengdu, Sichuan, 610041, China

19 [e]Infection Biology Unit, German Primate Center – Leibniz Institute for Primate Research,

20 Kellnerweg 4, 37077 Göttingen

21 [f]Department of Microbiology, Institute of Biological Sciences, Federal University of Minas

22 Gerais, Belo Horizonte, 31270-901, Minas Gerais, Brazil

23 [g]Center for Discovery and Innovation in Parasitic Diseases, Skaggs School of Pharmacy and

24 Pharmaceutical Sciences, University of California San Diego, 9500 Gilman Drive, La Jolla, CA

25 92093-0657, USA

26 [h]Faculty of Biology and Psychology, Georg-August University Göttingen, Göttingen 37073,

27 Germany

28 [i]School of Pharmacy, Faculty of Health Sciences, University of Eastern Finland, 70211,

29 Kuopio, Finland.

30 [j]German Center for Infection Research (DZIF), Partner Site Tübingen, Tübingen Germany.

31 [k]Department of Chemical Biology, Helmholtz Centre for Infection Research (HZI), 38124

32 Braunschweig, Germany

33 *l*German Center for Infection Research (DZIF), Partner Site Hannover-Braunschweig, 38124

34 Braunschweig, Germany

35 *m*Center for Biotechnology and Biomedicine, Leipzig University, Deutscher Platz 5, 04103

36 Leipzig, Germany

37

38

39 *#*These authors contributed equally.

40

41 ***Corresponding author**

42 Thanigaimalai Pillaiyar; − Institute of Pharmacy, Pharmaceutical/Medicinal Chemistry and

43 Tübingen Center for Academic Drug Discovery, Eberhard Karls University Tübingen, Auf der

44 Morgenstelle 8, 72076 Tübingen, Germany. E-mail: thanigaimalai.pillaiyar@uni-tuebingen.de.

45

46

Abstract

The main protease (M^{pro}) of SARS-CoV-2 is a key drug target for the development of antiviral therapeutics. Here, we designed and synthesized a series of small-molecule peptidomimetics with various cysteine-reactive electrophiles. Several compounds were identified as potent SARS-CoV-2 M^{pro} inhibitors, including compounds **8n** (IC_{50} = 0.0752 μM), **8p** (IC_{50} = 0.0887 μM), **8r** (IC_{50} = 0.0199 μM), **10a** (IC_{50} = 0.0376 μM), **10c** (IC_{50} = 0.0177 μM), and **10f** (IC_{50} = 0.0130 μM). Most of them additionally inhibited cathepsin L and were also active against SARS-CoV-1 and MERS-CoV M^{pro}. In Calu-3 cells, several inhibitors, including **8r**, **10**a, and **10c**, displayed high antiviral activity in the nanomolar range without showing cellular toxicity. The co-crystal structure of SARS-CoV-2 M^{pro} in complex with **8p** revealed covalent binding to the enzyme's catalytic residue Cys145 and showed specific, unprecedented interactions within the substrate binding pocket. Compounds **8n** and **10c**, especially **8n**, were effective against a panel of naturally occurring nirmatrelvir-resistant mutants, particularly E166V, and showed metabolic stability and additional favorable pharmacokinetic properties, making it a suitable candidate for further preclinical development.

**Keywords**: Antiviral, COVID-19, inhibitors, M^{pro}, peptidomimetics, SARS-CoV-2, X-ray structure.

Introduction

The severe acute respiratory syndrome-causing coronavirus type 2 (SARS-CoV-2),[1] the causative agent of the coronavirus disease 2019 (COVID-19), has spread worldwide, reaching pandemic status in March 2020. As of September 1st, 2024, more than 775 million cases have been reported worldwide, with 7 million associated deaths.[2,3] The pandemic led to extensive research on non-pharmacological and pharmacological approaches for preventing and treating the disease. Several successful vaccines were approved in a short time, and many antiviral drug candidates have been evaluated in clinical trials, a few of which reached the market.[3] However, emerging SARS-CoV-2 mutations pose a threat to the effectiveness of existing vaccines and antiviral therapies.[4, 5] Given the limited number of therapeutic options (e.g., nirmatrelvir and ensitrelvir) and reports of M^{pro} mutations associated with drug resistance,[6-9] alternative antiviral therapeutics are urgently needed.

SARS-CoV-2 is a member of the *Betacoronavirus* genus, together with SARS-CoV-1 and the Middle East respiratory syndrome coronavirus (MERS-CoV).[10] The single-stranded RNA genome of SARS-CoV-2 encodes two large polyproteins (PP1a and PP1ab), which are proteolytically cleaved into 16 non-structural proteins (nsp) by two viral proteases, the papain-like protease (PL^{pro}) and the main protease (M^{pro}). M^{pro}, also known as 3C-like protease (3CL^{pro}), is the key enzyme that is responsible for releasing at least 12 nsp, including the RNA-dependent RNA polymerase (RdRp), that are essential for the genomic replication and transcription processes.[11] M^{pro} is highly conserved among coronaviruses.[11-14] Thus, due to its pivotal role in the virus life cycle, the targeting of M^{pro} is a promising approach for developing antiviral therapeutics. The M^{pro} active site features a catalytic dyad comprised of His41 and Cys145, where the His deprotonates Cys resulting in a highly nucleophilic catalytic thiolate. Indeed, most of the reported M^{pro} inhibitors have electrophilic warheads that bind covalently to Cys145 (representative examples are depicted in Figure 1). For example, an indole-substituted peptidomimentic with an aldehyde warhead (FB2001) showed excellent M^{pro} inhibitory and

4

92   antiviral activity with acceptable pharmacokinetic properties and minimal toxicity and is

93   currently in phase II/III clinical trials.[15] GC376 is the bisulfite adduct of the aldehyde derivative

94   GC373, which showed high SARS-CoV-2 M^{pro} inhibitory activity with an IC_{50} value of 30 nM,

95   but low antiviral activity.[16] The benzothiazolyl ketone derivative YH-53 (see Figure 1),

96   previously identified as a SARS-CoV-1 M^{pro} inhibitor,[17] also exhibited SARS-CoV-2 M^{pro}

97   inhibitory and antiviral activity.[18] Nirmatrelvir, containing a nitrile warhead, is approved as an

98   oral M^{pro}-inhibitory antiviral drug in combination with the cytochrome P450 CYP3A4 inhibitor

99   ritonavir to prevent its fast metabolic inactivation.[19] Recently, the second-generation drug

100   ibuzatrelvir (PF-07817883) demonstrated better metabolic stability, suggesting that it could be

101   administered without a CYP3A4 inhibitor.[20-22] The peptidomimetic M^{pro} inhibitors simnotrelvir

102   (SIM0417)[23] and leritrelvir (RAY1216)[24] were approved in China for COVID-19 therapy (for

103   structures see Figure 1). In addition, several non-peptidic covalent SARS-CoV-2 M^{pro} inhibitors

104   have been reported, including chloropyridyl esters[25-28] and thioesters.[29] Also, potent non-

105   covalent inhibitors have been reported, e.g., GC-78-HCl[30] and S-217622 (ensitrelvir); the latter

106   compound was recently approved in Japan (see Figure 1).[31]

5
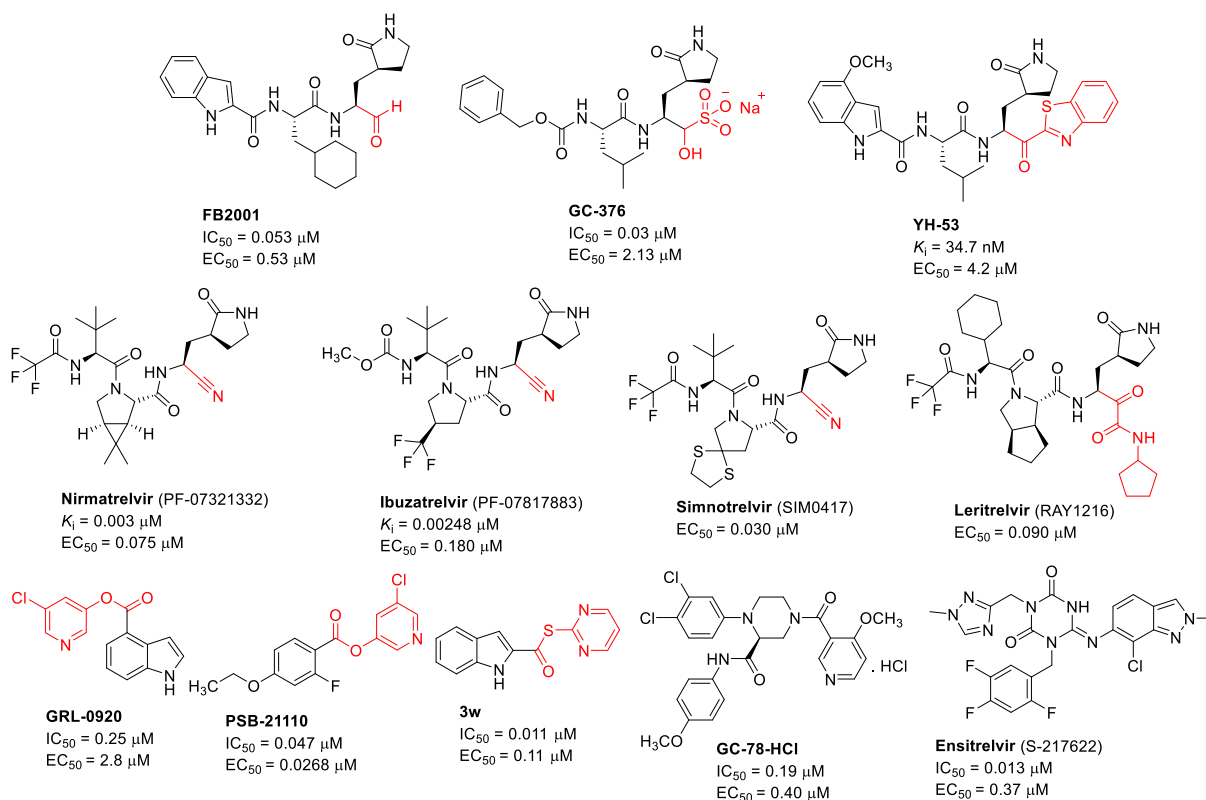
Figure 1. Structures of representative SARS-CoV-2 M^{pro} inhibitors with M^{pro}-inhibitory potency (IC_{50}) and antiviral activity (EC_{50}). The warhead groups are highlighted in red.

Considering the remarkable high mutation rates of SARS-CoV-2 lineages[10], it is not surprising that drug resistance is a major concern.[9] The effectiveness of nirmatrelvir and ensitrelvir is variable for different coronavirus species.[32] For instance, these drugs had less effect on the main proteases of HCoV-NL63 and HCoV-229E as compared that of SARS-CoV-2.[19, 33] Additionally, several mutations in M^{pro} have already been found that confer resistance against nirmatrelvir and ensitrelvir[7], as determined by *in vitro* and *in vivo* experiments.[8, 34] Therefore, it is critical to continue developing potent antivirals to prepare for the emergence of drug-resistant SARS-CoV-2 strains and for novel pandemic coronaviruses.[6, 35]

In the present study, we describe the design and synthesis of a new class of dipeptidic SARS-CoV-2 M^{pro} inhibitors with a vinyl ketone warhead group. A variety of compounds with low nanomolar M^{pro} inhibitory activity were developed based on analysis of structure-activity relationships (SARs). We determined the co-crystal structure of SARS-CoV-2 M^{pro} with one of

6

123 the potent inhibitors. Additionally, one of the most potent compounds was tested against

124 different M^{pro} mutants. For selected potent M^{pro} inhibitors, the antiviral activity against SARS-

125 CoV-2 was studied in a lung cell line (Calu-3) using a plaque assay. Finally, potent SARS-

126 CoV-2 M^{pro} inhibitors were additionally tested against the human cathepsin L (CatL) and M^{pro}

127 of other beta-coronaviruses, namely SARS-CoV-1 and MERS-CoV and were found to have

128 broad-spectrum protease inhibitory activity.

129

130 **Results and discussion**

131 **Design of new M^{pro} inhibitors.** Our previous study identified compound **I** (Figure 2) as a CatL

132 inhibitor (K_i = 0.152 μM), which was subsequently improved to produce CatL inhibitors with

133 low nanomolar potency.[36] While most of those compounds showed negligible or only weak

134 M^{pro} inhibitory activity, we discovered that **I** inhibits M^{pro} with an IC$_{50}$ of 9.50 μM, 60-fold less

135 potent than as a CatL inhibitor. Nevertheless, we utilized **I** as a starting compound with the aim

136 of improving activity against SARS-CoV-2 M^{pro}. Thus, the following structural modifications

137 were tackled (Figure 2): (i) First, we introduced several *N*-terminal capping groups, e.g.,

138 cinnamic acids and their hydrogenated derivatives, phenoxy, and 2-(phenylthio)acetic acid

139 derivatives. These are P3-P4 moieties (green) expected to occupy the corresponding S3-S4

140 positions in the M^{pro} active site. Additionally, rigidified, mono- or bicyclic moieties were

141 incorporated. (ii) *L*-leucine was used as a spacer instead of the P2-Boc group (blue) to allow

142 hydrophobic interactions with the S2 pocket. (iii) To optimize interactions with the S1 pocket,

143 the P1-phenyl ring (cyan) was substituted with electron-withdrawing groups and replaced with

144 an indole or a five-membered lactam ring. (iv) Finally, the Michael acceptor warhead of **I** (red)

145 was replaced by a dimethylaminobut-3-en-2-one, or a benzothiazolyl ketone moiety,

146 respectively.

7
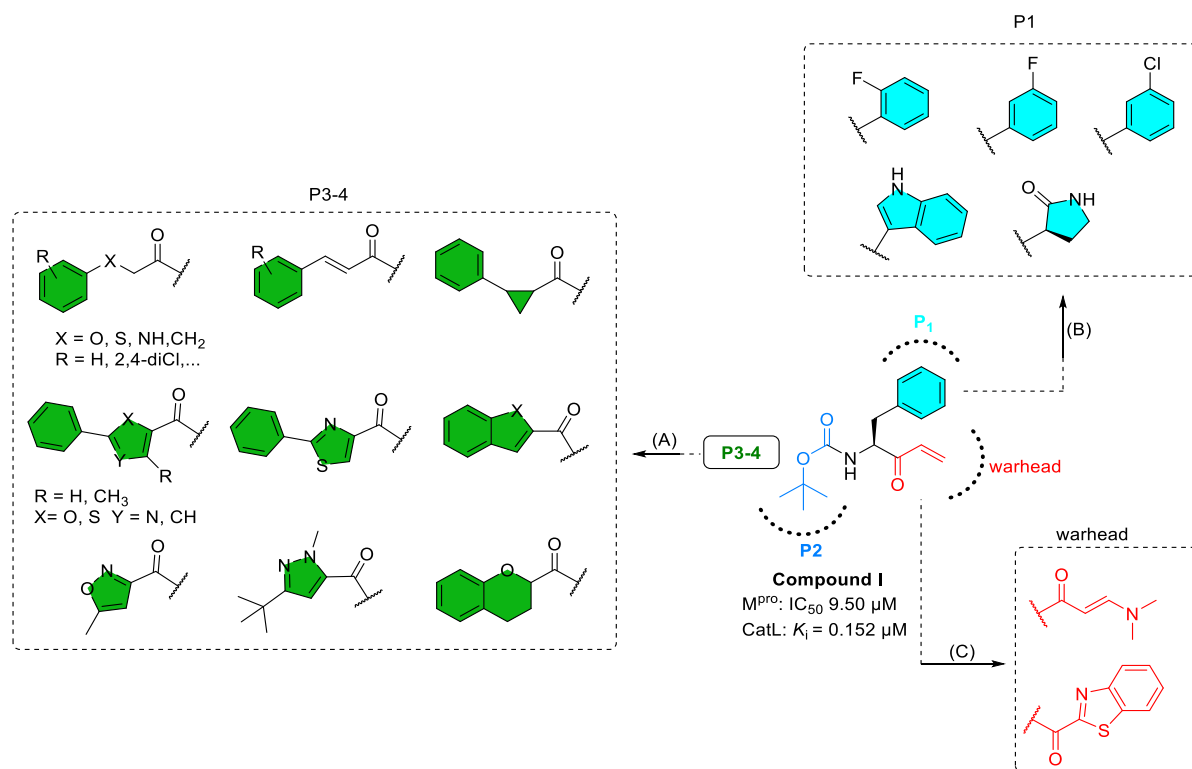
Figure 2. Design of new derivatives and analogs of lead compound **I** against SARS-CoV-2 M^{pro}.

Chemistry. A total of 42 new final compounds (**8a–z**, **8aa–ae**, **9a–b**, **10a–f**, **12a–b**, and **13a**) were synthesized as depicted in Schemes 1 and 2. The commercially available *N*-Boc-phenylalanine derivatives were used for the preparation of the corresponding Weinreb amides **1a–c** by 2,4,6-tripropyl-1,3,5,2,4,6-trioxatriphosphinane 2,4,6-trioxide (T3P)-mediated coupling reaction using *N,O*-dimethylhydroxylamine hydrochloride in the presence of diisopropylethylamine (DIPEA) in dichloromethane. The deprotection of **1a-c** with 4N HCl in dioxane yielded the corresponding free amines **2a-c**, which were subsequently reacted with N-Boc-leucine monohydrate through *O*-(7-azabenzotriazol-1-yl)-*N,N,N′,N′*-tetramethyluronium hexafluorophosphate (HATU)-supported amide coupling to give the corresponding dipeptides **3a-c**.

After deprotection of **3a-c**, the resulting free amines **4a-c** were coupled with a wide variety of carboxylic acids in the presence of HATU and DIPEA in DMF to produce the key intermediates **5a–z**, **5aa–ae**, **6a–b**, and **7a–c**. These intermediates were reacted with vinylmagnesium bromide

8

164 under Grignard reaction conditions to yield the α,β-unsaturated ketones (**8a–z**, **8aa–ae**, **9a,b**,

165 **10a–c**, Scheme 1). The intermediates bearing a benzofuranyl or a benzothiophenyl residue as

166 R^2 substitution (**5v** or **5z**) were converted to ketones **11a,b** with methylmagnesium bromide.

167 Compounds **11a,b** then underwent aldol condensation with *N,N*-dimethylformamide dimethyl

168 acetal to obtain the α,β-unsaturated ketones **12a,b** (Scheme 1), which were isolated as mixtures

169 of *cis/trans*-isomers. Lastly, the intermediate bearing a 2-(phenylthio)acetyl residue for R^2 (**5r**)

170 was reacted with 2-bromobenzothiophene in a Grignard reaction to produce the corresponding

171 benzothiazolyl ketone derivative **13a** (Scheme 1).

172

173 **Scheme 1. Synthesis of 8a-z, 8aa-ae, 9a-b, 10a-b, 12a-b, and 13a** [a]

174
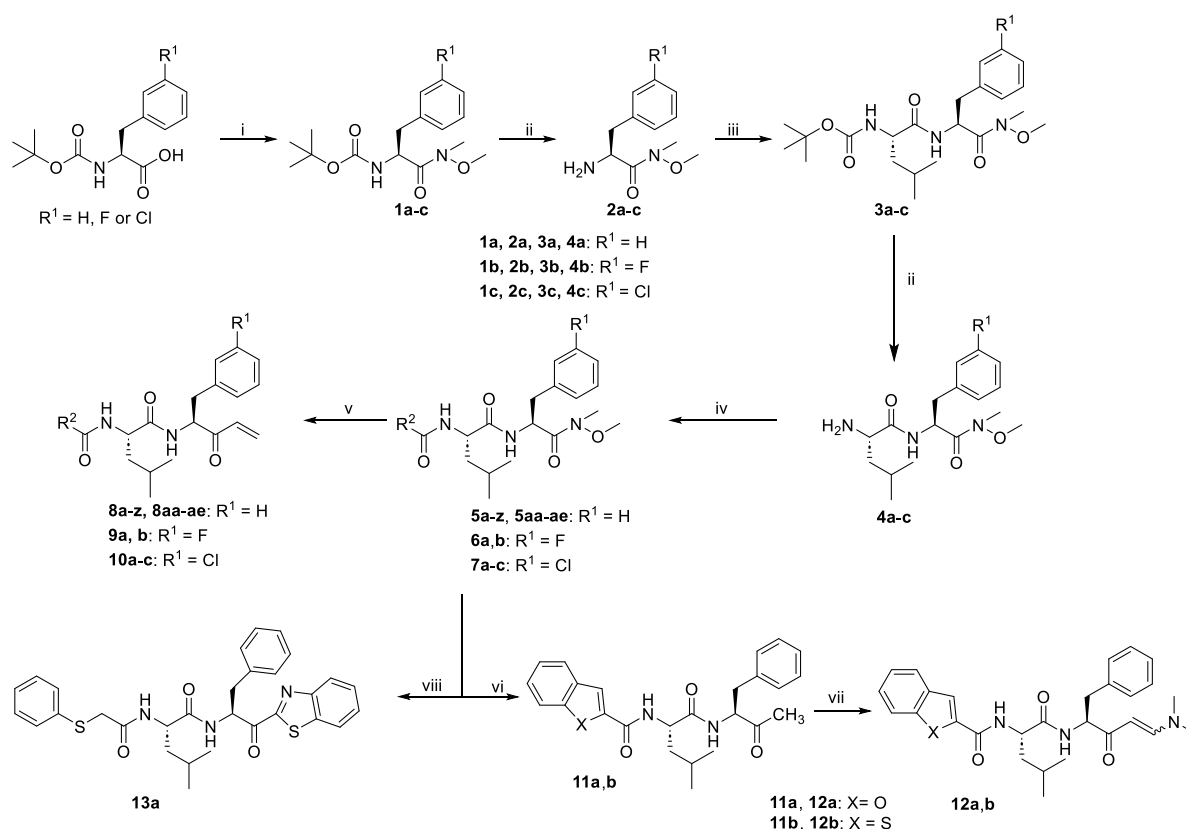
[a]Reagents and conditions: (i) T$_3$P, *N,O*-dimethylhydroxylamine hydrochloride, DIPEA, CH$_2$Cl$_2$, 0 °C, 12 h, 93-94%; (ii) 4N HCl in dioxane, 0 → 25 °C, 100%, NaOH, EtOAc, 25 °C; (iii) *N*-Boc-*L*-leucine, HATU, DIPEA, DMF, 0 → 25 °C, 84-85%; (iv) R^2-CO$_2$H, HATU, DIPEA, DMF, 0 → 25 °C, 44–95%; (v) 1M vinylmagnesium bromide solution in THF, Et$_2$O, -10 °C, 4 – 6 h, 8-93%; (vi) 3M methylmagnesium bromide solution in Et$_2$O, Et$_2$O, -10 °C,

4 – 6 h, 61-66%; (vii) *N,N*-dimethylformamidedimethyl acetal, DMF, 80 °C, 5 h, 61-77%; (viii) a. $(CH_3)_2CHMgCl \cdot LiCl$, 2-bromobenzothiazole, 30 min. at 0 °C, THF, b. Et_2O, -10 °C, 4 – 6 h, 45%. For R^1 and R^2, see Table 1.

175

176   Further compounds, **10d**–**f**, were synthesized as shown in Scheme 2. In the first step, the

177   corresponding amino acid methyl esters were coupled to *N*-Boc-protected leucine in a HATU-

178   supported amide coupling reaction in the presence of DIPEA. The amino group of the resulting

179   dipeptides **14a**–**c** was deprotected and subsequently acylated with 2-(2,4-

180   dichlorophenoxy)acetic acid or 2-(2,4,5-trichlorophenoxy)acetic acid using HATU and DIPEA

181   in DMF. The methyl esters **15a**–**c** were saponified using LiOH in THF/water. The resulting

182   carboxylic acids were reacted with *N,O*-dimethylhydroxylamine hydrochloride in the presence

183   of T3P to the corresponding Weinreb amides **16a**–**c**, which underwent a Grignard reaction using

184   vinylmagnesium bromide in diethyl ether to give the corresponding α,β-unsaturated ketones.

185

186   **Scheme 2. Synthesis of Compounds 10d–f**[a]
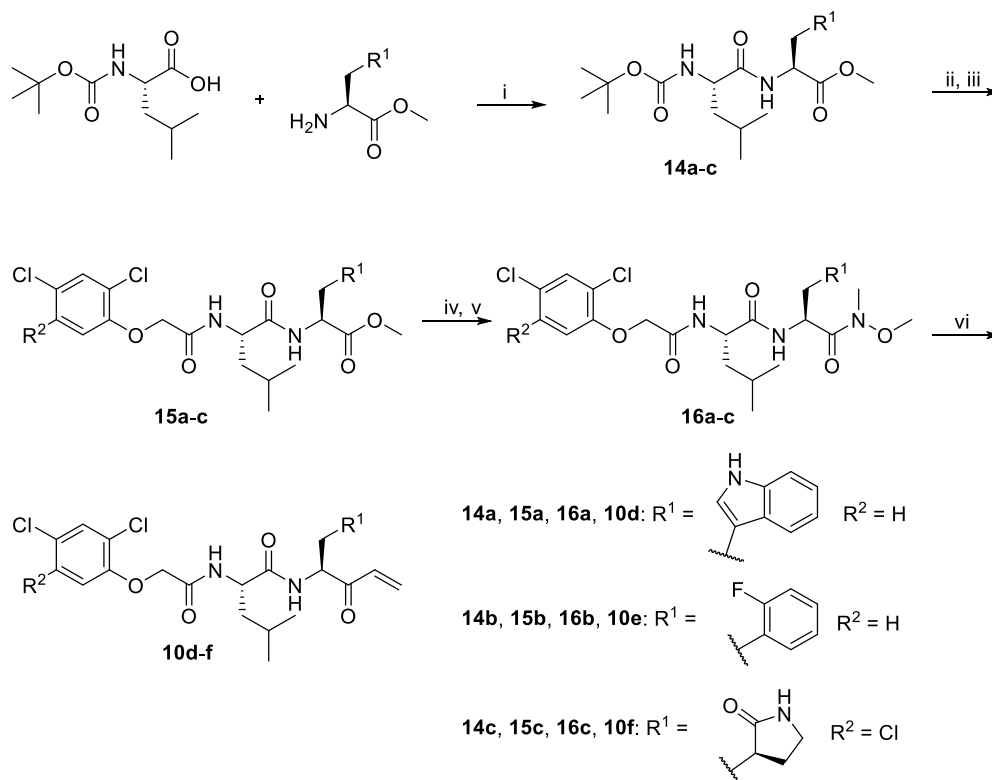
187

<superscript>a</superscript>Reagents and conditions: (i) HATU, DIPEA, DMF, 0 → 25 °C, 93%; (ii) 4N HCl in dioxane, 0 → 25 °C; (iii) R^2-CO$_2$H, HATU, DIPEA, DMF, 0 → 25 °C, 71–76%; (iv) 1M aqueous LiOH, THF, 25 °C, 2–3 h; (v) T$_3$P, *N*,*O*-dimethylhydroxylamine hydrochloride, DIPEA, CH$_2$Cl$_2$, 0 °C, 12 h, 50–95%; (vi) 1 M vinylmagnesium bromide solution in THF, Et$_2$O, -10 °C, 4–6 h, 25-66%.

188

189 The structures of the synthesized compounds were confirmed by ^{1}H (400 MHz) and ^{13}C (101

190 MHz) NMR spectroscopy. In addition, the purity of all final compounds was analyzed by HPLC

191 at wavelengths of 254 and 230 nm. The mass spectra for all final compounds were obtained

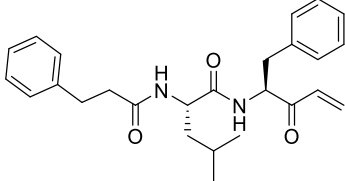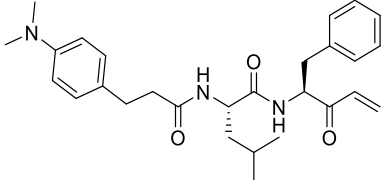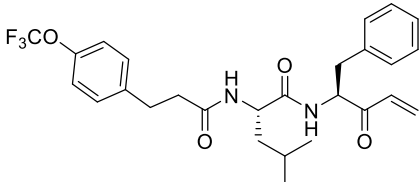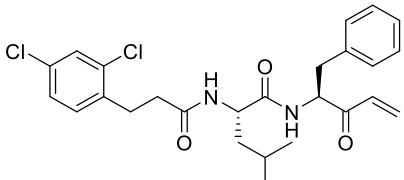192 using electrospray ionization mass spectrometry (ESI-MS).

193
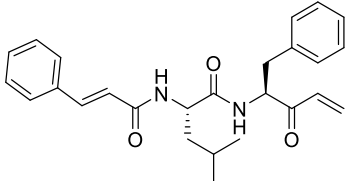
194 **SARS-CoV-2 M^{pro} Inhibition Assays.** Following a previously described procedure,[27] SARS-

195 CoV-2 M^{pro} inhibitory activity assays were performed using a fluorogenic substrate (Boc-Abu-
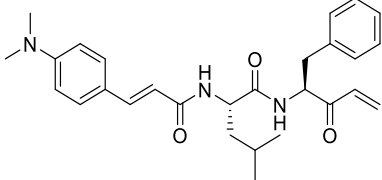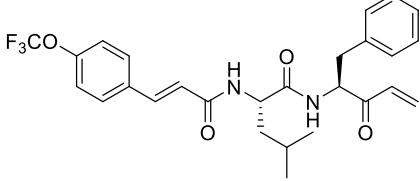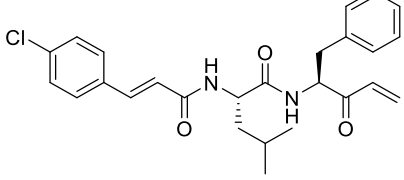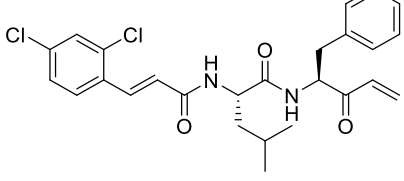
196 Tle-Leu-Gln-AMC). The compounds were initially screened at a concentration of 10 μM. For

197 compounds that showed at least 50% M^{pro} inhibition over 60 min, concentration-response

198 curves were determined with at least eight different inhibitor concentrations, and during the

199 first 10 min of the enzymatic reaction, the respective product formation rates were observed.

200 By using nonlinear regression analysis, IC$_{50}$ values were determined. Furthermore, the second-

201 order rate constant k_{inact}/K_i was established for inhibitors that showed a time-dependent

202 inhibition upon examining the effects of five different inhibitor concentrations on the product

203 formation rate for 60 min.

204
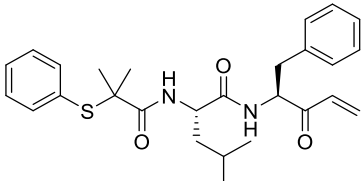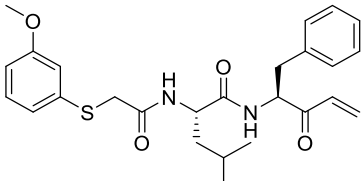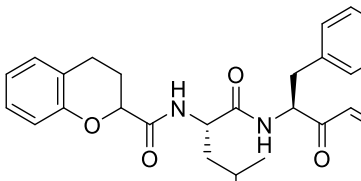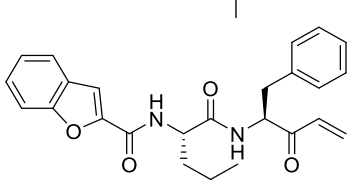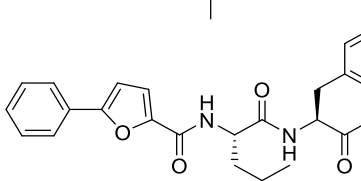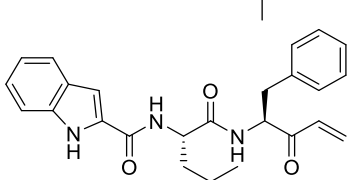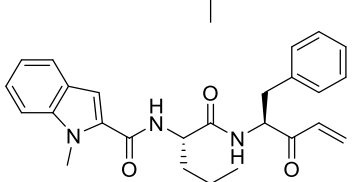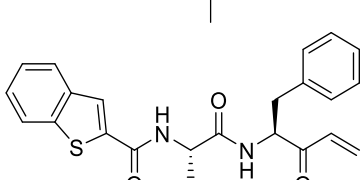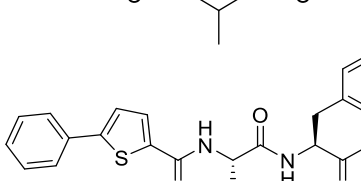
205 **Table 1. Structures and Activities of Investigated Compounds as SARS-CoV-2 M^{pro}**
206 **Inhibitors and Anticoronaviral Agents.**
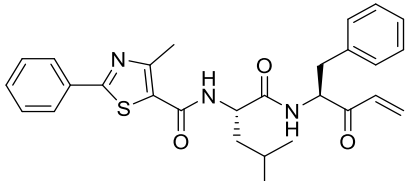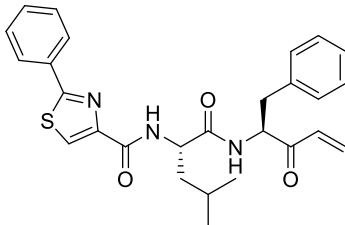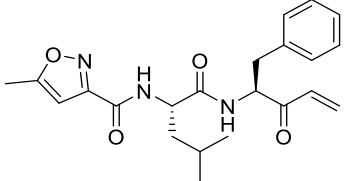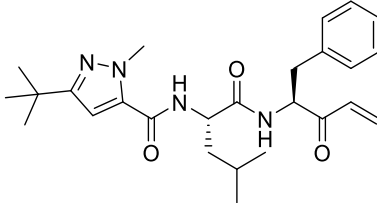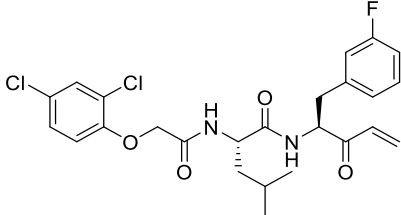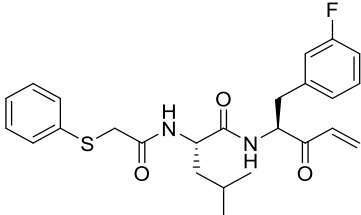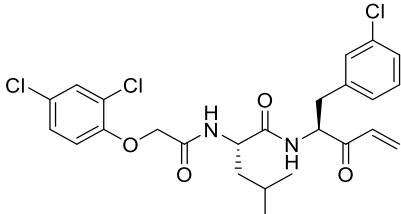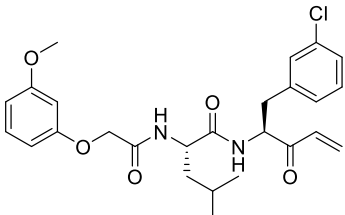
Cmpd.	Structure	SARS-CoV-2 M^{pro}		SARS-CoV-2 (Calu-3-cells)
		IC$_{50}$ (μM)[b]	k_{inact}/K_i (M^{-1}s^{-1})[c]	EC$_{50}$ (nM)[d]
-	Nirmatrelvir	**0.063**± 0.027	n.d.*e*	3.26

11

8a		$\mathbf{0.187} \pm 0.011$	$\mathbf{16{,}100} \pm 800$	n.d.[e]
8b		$\mathbf{0.152} \pm 0.007$	$\mathbf{14{,}700} \pm 400$	n.d.[e]
8c		$\mathbf{0.184} \pm 0.009$	$\mathbf{14{,}000} \pm 500$	n.d.[e]
8d		$\mathbf{0.0743} \pm 0.0135$	$\mathbf{35{,}800} \pm 2{,}800$	111
8e		$\mathbf{0.131} \pm 0.013$	$\mathbf{9{,}630} \pm 250$	n.d.[e]
8f		$\mathbf{0.279} \pm 0.060$	$\mathbf{9{,}200} \pm 700$	320
8g		$\mathbf{0.481} \pm 0.008$	$\mathbf{7{,}720} \pm 500$	34.4
8h		$\mathbf{0.0635} \pm 0.0127$	n.d.[e]	230
8i		$\mathbf{0.338} \pm 0.055$	$\mathbf{7{,}000} \pm 650$	n.d.[e]

Compound	Structure			
8j		**0.725** ± 0.168	**9,130** ± 737	n.d.[e]
8k		**0.138** ± 0.033	**14,500** ± 1,500	n.d.[e]
8l		**0.0625** ± 0.0124	**19,770** ± 1,460	12.4
8m		**0.0965** ± 0.0167	**23,800** ± 5,100	181
8n		**0.0752** ± 0.0227	**33,700** ± 5,600	16.5
8o		**0.134** ± 0.047	**26,500** ± 3,000	n.d.[e]
8p		**0.0887** ± 0.0334	**17,700** ± 1,300	557
8q		**0.131** ± 0.007	**22,600** ± 600	n.d.[e]
8r		**0.0199** ± 0.0042	**57,400** ± 8,300	10.6

8s		**0.0716** ± 0.0133	**73,700** ± 1,200	86.2
8t		**0.0473** ± 0.0062	n.d.[e]	173
8u		**0.227** ± 0.019	**14,900** ± 2,800	n.d.[e]
8v		**0.405** ± 0.045	**9,900** ± 700	n.d.[e]
8w		**0.363** ± 0.035	**16,400** ± 1,100	n.d.[e]
8x		**0.117** ± 0.047	**21,700** ± 2,700	2.57
8y		**0.0969** ± 0.0248	**41,000** ± 2,300	395
8z		**0.221** ± 0.032	**21,700** ± 1,200	n.d.[e]
8aa		**0.183** ± 0.043	**15,500** ± 500	n.d.[e]

8ab		0.117 ± 0.007	$29,900 \pm 2,700$	n.d.[e]
8ac		0.151 ± 0.015	$32,500 \pm 1,300$	n.d.[e]
8ad		0.449 ± 0.097	$21,300 \pm 3,200$	n.d.[e]
8ae		0.599 ± 0.173	$5,400 \pm 300$	n.d.[e]
9a		0.0442 ± 0.0071	$24,500 \pm 4,300$	3410
9b		0.0201 ± 0.0011	n.d.[e]	4.13
10a		0.0376 ± 0.0063	46900 ± 4700	n.d.[e]
10b		0.0247 ± 0.0035	57700 ± 24200	45.2

10c		**0.0177** ± 0.0057	n.d.[e]	n.d.[e]
10d		**0.316** ± 0.100	**11,900** ± 500	n.d.[e]
10e		**0.159** ± 0.041	**13,300** ± 900	n.d.[e]
10f		**0.0130** ± 0.0027	n.d.[e]	135
12a		>10[f]	n.d.[e]	n.d.[e]
12b		**18.9** ± 3.9	n.d.[e]	n.d.[e]
13a		>10[f]	n.d.[e]	n.d.[e]

[a]IC$_{50}$ values were obtained from duplicate measurements with at least five different inhibitor concentrations. The equation for non-linear regression was $v = v_0/(1 + [I]/IC_{50})$, where v is the product formation rate at different inhibitor concentrations, v_0 is the uninhibited product formation rate, [I] is the inhibitor concentration, and IC$_{50}$ is the half-maximal inhibitory concentration. The standard errors (SE) refer to the non-linear regression.
[b]The final substrate concentration of the fluorogenic substrate Boc-Abu-Tle-Leu-Gln-AMC was 50 µM and the formation of the product was monitored with excitation and emission wavelengths of 360 nm and 460 nm, respectively. The reactions were followed for 60 min at 37 °C. Detailed assay conditions are reported elsewhere.[27]
[c]Inhibitors showed a time-dependent inhibition. Progress curves in the presence of five different inhibitor concentrations were followed over 60 min and analyzed by nonlinear regression using the equation $[P] = v_i \times (1 - \exp(-k_{obs} \times t) / k_{obs} + d)$, where [P] is the product, v_i the initial rate, k_{obs} the observed first-order rate constant and d is the offset.[27]

16

225

226

227 **Structure-activity relationships**. In our previous study,[36] we developed a series of dipeptide

228 CatL inhibitors, which were mainly composed of leucine at P2 and phenylalanine at the P1

229 positions with different warheads and N-terminal P3 groups. Some compounds showed weak

230 inhibition of SARS-CoV-2 M^{pro}, but most of them were inactive against the viral protease.

231 In the present study, to develop potent M^{pro} inhibitors, lead compound **I** was structurally varied

232 to a large extent in order to improve M^{pro} inhibitory potency. In the first attempt, the C-terminus

233 of Leu-Phe (P2-P1 residues) was modified to an acryloyl group as a new warhead (compound

234 **8a**). This compound inhibited M^{pro} with an IC$_{50}$ value of 0.185 μM. An irreversible mode of

235 SARS-CoV-2 M^{pro} inhibition of **8a** was determined by kinetic studies, and the second-order

236 rate constant of inactivation, k_{inact}/K_i, was 16,000 M^{-1}s^{-1}. This result encouraged us to maintain

237 the Leu-Phe dipeptide portion with a vinyl ketone, and we explored a variety of N-terminal

238 substituents at the P3 position (**8b**-**z**, **8aa**-**ae**).

239 The *para*-dimethylamino- and trifluoromethoxy substitution at the terminal phenyl group led

240 to compound **8b** (IC$_{50}$ = 0.152 μM, k_{inact}/K_i = 14,700 M^{-1}s^{-1}), and **8c** (IC$_{50}$ = 0.184 μM,

241 k_{inact}/K_i = 14,000 M^{-1}s^{-1}), respectively, with similar inhibitory activity as **8a**. The introduction

242 of a 2,4-dichloro substitution improved the IC$_{50}$ and k_{inact}/K_i by more than two-fold compared

243 to **8a**-**c**, see **8d** (IC$_{50}$ = 0.0743 μM, k_{inact}/K_i = 35,800 M^{-1}s^{-1}), suggesting that a hydrophobic

244 substituent is favorable. The cinnamoyl derivatives **8f** (IC$_{50}$ = 0.279 μM), **8g** (IC$_{50}$ = 0.481 μM),

245 and **8i** (IC$_{50}$ = 0.338 μM) tended to reduce the M^{pro} inhibitory potency compared to their

246 saturated propionyl analogs, while **8e** (IC$_{50}$ = 0.131 μM, k_{inact}/K_i = 9,630 M^{-1}s^{-1}) and **8h**

247 (IC$_{50}$ = 0.279 μM) showed similar activities as **8a** and **8d**, respectively. The k_{inact}/K_i value for

17

8h was not calculated due to considerable M^{pro} reactivation within 1 h. Dimethoxy substitutions on the phenyl ring of **8e** further reduced the activity as in **8j** (IC$_{50}$ = 0.725 μM, k_{inact}/K_i = 9,100 M^{-1}s^{-1}). These findings suggested that the flexible, hydrophobic P3 moiety is favorable for M^{pro} inhibitory activity.

Next, the introduction of a cyclopropyl ring in the P3 alkyl moiety in compound **8k** did not change activity (IC$_{50}$ = 0.138 μM, k_{inact}/K_i = 14,500 M^{-1}s^{-1}), while the insertion of oxygen in the phenoxyacetyl derivative **8l** (IC$_{50}$ = 0.0625 μM) improved potency by nearly three-fold compared to **8a**, along with a k_{inact}/K_i value of 27,400 M^{-1}s^{-1} (K_i = 0.203 μM). The potency of analogs with substituents such as 4-chloro (**8m**), 2,4-dichloro (**8n**) and 3-methoxy (**8p**) on the N-terminal phenyl ring also retained the activity. However, 2,4,5-trichloro (**8o**) or 3-dimethylamino (**8q**) substitution resulted in analogs with slightly reduced potency. The M^{pro} inhibitory activity was further improved by replacing oxygen with sulfur. The resulting 2-(phenylthio)acetyl derivatives (**8r-t**) showed improved IC$_{50}$ values ranging from 0.0199 to 0.0752 μM, as compound **8r**, the second most potent M^{pro} inhibitor with an IC$_{50}$ of 0.0199 μM and a k_{inact}/K_i of 57,400 M^{-1}s^{-1}. The *gem*-dimethyl substitution at the linker of the 2-(phenylthio)acetyl moiety resulted in compound **8s** with slightly reduced inhibitory activity compared to **8r**, but k_{inact}/K_i was still high (57,400 M^{-1}s^{-1}). It was not possible to calculate the k_{inact}/K_i value for **8t** (IC$_{50}$ = 0.0473 μM) due to considerable M^{pro} reactivation.

In the next series of compounds, the impact of the N-terminal mono- or bi-cyclic capping group on the inhibitory potency was determined. In general, rigidization of the P3 group reduced the potency of the resulting compounds compared to those of analogs with acyclic, flexible moieties. For example, the chromane (**8u**, IC$_{50}$ = 0.227 μM; k_{inact}/K_i = 14,909 M^{-1}s^{-1}), benzofuran (**8v**, IC$_{50}$ = 0.405 μM; k_{inact}/K_i = 9,900 M^{-1}s^{-1}), and 5-phenylfuran derivative (**8w**, IC$_{50}$ = 0.363 μM; k_{inact}/K_i =16,400 M^{-1}s^{-1}) showed slightly reduced M^{pro} inhibitory activities compared to the phenoxyacetyl derivative **8l**. This trend was also observed by comparing **8r** with analogs bearing a benzothiophene (**8z**, IC$_{50}$ = 0.221 μM), and a 5-phenylthiophene residue

18

274 (**8aa**, IC_{50} = 0.183 µM). The k_{inact}/K_i values for **8z** and **8aa** were 21,700 $M^{-1}s^{-1}$ and 15,500

275 $M^{-1}s^{-1}$, respectively. The 2-phenylthiazole (**8ab**, IC_{50} = 0.117 µM; **8ac**, IC_{50} = 0.151 µM) and

276 the indole derivative (**8x**, IC_{50} = 0.117 µM; **8y**, IC_{50} = 0.0969 µM) showed slightly better M^{pro}

277 inhibitory activity along with k_{inact}/K_i values of up to 41,000 $M^{-1}s^{-1}$ than other bicycles and

278 monocycles, such as compounds with isoxazole (**8ad**, IC_{50} = 0.449 µM) and pyrazole rings

279 (**8ae**, IC_{50} = 0.599 µM). The k_{inact}/K_i values for **8ad** and **8ae** were 21,300 $M^{-1}s^{-1}$ and 5,400

280 $M^{-1}s^{-1}$, respectively.

281 Further, we explored the P1 phenyl group (**9a**,**b**, **10a**-**f**). The introduction of *m*-fluoro or

282 *m*-chloro substitution on the phenyl ring led to the inhibitors **9a,b,** and **10a-c** having improved

283 M^{pro} inhibitory activity compared to the corresponding unsubstituted derivatives. For example,

284 compounds **9a** (IC_{50} = 0.0422 µM) and **9b** (IC_{50} = 0.0377 µM) displayed nearly two-fold

285 improved IC_{50} values compared to **8n**. The k_{inact}/K_i values for **9a** and **10a** were 24,500 $M^{-1}s^{-1}$,

286 and 46,900 $M^{-1}s^{-1}$ respectively. However, *o*-fluoro substitution marginally reduced the activity

287 as in **10e** (IC_{50} = 0.159 µM; k_{inact}/K_i =16,400 $M^{-1}s^{-1}$). Comparing the activity of **10e** (*o*-fluoro)

288 with **9a** (*m*-fluoro), it was suggested that the *meta*-substitution is advantageous. Also, the

289 introduction of *m*-chloro substitution in **8p** or **8r** led to an increase in the inhibitory activity of

290 the resulting compounds such as **10b** (IC_{50} = 0.0247 µM) and **10c** (IC_{50} = 0.0177 µM),

291 respectively. The k_{inact}/K_i value for **10b** was 57,700 $M^{-1}s^{-1}$ but was not calculated for **10c** due

292 to considerable M^{pro} reactivation.

293 Additionally, the structure of the P1 side chain was also addressed. The replacement of the

294 phenyl ring with the indole system (**10c**, IC_{50} = 0.316 µM) reduced **8n** activity by four-fold,

295 suggesting that the indole ring is probably too large for the corresponding S1 pocket to be

296 optimally occupied**.** On the other hand, replacing the phenyl ring with a five-membered lactam

297 ring (**10f**) increased the activity by 10-fold compared to its P1-phenyl analog **8o.** This can be

298 explained by the additional hydrogen bond acceptor and donor properties of the lactam ring. In

19

fact, compound **10f** was our most potent M^{pro} inhibitor, with an IC_{50} value of 0.0130 µM, but its k_{inact}/K_i value was also not calculated due to considerable M^{pro} reactivation.

Finally, the warhead was investigated by incorporating a 3-(dimethylamino)acryloyl (**12a**, IC_{50} >10 µM; **12b**, IC_{50} = 18.9 µM) or a benzothiazolylcarbonyl moiety (**12a**, IC_{50} >10 µM). Unfortunately, both changes led to a strong decrease in activity or completely abolished it, reflecting a decrease in reactivity of the warhead towards the active site Cys145 of M^{pro}. Therefore, further changes in this position were avoided. Concentration-response curves for selected compounds are shown in Figure 3.
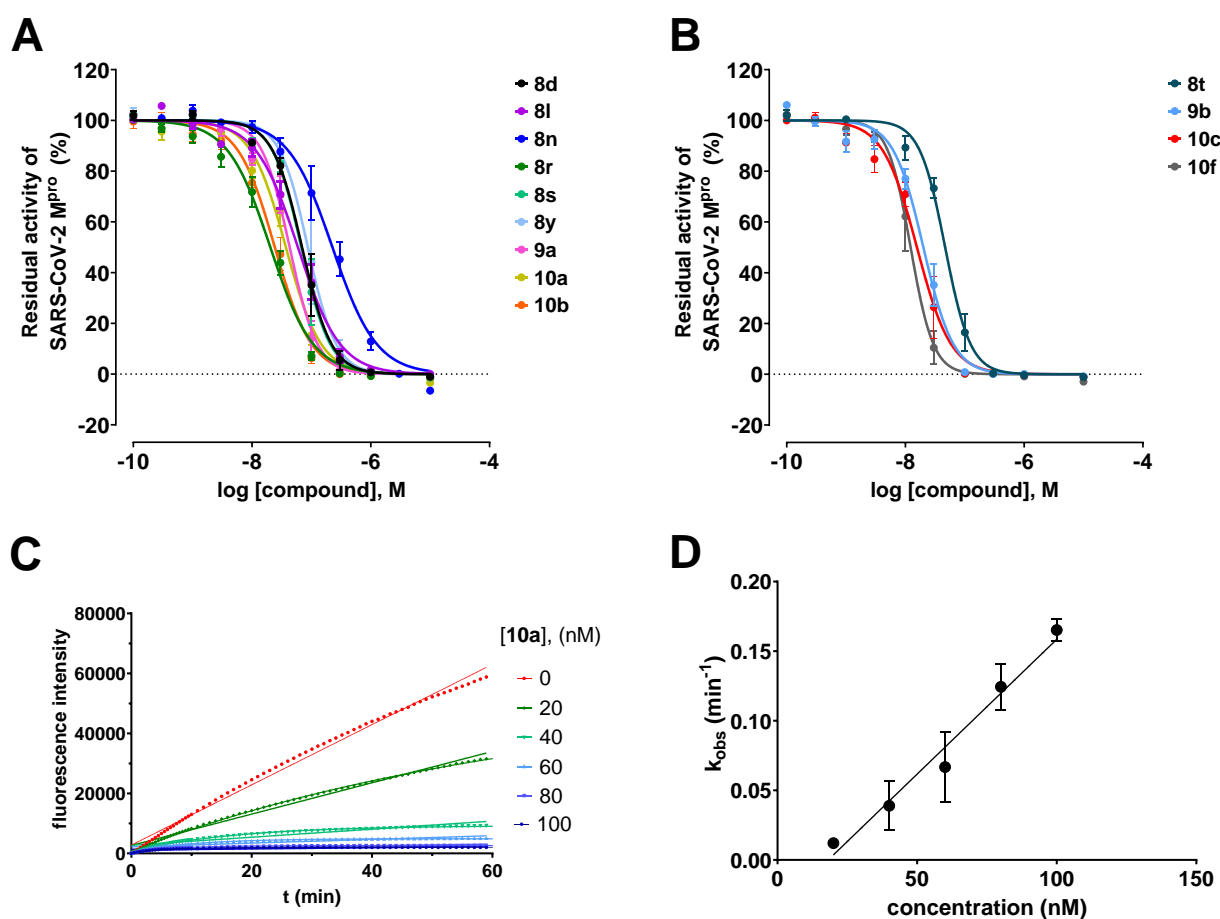
Figure 3. Concentration-dependent inhibition of SARS-CoV-2 M^{pro} by the best inhibitors of the present series, IC_{50} values are noted in parenthesis. (**A**) Irreversible inhibitors: **8d** (0.0743 ± 0.0135 µM), **8l** (0.0625 ± 0.0124 µM), **8n** (0.0752 ± 0.0227 µM), **8r** (0.0199 ± 0.0042 µM),

8s (0.0716 ± 0.0133 μM), **8y** (0.0969 ± 0.0248 μM), **9a** (0.0442 ± 0.0071), **10a** (0.0376 ± 0.0063), and **10b** (0.0247 ± 0.0035 μM). (**B**) Reversible inhibitors: **8t** (0.0473 ± 0.0062 μM), **9b** (0.0201 ± 0.0011 μM), **10c** (0.0177 ± 0.0057 μM), and **10f** (0.0130 ± 0.0027 μM). (**C**) Representative progress curves of enzyme-catalyzed hydrolysis of the substrate Boc-Abu-Tle-Leu-Gln-AMC in the absence (red) or presence of increasing concentrations of **10a** (from top to bottom: 20, 40, 60, 80, and 100 nM). (**D**) Plot of first-order rate constants k_{obs} versus inhibitor concentrations and linear regression resulting in a k_{inac}/K_i value of 46,900 ± 4,700 M^{-1}s^{-1} (n = 3).

Cytotoxicity and antiviral activity of M^{pro} inhibitors against SARS-CoV-2.

Potent M^{pro} inhibitors (**8d**, **8f-h**, **8l-n**, **8p-t**, **8x-y**, **9a-b**, **10a-c**, and **10f**) were initially tested at a high concentration of 10 μM for cytotoxic effects on Calu-3 cells. At the specified concentration, none of the compounds displayed cytotoxicity. Subsequently, the compounds were tested for their antiviral activity against Pango lineage B.1.513 of SARS-CoV-2 using Calu-3 cells according to previously reported procedures.[29] Molnupiravir (RdRp inhibitor) and nirmatrelvir (M^{pro} inhibitor), two approved SARS-CoV-2 drugs, were employed as positive controls.[37] The cells were incubated for 1 h before infection and 24 h post-infection (*h.p.i.*) with 10-fold serial dilutions (10 – 0.001 μM) of each inhibitor and infected with SARS-CoV-2 at a multiplicity of infection (MOI) of 0.01. Viral titers in culture supernatants were determined at 24 *h.p.i* by titration on Vero E6 cells and are expressed as plaque-forming units per milliliter (PFU/mL).

Overall, 18 of the 19 tested compounds showed EC$_{50}$ values in the (sub)micromolar to low nanomolar range (Table 1). Strikingly, compounds **8r**, **8x**, and **9b**, possess extremely potent antiviral activity ranging from 2.57 to 10.6 nM, which is comparable to or even lower than that of the control compounds (5.448 nM for molnuprevir and 3.255 nM for nirmatrelvir). Accordingly, these compounds are potent M^{pro} inhibitors. Compounds **8g**, **8l**, **8n**, and **10b** also proved to be highly effective antiviral agents, with EC$_{50}$ values ranging from 12.4 to 45.2 nM. The M^{pro} inhibitors **10f**, **8d**, **8m**, **8s**, and **8f** exhibited good antiviral activities with EC$_{50}$ values

21

ranging from 86.2 to 320 nM. Compounds **8h**, **8p**, **8y**, and **9a** showed only moderate antiviral activity, while **10a** and **10c** did not show any antiviral activity. The concentration-dependent inhibition curves for most active compounds are depicted in Figure 4 and Figure S1.
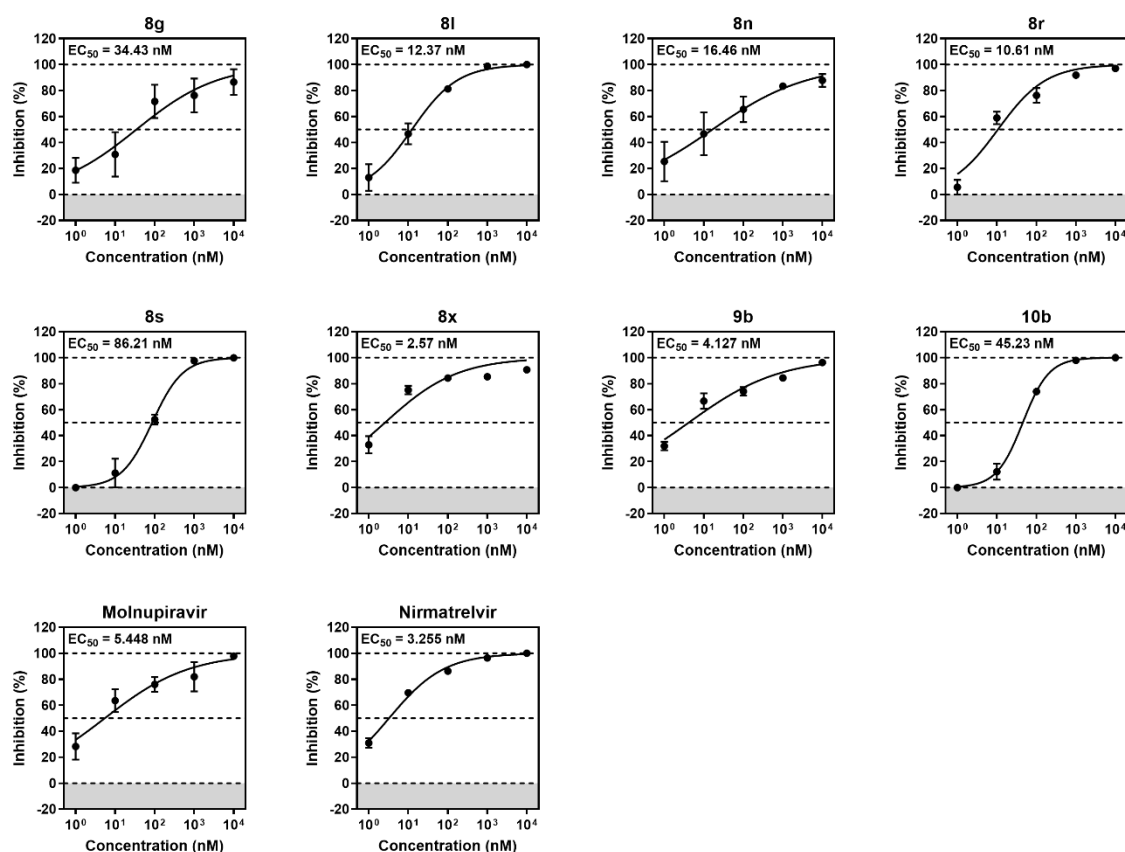
Figure 4. EC_{50} values for antiviral activity of M^{pro} inhibitors determined on SARS-CoV-2 in Calu-3 cells. Concentration-response curves of **8g**, **8l**, **8n**, **8r**, **8s, 8x**, **9b**, and **10b** were determined after treatment of Calu-3 cells infected with SARS-CoV-2 lineage B.1.513 at a MOI of 0.01. After 24 h of incubation with the compounds, virus-containing supernatants were collected, titrated in Vero E6 cells and expressed as PFU/mL. EC_{50} values were calculated for each compound compared to the DMSO control. Means $\pm$ SDs from three biological replicates are presented; in some cases, error bars are not visible as they are smaller than the symbols.

Effects of selected compounds against SARS-CoV-1 M^{pro}, MERS-CoV $M^{pro,}$ and CatL. Given their promising M^{pro} inhibition and antiviral efficacy against SARS-CoV-2, several compounds were evaluated for their ability to inhibit the M^{pro} of SARS-CoV-1 and MERS-CoV. The compounds were initially tested at 10 µM against recombinant SARS-CoV-1 M^{pro}

22

and MERS-CoV M^{pro} and those that showed at least 50% inhibition were assessed in concentration-response curves. Enzyme activity was measured with the fluorogenic substrate Ac-Abu-Tle-Leu-Gln-ACC[29] and GC-373[38] and nirmatrelvir were used as positive controls (See Table 2 for IC$_{50}$ values, and Figures S2-3 for concentration-dependent curves).

Table 2. SARS-CoV-1 M^{pro}, MERS-CoV M^{pro,} and cathepsin L inhibitory activity of selected compounds

Cmpd.	SARS-CoV-1 M^{pro} IC$_{50}$ (µM)^a or % inhibition at 10 µM	MERS-CoV M^{pro} IC$_{50}$ (µM)^a or % inhibition at 10 µM	Cathepsin L K_i (µM)^b
8e	**0.110** ± 0.008	n.d.^{c}	n.d.
8f	**0.0578** ± 0.0197	>10 (40%)	n.d.
8g	**0.0727** ± 0.0197	>10 (32%)	n.d.
8j	**0.0233** ± 0.0018	>10 (48%)	n.d.
8l	**0.0270** ± 0.0130	**0.138** ± 0.051	**0.0126** ± 0.0003
8m	**0.203** ± 0.015	**1.42** ± 0.004	n.d.
8n	**0.0357** ± 0.0110	**2.64** ± 0.02	**0.0305** ± 0.0018
8p	**0.0574** ± 0.0172	**0.565** ± 0.237	**0.0259** ± 0.0025
8q	**0.00945** ± 0.00430	**0.111** ± 0.018	**0.0259** ± 0.0035
8v	**0.0203** ± 0.0048	**0.942** ± 0.002	n.d.
8w	**0.0219** ± 0.0032	**0.538** ± 0.050	n.d.
8x	**0.357** ± 0.091	**0.0697** ± 0.0254	**0.169** ± 0.018
10a	**0.0130** ± 0.0031	>10 (44%)	**0.0595** ± 0.0013
10b	n.d.	n.d.	**0.0167** ± 0.0012
10d	**0.0574** ± 0.0062	**1.08** ± 0.25	**0.105** ± 0.008
10f	**0.0316** ± 0.0005	**0.0709** ± 0.0024	**0.145** ± 0.003
Nirmatrelvir	**0.0278** ± 0.0024	**0.0881** ± 0.0074	n.d.
GC373$^{d\ 29}$	**0.0446** ± 0.0023	**0.0780** ± 0.0168	n.d.

^{a}IC$_{50}$ values represent the average of two independent experiments determined in triplicate. Errors are given by the ratio between the standard deviation and the square root of the number of measurements. (n = 6)
^{b}The final substrate concentration of the chromogenic substrate Z-Phe-Arg-pNA was 100 µM and the formation of the product was monitored at 405 nm. Reactions were followed at 37 °C for 60 min. Detailed assay conditions are reported elsewhere.[39, 40] The progress curves were analyzed by linear regression. K_i values were obtained from duplicate measurements with five different inhibitor concentrations and analyzed by non-linear regression using the equation $v = v_0/(1 + [I]/(K_i \times (1 + [S]/K_m)))$, where v and v_0 are the product formation rates in the presence and absence of inhibitor, [S] is the substrate concentration and K_m is the Michaelis constant, being 17 µM. The standard errors (SE) refer to the non-linear regression.

376 All investigated SARS-CoV-2 M^{pro} inhibitors also displayed similar inhibitory activity against

377 SARS-CoV-1 M^{pro}. Compounds **8j**, **8l**, **8n**, **8n**, **8q**, **8v**, **8w**, **10a**, and **10f** showed potent activity

378 (IC_{50} ranging from 0.00945 to 0.0316 μM) in the same range or lower as the controls

379 nirmatrelvir and GC373. Compound **8r** had the highest potency with an IC_{50} of 0.00945 μM.

380 In general, there was a considerable difference in the potency of inhibiting MERS-CoV M^{pro}

381 compared to SARS-CoV-1 and SARS-CoV-2 M^{pro}. For example, compounds **8e**-**g** and **10a**,

382 which were active on SARS-CoV-1 and SARS-CoV-2 M^{pro}, only weekly inhibited MERS-CoV

383 M^{pro} ($IC_{50} > 10$ μM), with a maximum inhibition of 48% at 10 μM. Compounds **8m**, **8n**, **8v**,

384 and **10d** moderately inhibited MERS-CoV M^{pro} ($IC_{50} \approx 1$ μM) while compounds **8l**, **8p**, **8r**, **8w**,

385 **8x**, and **10f**, inhibited MERS-CoV M^{pro} in the nanomolar range, with compounds **8x** and **10f**

386 having IC_{50} values of 0.0697 and 0.0709 μM, respectively. Thus, these dipeptides represent a

387 novel class of broad-spectrum inhibitors that target the main protesase of SARS-CoV-1, SARS-

388 CoV-2, and MERS-CoV.

389 Next, considering that dipeptides composed of a Leu-Phe at the P2 and P1 positions had been

390 reported as CatL inhibitors in our previous study,[36] we selected potent M^{pro} inhibitors to assess

391 their activity against CatL, which plays an important role in viral entry.[41-43] The CatL inhibition

392 assay was performed according to the previously reported procedures with a chromogenic

393 peptide substrate.[39] Compounds were initially tested at a concentration of 10 μM (Table 2), and

394 for those compounds that showed more than 30% inhibition of CatL, dose-response curves were

395 determined using five different concentrations. K_i values were calculated using non-linear

396 regression for the inhibition over 60 min.

397 Overall, most of the compounds showed inhibitory potency for CatL in the same range as

398 observed for M^{pro}, e.g. **8x** (M^{pro} $IC_{50} = 0.117$ μM, CatL $K_i = 0.169$ μM), **10a** (M^{pro} $IC_{50} = 0.0376$

399 μM, CatL $K_i = 0.0595$ μM), and **10b** (M^{pro} $IC_{50} = 0.0247$ μM, CatL $K_i = 0.0167$ μM). In some

24

cases, CatL inhibitory potency was higher than that of M[pro]. For example, compounds **8l** (CatL K_i = 0.0126 μM), **8n** (CatL K_i = 0.0305 μM), and **8p** (CatL K_i = 0.0259 μM) showed significantly better CatL inhibitory potency than their M[pro] inhibitory activity. This could be explained by the preference of the phenyl residue at the P1 position for CatL over M[pro]. On the other hand, the inhibitor **10f** with a P1 pyrrolidin-2-one, a surrogate for glutamine critical for M[pro] selectivity in cleaving the natural peptide substrate, showed 11-fold selectivity for M[pro] vs. CatL. Interestingly, compound **10d** (CatL K_i = 0.105 μM) with a P1 indole also showed selectivity for M[pro] over CatL. Thus, these compounds could be developed as potent dual inhibitors of M[pro] and CatL. This might be an advantage as both proteases are important for the viral replication cycle.[44]

X-ray co-crystal structure of 8p. The crystal structure of SARS-CoV-2 M[pro] in complex with the M[pro] inhibitor **8p** (PDB 9GV2) was determined to characterize the binding mode of the inhibitor (Figure 5A). Table S1 shows the X-ray data and refinement statistics for the complex. The electron density clearly shows that the electrophilic acryl ketone forms a covalent bond to Cys145 via the β-carbon. Unexpectedly, the phenyl residue of **8p** does not serve as a P1 residue, instead it binds to the S2 pocket. It is stabilized by hydrophobic interactions with Met165 and Met49, which flank the phenyl residue as a kind of bracket. This leaves the S1 pocket unoccupied. The backbone atoms of Glu166 fix **8p** in the binding pocket via two polar interactions.
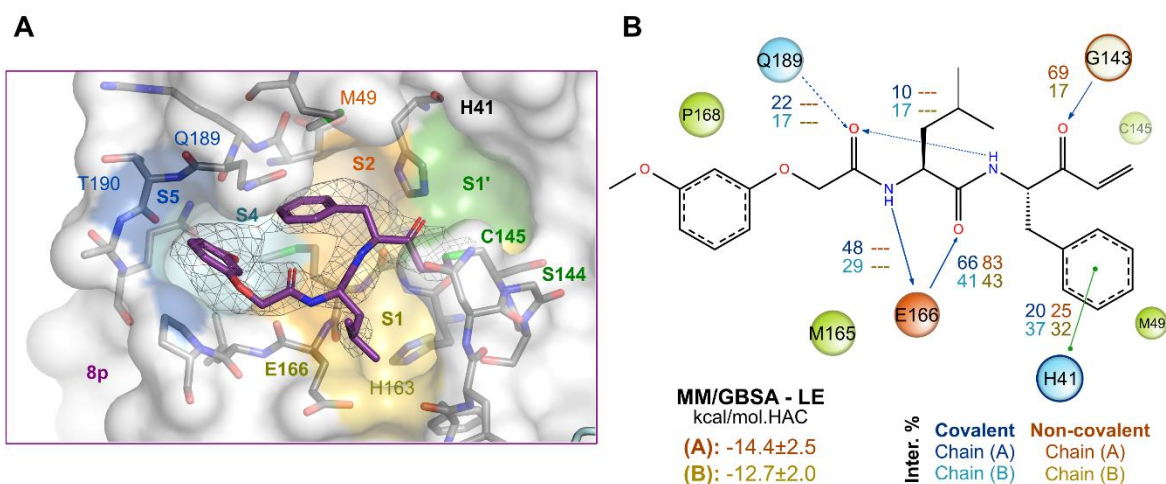
Figure 5. **A**) Crystal structure of SARS-CoV-2 M^{pro} in complex with the M^{pro} inhibitor **8p** (PDB 9GV2). The polder omits electron density map is shown at a contour level of 2.5 σ$_{rms}$. The P1 residue, which binds above the S1 pocket, has weak density indicating flexibility **B**) Protein-ligand interaction for **8p** along the analyzed trajectory (10x replicas of 200 ns per system). The interaction frequency for non-covalently and covalently bound ligands is displayed in blue and orange, respectively, and separated by individual protomers/chains (chains A and B). Non-covalently bound system simulations were used to predict the cumulative predicted binding energy using Molecular Mechanics, generalized Born surface area (MM/GBSA) and are represented by their ligand efficiency values (LE, as described in the methods section). Representative 3D confirmations are available as Supporting Information.

Subsequently, the determined complex was subjected to molecular dynamics simulations with or without the covalent bond attaching compound **8p** to the catalytic Cys145 (see Supporting Information – extended methods and discussion for the modeling contents), and the interaction frequencies between the compound and relevant amino acids were compared (Figure 5B and Supporting Information Figure **S4**). Interactions between the compound's peptidic backbone and the active site were more frequently observed in the pre-reaction complex, which suggested they are essential to orient the compound prior to formation of the covalent bond with Cys145. **8p** displays further polar contacts with the side chain of Gln189 in about 20% of the MD frames (Figure 5B and Supporting Information, Figure **S4**). The phenyl group was–stabilized by hydrophobic contacts with Met49 and Met165 and further π-mediated interactions with His41.

26

Testing at M^pro mutants. SARS-CoV-2 M^{pro} bearing Glu166Asn/Val, Met165Thr, Gly143Ser, Gln189Glu, Ala173Val, His172Phe/Gln/Tyr, or Gln192Ser/Thr/Val mutations have been reported to display resistance against approved drugs, including nirmatrelvir.[45-51] Due to concerns regarding drug-resistance, we investigated the efficacy of the selected potent compounds **8n** and **10c** at several naturally occurring M^{pro} variants. A panel of 16 mutated M^{pro} enzymes was expressed and assessed for inhibition of their enzymatic activity by **8n**, **10c**, and nirmatrelvir (Figure 6A,B) using a FRET assay as described.[52]

Nimatrelvir demonstrated reduced efficacy against each of the M^{pro} mutants. (Table 3). Glu166Val was the most resistant mutant to nirmatrelvir, resulting in an IC$_{50}$ value of 2.62 μM that corresponds to a 243-fold reduction in potency when compared to the wild-type enzyme. Compound **10c** exhibited a profile similar to nirmatrelvir against most of the assessed mutations. However, activity against the Glu166Val mutant was reduced by only 20-fold when compared to the control, resulting in an IC$_{50}$ value of 0.236 μM. Interestingly, compound **8n** showed more robust activity (less decrease in activity) against all mutants, as compared to nirmatrelvir and **10c**. Compound **8n** had remarkable potency at the Glu166Val mutant, with an IC$_{50}$ value of 0.406 μM (5-fold decrease in comparison to the wildtype enzyme), suggesting that **8n** can, to some extent, overcome these resistances to nirmatrelvir.

Table 3. The impact of resistance mutations on the inhibition of SARS-CoV-2 M^{pro} by **Nirmatrelvir**, **8n**, and **10c**.[a]

M^{pro} variant	Nirmatrelvir		8n		10c	
	IC$_{50}$ (nM)	IC$_{50}$ (fold increase)	IC$_{50}$ (nM)	IC$_{50}$ (fold increase)	IC$_{50}$ (nM)	IC$_{50}$ (fold increase)
WT	10.9 ± 0.2	1.0	68 ± 6	1.0	11.7 ± 0.2	1.0
S144A	41.7 ± 0.2	3.9	328 ± 28	4.8	42.5 ± 0.5	3.6
S144F	176 ± 11	16.3	636 ± 4	9.4	219 ± 8	18.7
S144G	191 ± 8	17.7	472 ± 16	6.9	254 ± 32	21.7
S144M	426 ± 26	39.4	745 ± 29	11.0	414 ± 30	35.4
S144Y	203 ± 15	18.8	497 ± 19	7.3	244 ± 30	20.9

27

	8n IC$_{50}$	8n fold	10c IC$_{50}$	10c fold	nirmatrelvir IC$_{50}$	nirmatrelvir fold
M165T	181 ± 69	16.8	1390 ± 20	20.4	260 ± 23	22.2
H172F	1700 ± 10	15.8	313 ± 14	4.6	146 ± 23	12.5
H172Q	166 ± 4	15.4	390 ± 30	5.7	159 ± 12	13.6
Q192S	274 ± 15	25.4	488 ± 2	7.2	261 ± 20	22.3
L50F/ E166A/ L167F	512 ± 2	47.4	392 ± 17	5.8	239 ± 11	20.4
G143S	151 ± 4	14.0	230 ± 8	3.4	155 ± 13	13.2
E166V	2620 ± 60	243	409 ± 18	6.0	236 ± 3	20.2
H172Y	283 ± 28	26.2	1280 ± 70	18.8	297 ± 27	25.4
Q189E	199 ± 19	18.4	714 ± 15	10.5	211 ± 12	18.0
ΔP168	47.0 ± 2.0	4.4	368 ± 7	5.4	65.4 ± 1.0	5.6
A173V	85.5 ± 6.0	7.9	140 ± 3	2.1	82.4 ± 8.0	7.0

30-100	10-30	>100

[a]IC$_{50}$ determination of **8n** and **10c** and nirmatrelvir against M^{pro} mutants. Data are shown as mean ± SD based on three independent experiments.

The proposed binding mode of 8n in SARS-CoV-2 M^{pro}

In all dimeric M^{pro} crystal structures, the side chain of Glu166 interacted with the N-terminal Ser1 of the other monomer, and was involved in the substrate-induced M^{pro} dimerization.[53] Dimerization is essential for M^{pro} activity, as monomers are not catalytically active.[54] (see Supporting Information Figure S5 for representation of the overall M^{pro} architecture and 3D conformation of the relevant mutant sites) Accordingly, Glu166Val mutants have lower enzymatic activity (with a k_{cat}/K_m value of only 3% of that of the wildtype M^{pro} [55]), which is linked to the collapse of the S1 pocket (see PDB ID 8H82). The Glu166Val mutation disrupted four hydrogen bonds with Ser1, as proposed by the original crystal structure (see PDB ID 8H82), but also with the main chain of the Phe140 backbone (observed in ~40% of the analyzed simulation time, Figure 6). The Ser1 side chain formed an additional hydrogen bond with the carbonyl group of Phe140, which likely compensates for the role of Glu166 in maintaining the S1 site. All these changes help to rationalize the reduced nirmatrelvir binding and consequent resistance.

The crystal structure of **8p** in the M^{pro} site suggests that its binding is independent of interactions with the side chain of Glu166 (Figure 5), and we hypothesize that **8n** would also display similar binding. To validate this hypothesis, we simulated nirmatrelvir and **8n** in wildtype M^{pro} and the Glu166Val mutant and evaluated the protein-ligand interaction frequency and potential binding energy (Figure 6A illustrates the modeling pipeline; detailed methods are described in Supporting Information). Nirmatrelvir's predicted binding energy along the simulation trajectory is significantly affected by the Glu166Val mutation, whereas that of **8n** is not affected (Figure 6B). The wider variation in the **8n** binding energy also suggests large ligand conformational changes, which are shown in the most prominent clusters (Figure 6C, D). The proposed binding mode of **8n** is stabilized by π-π-interactions between the phenyl group and His41, and polar interactions between the amide core and the backbone of residue Glu166. Interestingly, the interactions between Val166 and **8n** interaction is calculated to be more frequent than the Glu166 counterpart (Figure 6E,F).
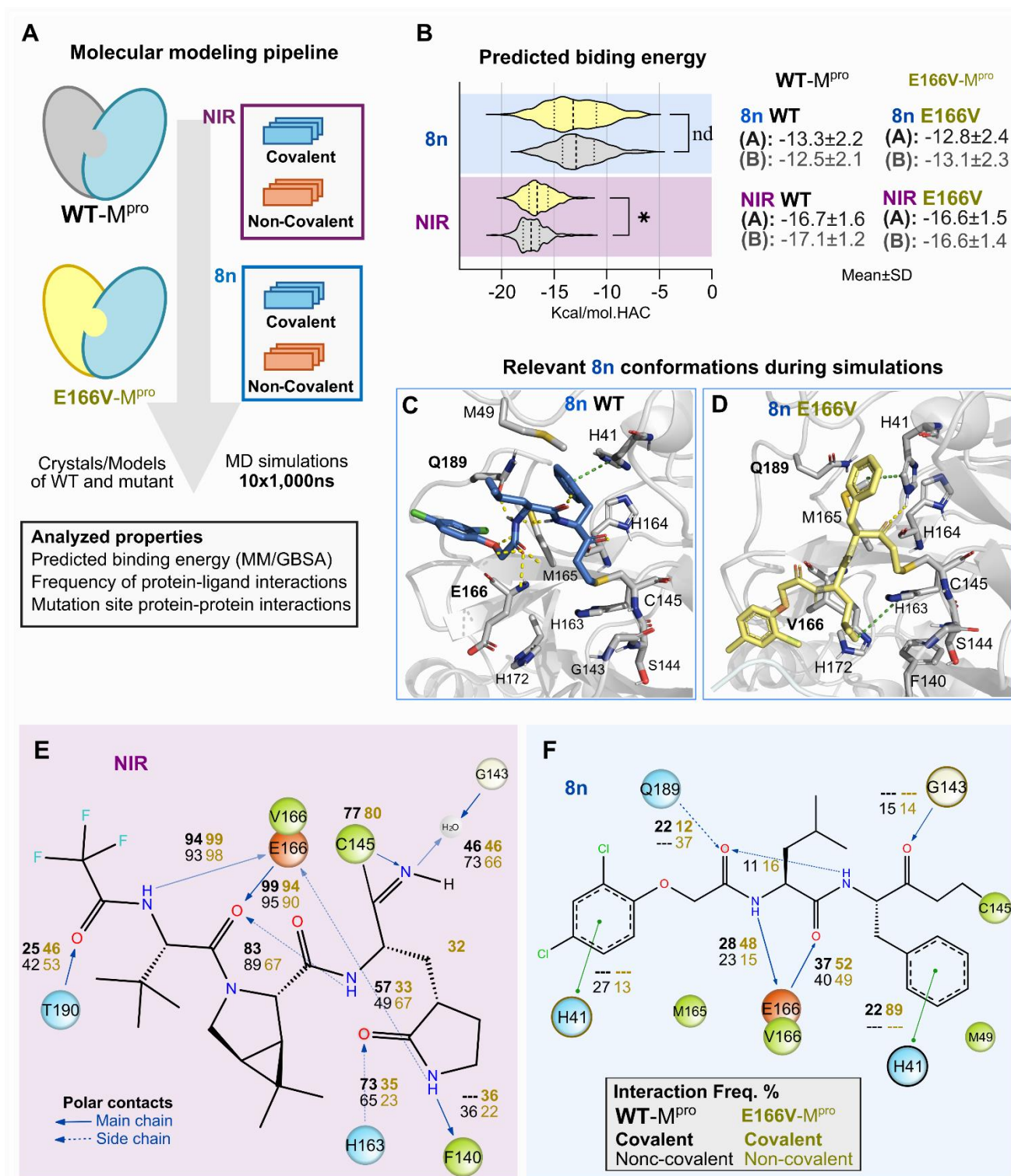
Figure 6. **A**) Illustration of the modeling pipeline. **B**) Non-covalently bound system simulations were used to predict their cumulative binding energy using MM/GBSA normalized by the number of heavy atoms (heavy atom count, HAC). Mann-Whitney test was used to compare the effect between both compounds on wildtype (gray) and Glu166Val (yellow) simulations, with p-values of 0.28 and <0.0001 (*) and for **8n** and nirmatrelvir, respectively. (**C,D**) The proposed binding mode of **8n** was derived from relevant frames of the simulation by clustering for the WT (**C**) and Glu166Val (**D**) trajectories. Polar contacts are depicted by yellow dashed lines and π-mediated interactions by green lines. Protein-ligand interaction for nirmatrelvir

(NIR, **E**) and compound **8n** (**F**) along the analyzed trajectory (10 replicas of 1,000 ns per system). Their interaction frequency are displayed for non-covalently bound and covalently bound ligands in bold and normal fonts, respectively, as an average of the individual chains' values.

In vitro **ADME studies.** The most promising compound (**8n**) was selected with another close analog and potent promising inhibitor (**8r**), for comparison and further characterization (Table 4). First, the metabolic stability in mouse liver microsomes (MLMs) and human liver microsomes (HLMs) was investigated. Both compounds were metabolically stable in mouse as well as human microsomes, with half-lives ($t_{1/2}$) of more than 60 min each. Additionally, the intrinsic clearance of **8n** and **8r** in the mouse and human models was determined to be below 23 μL/min/mg, indicating that the compounds are stable. Encouraged by these results, in the next step, plasma stability as well as plasma protein binding (PPB) were assessed. The compound **8n** was stable in mouse and human plasma, and no degradation was observed during up to 240 min, while **8r** had a half-life in mouse plasma of around 140 min. **8r** was nearly entirely plasma protein bound, whereas the free fraction of **8n** in mouse was around 4 % and < 0.4 % in human plasma. Thus, both compounds had quite high plasma protein binding in mice and humans. In summary, **8n** and **8r** showed favorable in vitro ADME properties suitable for further preclinical development. Moreover, **8n** exhibited better properties than **8r**. However, decreasing plasma protein binding would be the goal for further optimization of these inhibitors.

Table 4. Pharmacokinetic properties of **8n** and **8r** in human and mouse plasma

Compd.	$t_{1/2}$ (min) mouse	Cl_{int} mouse (μl/min/mg protein)	$t_{1/2}$ (min) human	Cl_{int} human (μl/min/mg protein)	Mouse plasma $t_{1/2}$ (min)	Human plasma $t_{1/2}$ (min)	PPB mouse (%)[a]	PPB human (%)[a]
8n	> 60	< 23	> 60	< 23	>240	>240	95.8 ± 4.8	99.6 ± 0.6
8r	> 60	< 23	> 60	< 23	>240	143.1	99.7 ± 0.1	100 ± 0.0

[a]Means ± SDs from 3 replicates are presented.

CONCLUSIONS

In summary, we designed and synthesized a series of novel small-molecule peptidomimetics based on an initial hit compound to optimize them for inhibition of M^{pro}, an essential protease for replication of SARS-CoV-2. The dipeptides are composed of a variety of N-terminal capping groups, P3-Leu, P2-aryl groups and a C-terminal warhead. This resulted in several potent inhibitors with IC_{50} values in the low micromolar to low nanomolar range against SARS-CoV-2 M^{pro}. In particular, compounds **8r** ($IC_{50} = 0.0199$ μM), **10c** ($IC_{50} = 0.0177$ μM), and **10f** ($IC_{50} = 0.0130$ μM) were potent M^{pro} inhibitors, with 480- to 730-fold improved inhibitory activity when compared to the initial hit compound **I** ($IC_{50} = 9.50$ μM). The covalent irreversible binding mode of the compounds was validated by an X-ray co-crystal structure of M^{pro} in complex with **8p**. These structure studies supported by **8p** structure and MD simulations using **8n** suggest that their binding is independent of interactions with the side chain of Glu166.

Several compounds showed excellent antiviral activity in Calu-3 cells against SARS-CoV-2 and displayed no cytotoxicity. Most of the investigated SARS-CoV-2 M^{pro} inhibitors were found to additionally inhibit SARS-CoV-1 and MERS-CoV M^{pro}, as well as CatL, a host cysteine protease involved in the viral entry of coronaviruses. Compound **8n** displayed remarkable efficacy against a panel of naturally occurring nirmatrelvir-resistant mutants, especially the Glu166Val mutant of M^{pro}, and exhibited high metabolic stability, making it an attractive early hit for further preclinical development.

32

EXPERIMENTAL SECTION

General Chemistry. All commercially available starting materials, reagents, and (anhydrous) solvents were used without further purification. Reaction controls were performed by thin-layer chromatography (TLC) on Macherey-Nagel-precoated 60 F254 silica plates. Spots were visualized either by ultraviolet (UV) light (254 nm) or staining solutions. Flash column chromatography was carried out using Grace Davison Davisil LC60A (20–45 μm) or Merck Geduran Si60 (mesh 63–200 μm) with a LaFlash automated flash chromatography system. NMR spectra were recorded on a Bruker Avance 400 MHz spectrometer at ambient temperature. Chemical shifts (δ) are reported in parts per million (ppm) relative to the internal control tetramethylsilane (TMS), and the spectra were calibrated against the residual solvent peak of the used deuterated solvent. Coupling constants (*J*) are expressed in Hz. Purities of final compounds were determined by RP-HPLC using an Agilent 1100 Series LC with a Phenomenex Luna C8 analytical column (150 × 4.6 mm, 5 μm) and detected by a UV-DAD detector at 254 nm and 230 nm wavelength. The eluting was carried out with the following gradient: (A = 0.01 M KH_2PO_4, pH 2.30, B = MeOH) 40% B to 85% B in 8 min, 85% B for 5 min, 85% to 40% B in 1 min, 40% B for 2 min, stop time 16 min, flow 1.5 mL/min. Standard mass spectra were obtained from an Advion expression compact mass spectrometer (electron spray ionization, ESI) with a TLC plate reader system (using the following settings: ESI voltage 3.50 kV, capillary voltage 187 V, source voltage 44 V, capillary temperature 250 °C, desolvation gas temperature 250 °C, gas flow 5 L/min). All final compounds are ≥ 95% pure by HPLC.

General Procedure A for the Synthesis of Weinreb Amides

A mixed suspension of the appropriate carboxylic acid (1 equiv., 1 mmol), *N,O*-dimethylhydroxylamine • HCl (1.5 equiv., 1.5 mmol), and DIPEA (3.5 equiv., 3.5 mmol) in CH_2Cl_2 (7 mL) was cooled to 0 °C, followed by the dropwise addition of T_3P (1.5 equiv., 1.5

33

mmol). The resulting mixture was stirred at room temperature for 2 h. The reaction was concentrated under reduced pressure, diluted with EtOAc (20 mL), and washed successively with saturated aqueous $NaHCO_3$ solution (2 × 15 mL) and brine (15 mL). The organic layer was dried over anhydrous Na_2SO_4, filtered, and concentrated under reduced pressure to obtain the product.

General Procedure B for the Boc-Deprotection

The *N-Boc-protected* amine (1 equiv., 0.75 mmol) was dissolved in CH_2Cl_2 (3 mL), and 4N HCl in dioxane (10 equiv., 7.5 mmol) was added at 0 °C. The mixture was stirred for 3 h at 0 °C. The reaction was concentrated under reduced pressure to give the HCl salt, which was dissolved in aqueous 0.05 M NaOH and extracted with EtOAc (3 × 15 mL). The combined organic layers were dried over anhydrous Na_2SO_4, filtered, and concentrated under reduced pressure. The product was used without further purification.

General *Procedure C for the Synthesis of Amides*

HATU (1.2 equiv.) was added sequentially at 0 °C to a solution of the carboxylic acid (1 equiv.) in DMF (5 mL). The solution was kept at 0 °C for 30 min. After 30 minutes, DIPEA (3 equiv.) and the amine (1 equiv.) were added slowly. The mixture was stirred at 0 °C for 1 h and at 25 °C for 12 h. The reaction was quenched by adding water and extracted with EtOAc (3 × 15 mL). The combined organic phases were washed with saturated aqueous NH_4Cl solution (2 × 50 mL), saturated aqueous $NaHCO_3$ solution (2 × 50 mL), and brine (2 × 50 mL). The organic layer was dried over anhydrous Na_2SO_4 and concentrated under reduced pressure to afford the crude product.

General Procedure D for the Synthesis of Vinylketones

The Weinreb amide (1 equiv., 0.5 mmol) was dissolved in Et_2O (dry). The reaction mixture was cooled to -10 °C in a salt-ice bath, and 1M vinylmagnesium bromide in THF (3.2 equiv., 1.6 mmol) was added dropwise. After 1 h additional 1M vinylmagnesium bromide in THF (3.2 equiv., 1.6 mmol) was added dropwise. After 5 - 6 h of stirring at 0 °C, the reaction mixture was quenched with 1N HCl. The mixture was extracted with EtOAc (3×20 mL). The combined organic layers were dried over anhydrous Na_2SO_4 and concentrated under reduced pressure to afford the crude product as a solid.

General Procedure E for the Synthesis of Methylketones

The Weinreb amide (1 equiv., 0.5 mmol) was dissolved in Et_2O (dry). The reaction mixture was cooled to -10 °C in a salt-ice bath, and 3M methylmagnesium bromide in Et_2O (3.2 equiv., 1.6 mmol) was added dropwise. After 5 to 6 h of stirring at 0 °C, the reaction mixture was quenched with 1N HCl. The mixture was extracted with EtOAc (3×20 mL). The combined organic layers were dried over anhydrous Na_2SO_4, filtered, and concentrated under reduced pressure to get the crude product.

General Procedure F for the Aldol Condensation

A mixture of the ketone (1 equiv., 0.3 mmol) and *N*, *N*-dimethylformamide dimethyl acetal (2 equiv., 0.6 mmol) was dissolved in DMF (1 mL). The mixture was stirred for 5 h at 80 °C. Upon the completion of the reaction, the mixture was cooled to room temperature, and the solvent was removed under reduced pressure to obtain the crude compound.

General Procedure G for the Saponification of Methylester

To a solution of ester (1 equiv., 0.7 mmol) in THF (5 mL) cooled in an ice bath was added a 1.0 M LiOH aqueous solution (4 mL). After 2 h, the pH of the reaction mixture was adjusted to

3 by adding a 1.0 M HCl aqueous solution. The two layers were separated, and the aqueous layer was extracted with EtOAc (3 × 20 mL). The combined organic layers were washed with brine (10 mL), dried over anhydrous Na_2SO_4, filtered, and concentrated under reduced pressure to afford the product. The product was used without further purification.

(S)-4-Methyl-N-((S)-3-oxo-1-phenylpent-4-en-2-yl)-2-(3-phenylpropanamido)pentanamide (8a). Obtained from the reaction of **5a** (227 mg, 0.5 mmol) and 1 M vinylmagnesium bromide in THF (3.2 mL, 0.5 mmol) following general procedure D. Flash purification with petroleum ether/EtOAc (0 - 60% EtOAc). Yield: 109 mg (52%) of **8a** as a white solid. ^{1}H NMR (400 MHz, CDCl_3) δ 7.29 – 7.27 (m, 1H), 7.26 – 7.24 (m, 1H), 7.24 – 7.22 (m, 2H), 7.21 – 7.20 (m, 2H), 7.19 – 7.17 (m, 2H), 7.10 – 7.05 (m, 2H), 6.67 (d, *J* = 7.5 Hz, 1H), 6.42 (dd, *J* = 17.4, 9.7 Hz, 1H), 6.35 (dd, *J* = 17.4, 2.0 Hz, 1H), 5.86 (dd, *J* = 9.7, 2.0 Hz, 1H), 5.73 (d, *J* = 8.1 Hz, 1H), 5.11 – 5.05 (m, 1H), 4.46 – 4.38 (m, 1H), 3.15 (dd, *J* = 14.0, 6.5 Hz, 1H), 3.01 – 2.97 (m, 1H), 2.96 – 2.92 (m, 2H), 2.51 – 2.42 (m, 2H), 1.57 – 1.49 (m, 1H), 1.42 – 1.35 (m, 2H), 0.85 (d, *J* = 5.6 Hz, 3H), 0.84 (d, *J* = 5.6 Hz, 3H). ^{13}C NMR (101 MHz, CDCl_3) δ 197.05, 172.06, 171.76, 140.70, 135.74, 133.33, 130.64, 129.57 (2 x C), 128.71 (2 x C), 128.66 (2 x C), 128.45 (2 x C), 127.22, 126.46, 57.19, 51.66, 41.34, 38.28, 37.71, 31.64, 24.73, 22.96, 22.18. ESI-MS [M + Na]$^+$ = 443.3. HPLC t$_R$ = 8.70 min.

(S)-2-(3-(4-(Dimethylamino)phenyl)propanamido)-4-methyl-N-((S)-3-oxo-1-phenylpent-4-en-2-yl)pentanamide (8b). Obtained from the reaction of **5b** (248 mg, 0.5 mmol) and 1 M vinylmagnesium bromide in THF (3.2 mL, 0.5 mmol) following general procedure D. Flash purification with petroleum ether/EtOAc (0 - 60% EtOAc). Yield: 72 mg (31%) of **8b** as a white solid. ^{1}H NMR (400 MHz, CDCl_3) δ 7.26 – 7.23 (m, 2H), 7.23 – 7.20 (m, 1H), 7.11 – 7.07 (m, 2H), 7.07 – 7.04 (m, 2H), 6.74 – 6.70 (m, 1H), 6.70 – 6.65 (m, 2H), 6.42 (dd, *J* = 17.4, 9.7 Hz, 1H), 6.35 (dd, *J* = 17.4, 1.9 Hz, 1H), 5.85 (dd, *J* = 9.8, 1.9 Hz, 1H), 5.69 (d, *J* = 8.1 Hz, 1H),

36

5.11 – 5.03 (m, 1H), 4.45 – 4.36 (m, 1H), 3.15 (dd, J = 14.0, 6.4 Hz, 1H), 2.97 (dd, J = 14.0, 6.2 Hz, 1H), 2.90 (s, 6H), 2.88 – 2.81 (m, 2H), 2.51 – 2.38 (m, 2H), 1.57 – 1.47 (m, 1H), 1.43 – 1.31 (m, 2H), 0.85 (d, J = 6.4 Hz, 3H), 0.83 (d, J = 6.4 Hz, 3H) ^{13}C NMR (101 MHz, CDCl$_3$) δ 197.11, 172.51, 171.81, 149.35, 135.81, 133.31, 130.58, 129.57 (2 x C), 129.06 (2 x C), 128.63 (2 x C), 127.18, 113.27, 57.19, 51.61, 41.18, 40.99, 38.66, 37.65, 30.74, 24.67, 23.00, 22.16. ESI-MS [M + Na]$^+$ = 486.2. HPLC t$_R$ = 6.78 min.

(S)-4-Methyl-N-((S)-3-oxo-1-phenylpent-4-en-2-yl)-2-(3-(4-(trifluoromethoxy)phenyl)

propanamido)pentanamide (8c). Obtained from the reaction of **5c** (26 9 mg, 0.5 mmol) and 1 M vinylmagnesium bromide in THF (3.2 mL, 0.5 mmol) following general procedure D. Flash purification with petroleum ether/EtOAc (0 - 50% EtOAc). Yield: 76 mg (30%) of **8c** as a white solid. ^{1}H NMR (400 MHz, CDCl$_3$) δ 7.25 – 7.24 (m, 1H), 7.24 – 7.21 (m, 2H), 7.21 – 7.18 (m, 2H), 7.11 (d, J = 8.0 Hz, 2H), 7.09 – 7.05 (m, 2H), 6.66 (d, J = 7.5 Hz, 1H), 6.46 – 6.32 (m, 2H), 5.89 – 5.84 (m, 1H), 5.81 (d, J = 8.2 Hz, 1H), 5.12 – 5.05 (m, 1H), 4.47 – 4.40 (m, 1H), 3.15 (dd, J = 14.0, 6.5 Hz, 1H), 3.04 – 2.98 (m, 1H), 2.98 – 2.90 (m, 2H), 2.53 – 2.40 (m, 2H), 1.56 – 1.49 (m, 1H), 1.44 – 1.35 (m, 2H), 0.86 (d, J = 3.7 Hz, 3H), 0.84 (d, J = 3.7 Hz, 3H). ^{13}C NMR (101 MHz, CDCl$_3$) δ197.00, 171.76, 171.61, 147.88, 139.51, 135.65, 133.32, 130.72, 129.80 (2 x C), 129.57 (2 x C), 128.67 (2 x C), 127.25, 121.19 (2 x C), 120.63 (d, J = 256.8 Hz), 57.21, 51.71, 41.50, 38.04, 37.75, 30.82, 24.79, 22.89, 22.13. ESI-MS [M + Na]$^+$ = 527.1. HPLC t$_R$ = 9.80 min.

(S)-2-(3-(2,4-Dichlorophenyl)propanamido)-4-methyl-N-((S)-3-oxo-1-phenylpent-4-en-2-

yl)pentanamide (8d). Obtained from the reaction of **5d** (261 mg, 0.5 mmol) and 1 M vinylmagnesium bromide in THF (3.2 mL, 0.5 mmol) following general procedure D. Flash purification with petroleum ether/EtOAc (0 - 50% EtOAc). Yield: 157 mg (64%) of **8d** as a white solid. ^{1}H NMR (400 MHz, CDCl$_3$) δ 7.35 (d, J = 2.0 Hz, 1H), 7.26 – 7.23 (m, 2H), 7.22

37

– 7.16 (m, 2H), 7.16 – 7.11 (m, 1H), 7.09 – 7.04 (m, 2H), 6.66 (d, J = 7.5 Hz, 1H), 6.42 (dd, J = 17.5, 9.5 Hz, 1H), 6.35 (dd, J = 17.4, 2.1 Hz, 1H), 5.87 (dd, J = 9.5, 2.1 Hz, 1H), 5.82 (d, J = 8.2 Hz, 1H), 5.12 – 5.05 (m, 1H), 4.46 – 4.38 (m, 1H), 3.15 (dd, J = 14.0, 6.5 Hz, 1H), 3.02 (t, J = 7.6 Hz, 2H), 3.00 – 2.96 (m, 1H), 2.47 (t, J = 7.6 Hz, 2H), 1.58 – 1.49 (m, 1H), 1.45 – 1.36 (m, 2H), 0.86 (d, J = 5.2 Hz, 3H), 0.85 (d, J = 5.3 Hz, 3H). ^{13}C NMR (101 MHz, CDCl$_3$) δ 196.87, 171.53, 171.25, 136.73, 135.48, 134.48, 133.16, 132.84, 131.60, 130.66, 129.43 (2 x C), 129.31, 128.53 (2 x C), 127.21, 127.14, 57.06, 51.55, 41.37, 37.62, 35.76, 28.90, 24.65, 22.81, 22.09. ESI-MS [M - H]$^-$ = 487.3. HPLC t$_R$ = 9.82 min.

(S)-2-Cinnamamido-4-methyl-N-((S)-3-oxo-1-phenylpent-4-en-2-yl)pentanamide **(8e)**. Obtained from the reaction of **5e** (226 mg, 0.5 mmol) and 1 M vinylmagnesium bromide in THF (3.2 mL, 3.2 mmol) following general procedure D. Flash purification with CH$_2$Cl$_2$/MeOH (0 - 5% MeOH). Yield: 54 mg (26%) of **8e** as a white solid. ^{1}H NMR (400 MHz, CDCl$_3$) δ 7.67 – 7.59 (m, 1H), 7.53 – 7.48 (m, 1H), 7.48 – 7.44 (m, 1H), 7.40 – 7.32 (m, 3H), 7.25 – 7.21 (m, 2H), 7.20 – 7.14 (m, 1H), 7.14 – 7.07 (m, 2H), 7.03 – 6.94 (m, 1H), 6.44 (dd, J = 17.2, 7.8 Hz, 1H), 6.45 – 6.43 (m, 1H), 6.38 (dd, J = 17.1, 1.7 Hz, 1H), 5.88 – 5.80 (m, 1H), 5.16 – 5.09 (m, 1H), 4.68 – 4.60 (m, 1H), 3.18 (dd, J = 14.0, 6.2 Hz, 1H), 3.01 (dd, J = 13.9, 6.7 Hz, 1H), 1.69 – 1.60 (m, 1H), 1.59 – 1.49 (m, 2H), 0.91 (d, J = 5.8 Hz, 3H), 0.88 (d, J = 5.8 Hz, 3H). ^{13}C NMR (101 MHz, CDCl$_3$) δ 197.06, 171.94, 165.78, 141.77, 135.70, 134.68, 133.26, 133.08, 130.54, 129.81, 129.44 (2 x C), 128.82, 128.56 (2 x C), 127.88 (2 x C), 127.09, 120.07, 57.17, 51.78, 41.52, 37.51, 24.81, 22.91, 22.14. ESI-MS [M + Na]$^+$ = 441.3. HPLC t$_R$ = 11.22 min.

(S)-2-((E)-3-(4-(Dimethylamino)phenyl)acrylamido)-4-methyl-N-((S)-3-oxo-1-phenylpent-4-en-2-yl)pentanamide (8f). Obtained from the reaction of **5f** (247 mg, 0.5 mmol) and 1 M vinylmagnesium bromide in THF (3.2 mL, 0.5 mmol) following general procedure D. Flash purification with petroleum ether/EtOAc (0 - 70% EtOAc). Yield: 65 mg (28%) of **8f** as a

38

yellow solid. ^{1}H NMR (400 MHz, CDCl$_3$) δ 7.57 (d, J = 15.5 Hz, 1H), 7.46 – 7.35 (m, 2H), 7.25 – 7.18 (m, 2H), 7.18 – 7.14 (m, 1H), 7.14 – 7.06 (m, 2H), 6.97 – 6.88 (m, 1H), 6.72 – 6.61 (m, 2H), 6.44 (dd, J = 17.4, 10.0 Hz, 1H), 6.36 (dd, J = 17.2, 2.3 Hz, 1H), 6.18 (dd, J = 15.4, 4.8 Hz, 1H), 5.93 (dd, J = 40.2, 9.6 Hz, 1H), 5.87 – 5.80 (m, 1H), 5.15 – 5.03 (m, 1H), 4.66 – 4.55 (m, 1H), 3.16 (dd, J = 13.9, 6.1 Hz, 1H), 3.01 (s, 6H), 2.98 – 2.91 (m, 1H), 1.71 – 1.58 (m, 2H), 1.57 – 1.47 (m, 1H), 0.97 – 0.91 (m, 3H), 0.92 – 0.87 (m, 3H). ^{13}C NMR (101 MHz, CDCl$_3$) δ 197.19, 172.04, 166.80, 151.64, 142.37, 135.87, 133.38, 130.50, 129.59 (3 x C), 128.65 (2 x C), 127.07, 122.63, 114.76, 112.04 (2 x C), 57.29, 51.69, 41.27, 40.31 (2 x C), 37.68, 24.93, 23.04, 22.32, 22.23. ESI-MS [M + Na]$^+$ = 483.9. HPLC t$_R$ = 9.07 min.

(S)-4-Methyl-N-((S)-3-oxo-1-phenylpent-4-en-2-yl)-2-((E)-3-(4-(trifluoromethoxy)phenyl) acrylamido)pentanamide (8g). Obtained from the reaction of **5g** (251 mg, 0.5 mmol) and 1 M vinylmagnesium bromide in THF (3.2 mL, 0.5 mmol) following general procedure D. Flash purification with petroleum ether/EtOAc (0 - 70% EtOAc). Yield: 146 mg (58%) of **8g** as a white solid. ^{1}H NMR (400 MHz, CDCl$_3$) δ 7.60 (d, J = 15.6 Hz, 1H), 7.54 – 7.48 (m, 2H), 7.25 – 7.15 (m, 5H), 7.12 – 7.05 (m, 2H), 6.87 (d, J = 7.7 Hz, 1H), 6.44 (dd, J = 17.4, 9.7 Hz, 1H), 6.38 (d, J = 15.6 Hz, 1H), 6.37 (dd, J = 17.4, 1.9 Hz, 1H), 6.28 (d, J = 8.3 Hz, 1H), 5.87 (dd, J = 9.7, 1.9 Hz, 1H), 5.18 – 5.10 (m, 1H), 4.68 – 4.60 (m,1H), 3.17 (dd, J = 14.0, 6.4 Hz, 1H), 3.01 (dd, J = 14.0, 6.0 Hz, 1H), 1.67 – 1.60 (m, 1H), 1.59 – 1.53 (m, 1H), 0.95 – 0.92 (m, 3H), 0.93 – 0.89 (m, 3H). ^{13}C NMR (101 MHz, CDCl$_3$) δ 197.05, 171.86, 165.40, 150.24, 140.20, 135.64, 133.45, 133.36, 130.73, 129.59 (2 x C), 129.38 (2 x C), 128.68 (2 x C), 127.18, 121.28 (2 x C), 121.16, 120.52 (d, J = 258.1 Hz), 57.29, 51.96, 41.64, 37.77, 24.97, 23.00, 22.32. ESI-MS [M + Na]$^+$ = 524.8. HPLC t$_R$ = 9.38 min.

(S)-2-((E)-3-(4-Chlorophenyl)acrylamido)-4-methyl-N-((S)-3-oxo-1-phenylpent-4-en-2-yl)pentanamide (8h). Obtained from the reaction of **5h** (243 mg, 0.5 mmol) and 1 M

39

vinylmagnesium bromide in THF (3.2 mL, 0.5 mmol) following general procedure D. Flash purification with CH$_2$Cl$_2$/MeOH (0 - 3% MeOH). Yield: 41 mg (18%) of **8h** as a white solid. ^{1}H NMR (400 MHz, CDCl$_3$) δ 7.61 – 7.53 (m, 1H), 7.45 – 7.38 (m, 2H), 7.36 – 7.30 (m, 2H), 7.24 (d, *J* = 7.4 Hz, 1H), 7.25 – 7.16 (m, 2H), 7.13 – 7.09 (m, 1H), 7.09 – 7.05 (m, 1H), 6.89 – 6.79 (m, 1H), 6.49 – 6.41 (m, 1H), 6.37 (d, *J* = 15.7 Hz, 2H), 6.28 – 6.14 (m, 1H), 5.91 – 5.82 (m, 1H), 5.16 – 5.09 (m, 1H), 4.66 – 4.56 (m, 1H), 3.22 – 3.13 (m, 1H), 3.05 – 2.97 (m, 1H), 1.70 – 1.62 (m, 2H), 1.56 – 1.51 (m, 1H), 0.92 (d, *J* = 6.1 Hz, 3H), 0.89 (d, *J* = 6.1 Hz, 3H).^{13}C NMR (101 MHz, CDCl$_3$) δ 197.13, 171.87, 165.54, 140.56, 135.84, 135.73, 133.35, 133.23, 130.70, 129.58, 129.30 , 129.25 (3 x C), 129.17, 128.68, 127.23, 120.77, 120.72, 57.29, 51.92, 41.71, 37.69, 24.96, 23.03, 22.30. ESI-MS [M + Na]$^+$ = 475.4. HPLC t$_R$ = 9.68 min.

(S)-2-((E)-3-(2,4-Dichlorophenyl)acrylamido)-4-methyl-N-((S)-3-oxo-1-phenylpent-4-en-2-yl)pentanamide (8i). Obtained from the reaction of **5i** (260 mg, 0.5 mmol) and 1 M vinylmagnesium bromide in THF (3.2 mL, 0.5 mmol) following general procedure D. Flash purification with petroleum ether/EtOAc (0 - 50% EtOAc). Yield: 107 mg (44%) of **8i** as a white solid. ^{1}H NMR (400 MHz, CDCl$_3$) δ 7.92 (d, *J* = 15.6 Hz, 1H), 7.48 (d, *J* = 8.5 Hz, 1H), 7.44 – 7.39 (m, 1H), 7.25 – 7.15 (m, 4H), 7.12 – 7.06 (m, 2H), 6.83 (d, *J* = 7.6 Hz, 1H), 6.45 (dd, *J* = 15.2, 7.5 Hz, 1H), 6.39 (d, *J* = 15.6 Hz, 2H), 6.37 (dd, *J* = 17.4, 1.9 Hz, 1H), 5.88 (dd, *J* = 9.7, 1.9 Hz, 1H), 5.17 – 5.09 (m, 1H), 4.67 – 4.58 (m, 1H), 3.16 (dd, *J* = 14.0, 6.4 Hz, 1H), 3.02 (dd, *J* = 14.0, 6.0 Hz, 1H), 1.69 – 1.61 (m, 2H), 1.62 – 1.53 (m, 1H), 0.93 (d, *J* = 6.1 Hz, 3H), 0.92 (d, *J* = 6.1 Hz, 3H). ^{13}C NMR (101 MHz, CDCl$_3$) δ 197.02, 171.89, 165.06, 136.59, 135.97, 135.55, 135.53, 133.30, 131.73, 130.78, 130.11, 129.58 (2 x C), 128.70 (2 x C), 128.43, 127.60, 127.22, 123.43, 57.35, 52.01, 41.60, 37.75, 24.95, 23.00, 22.31. ESI-MS [M + Na]$^+$ = 509.2. HPLC t$_R$ = 9.78 min.

(S)-2-((E)-3-(3,5-Dimethoxyphenyl)acrylamido)-4-methyl-N-((S)-3-oxo-1-phenylpent-4-en-2-yl)pentanamide (8j). Obtained from the reaction of **5j** (255 mg, 0.5 mmol) and 1 M vinylmagnesium bromide in THF (3.2 mL, 0.5 mmol) following general procedure D. Flash purification with petroleum ether/EtOAc (0 - 50% EtOAc). Yield: 67 mg (28%) of **8j** as a white solid. ^{1}H NMR (400 MHz, CDCl$_3$) δ 7.54 (d, *J* = 15.5 Hz, 1H), 7.24 – 7.17 (m, 2H), 7.17 – 7.12 (m, 1H), 7.11 – 7.05 (m, 2H), 6.98 (d, *J* = 7.0 Hz, 1H), 6.64 (d, *J* = 2.1 Hz, 2H), 6.49 – 6.46 (m, 1H), 6.45 – 6.34 (m, 3H), 6.31 (d, *J* = 6.6 Hz, 1H), 5.85 (d, *J* = 9.9 Hz, 1H), 5.12 (dd, *J* = 13.8, 6.4 Hz, 1H), 4.71 – 4.63 (m, 1H), 3.79 (s, 6H), 3.15 (dd, *J* = 14.0, 6.3 Hz, 1H), 2.99 (dd, *J* = 14.0, 6.2 Hz, 1H), 1.70 – 1.62 (m, 2H), 1.60 – 1.50 (m, 1H), 0.93 (d, *J* = 6.0 Hz, 3H), 0.91 (d, *J* = 6.0 Hz, 3H). ^{13}C NMR (101 MHz, CDCl$_3$) δ 197.14, 171.92, 165.75, 161.21 (2 x C), 141.85, 136.81, 135.81, 133.46, 130.48, 129.58 (2 x C), 128.66 (2 x C), 127.12, 120.90, 106.04 (2 x C), 102.30, 57.28, 55.54 (2 x C), 51.92, 41.56, 37.73, 24.98, 22.98, 22.36. ESI-MS [M + Na]$^{+}$ = 501.6. HPLC t$_R$ = 8.67 min.

N-((S)-4-Methyl-1-oxo-1-(((S)-3-oxo-1-phenylpent-4-en-2-yl)amino)pentan-2-yl)-2-phenylcyclopropane-1-carboxamide (8k). Obtained from the reaction of **5k** (232 mg, 0.5 mmol) and 1 M vinylmagnesium bromide in THF (3.2 mL, 0.5 mmol) following general procedure D. Flash purification with petroleum ether/EtOAc (0 - 70% EtOAc). Yield: 139 mg (64%) of **8k** as a white solid. ^{1}H NMR (400 MHz, CDCl$_3$) δ 7.31 – 7.26 (m, 2H), 7.26 – 7.23 (m, 1H), 7.22 – 7.12 (m, 3H), 7.11 – 7.04 (m, 4H), 6.79 – 6.69 (m, 1H), 6.47 – 6.39 (m, 1H), 6.39 – 6.33 (m, 1H), 6.14 – 6.05 (m, 1H), 5.89 – 5.83 (m, 1H), 5.14 – 5.06 (m, 1H), 4.54 – 4.44 (m, 1H), 3.20 – 3.12 (m, 1H), 3.05 – 2.95 (m, 1H), 2.54 – 2.44 (m, 1H), 1.67 – 1.56 (m, 4H), 1.52 – 1.42 (m, 1H), 1.28 – 1.23 (m, 1H), 0.93 – 0.91 (m, 3H), 0.91 – 0.88 (m, 3H). ^{13}C NMR (101 MHz, CDCl$_3$) δ 196.94, 171.76, 171.57, 140.57, 135.54, 133.19, 130.57, 129.46, 128.54 (3 x C), 128.51 (3 x C), 127.10, 126.38, 126.09, 57.09, 51.95, 41.52, 37.68, 26.39, 25.26, 24.77, 22.77, 22.24, 16.33. ESI-MS [M - H]$^{-}$ = 430.9. HPLC t$_R$ = 8.83 & 8.94 min (isomeric mixture).

41

786

(S)-4-Methyl-N-((S)-3-oxo-1-phenylpent-4-en-2-yl)-2-(2-phenoxyacetamido)pentanamide (8l).
Obtained from the reaction of **5l** (228 mg, 0.5 mmol) and 1 M vinylmagnesium bromide in THF
(3.2 mL, 0.5 mmol) following general procedure D. Flash purification with petroleum
ether/EtOAc (0 - 50% EtOAc). Yield: 57 mg (27%) of **8l** as a white solid. ^{1}H NMR (400 MHz,
CDCl$_3$) δ 7.36 – 7.29 (m, 2H), 7.25 – 7.20 (m, 2H), 7.19 – 7.13 (m, 1H), 7.09 – 7.01 (m, 3H),
6.96 – 6.90 (m, 2H), 6.81 (d, *J* = 8.2 Hz, 1H), 6.69 (d, *J* = 7.5 Hz, 1H), 6.45 (dd, *J* = 17.4, 9.8
Hz, 1H), 6.37 (dd, *J* = 17.4, 1.9 Hz, 1H), 5.88 (dd, *J* = 9.8, 1.9 Hz, 1H), 5.15 – 5.09 (m, 1H),
4.55 – 4.50 (m, 1H), 4.49 – 4.41 (m, 2H), 3.18 (dd, *J* = 14.1, 6.4 Hz, 1H), 2.99 (dd, *J* = 14.1,
6.1 Hz, 1H), 1.68 – 1.63 (m, 1H), 1.56 – 1.47 (m, 2H), 0.89 (d, *J* = 6.1 Hz, 3H), 0.88 (d, *J* = 6.1
Hz, 3H). ^{13}C NMR (101 MHz, CDCl$_3$) δ 197.01, 171.12, 168.42, 157.20, 135.64, 133.31,
130.71, 129.97 (2 x C), 129.53 (2 x C), 128.63 (2 x C), 127.23, 122.38, 114.84 (2 x C), 67.25,
57.12, 51.33, 40.92, 37.63, 24.84, 22.96, 22.14. ESI-MS [M + Na]$^+$ = 445.4. HPLC t$_R$ = 8.94
min.

(S)-2-(2-(4-Chlorophenoxy)acetamido)-4-methyl-N-((S)-3-oxo-1-phenylpent-4-en-2-
yl)pentanamide (8m). Obtained from the reaction of **5m** (245 mg, 0.5 mmol) and 1 M
vinylmagnesium bromide in THF (3.2 mL, 0.5 mmol) following general procedure D. Flash
purification with petroleum ether/EtOAc (0 - 50% EtOAc). Yield: 107 mg (47%) of **8m** as a
white solid. ^{1}H NMR (400 MHz, CDCl$_3$) δ 7.24 – 7.19 (m, 2H), 7.18 – 7.13 (m, 2H), 7.12 –
7.07 (m, 1H), 7.02 – 6.98 (m, 2H), 6.82 – 6.76 (m, 2H), 6.73 (d, *J* = 8.1 Hz, 1H), 6.61 (d, *J* =
7.5 Hz, 1H), 6.38 (dd, *J* = 17.4, 9.7 Hz, 1H), 6.31 (dd, *J* = 17.4, 1.9 Hz, 1H), 5.82 (dd, *J* = 9.7,
1.9 Hz, 1H), 5.09 – 5.03 (m, 1H), 4.49 – 4.42 (m, 1H), 4.41 – 4.29 (m, 2H), 3.11 (dd, *J* = 14.1,
6.4 Hz, 1H), 2.94 (dd, *J* = 14.1, 6.0 Hz, 1H), 1.60 – 1.56 (m, 1H), 1.50 – 1.42 (m, 2H), 0.83 (d,
J = 5.7 Hz, 3H), 0.82 (d, *J* = 5.7 Hz, 3H). ^{13}C NMR (101 MHz, CDCl$_3$) δ 196.96, 171.08,
167.88, 155.78, 135.55, 133.26, 130.84, 129.86 (2 x C), 129.53 (2 x C), 128.63 (2 x C), 127.40,

42

127.24, 116.16 (2 x C), 67.53, 57.13, 51.34, 41.08, 37.64, 24.85, 22.94, 22.16. ESI-MS [M + Na]$^+$ = 479.3. HPLC t$_R$ = 9.04 min.

(S)-2-(2-(2,4-Dichlorophenoxy)acetamido)-4-methyl-N-((S)-3-oxo-1-phenylpent-4-en-2-yl)pentanamide (8n). Obtained from the reaction of **5n** (262 mg, 0.5 mmol) and 1 M vinylmagnesium bromide in THF (3.2 mL, 0.5 mmol) following general procedure D. Flash purification with petroleum ether/EtOAc (0 - 70% EtOAc). Yield: 103 mg (42%) of **8n** as a white solid. ^{1}H NMR (400 MHz, CDCl$_3$) δ 7.43 – 7.41 (m, 1H), 7.24 – 7.19 (m, 3H), 7.17 – 7.12 (m, 1H), 7.09 – 7.05 (m, 2H), 7.02 (d, *J* = 8.0 Hz, 1H), 6.82 (d, *J* = 8.8 Hz, 1H), 6.72 (d, *J* = 7.5 Hz, 1H), 6.45 (dd, *J* = 17.4, 9.8 Hz, 1H), 6.37 (dd, *J* = 17.4, 1.8 Hz, 1H), 5.89 (dd, *J* = 9.8, 1.8 Hz, 1H), 5.17 – 5.12 (m, 1H), 4.53 – 4.49 (m, 1H), 4.48 – 4.41 (m, 2H), 3.20 (dd, *J* = 14.1, 6.5 Hz, 1H), 3.03 (dd, *J* = 14.1, 5.8 Hz, 1H), 1.73 – 1.66 (m, 1H), 1.60 – 1.52 (m, 2H), 0.92 (d, *J* = 6.2 Hz, 3H), 0.90 (d, *J* = 6.2 Hz, 3H). ^{13}C NMR (101 MHz, CDCl$_3$) δ 197.01, 170.97, 167.40, 151.67, 135.58, 133.28, 130.80, 130.44, 129.56 (2 x C), 128.60 (2 x C), 128.16, 127.76, 127.21, 124.13, 114.87, 68.29, 57.07, 51.53, 40.98, 37.60, 24.92, 23.02, 22.13. ESI-MS [M - H]$^-$ = 488.9. HPLC t$_R$ = 10.09 min.

(S)-4-Methyl-N-((S)-3-oxo-1-phenylpent-4-en-2-yl)-2-(2-(2,4,5-trichlorophenoxy)acetamido)pentanamide (8o). Obtained from the reaction of **5o** (279 mg, 0.5 mmol) and 1M vinylmagnesium bromide in THF (3.2 mL, 0.5 mmol) following general procedure D. Flash purification with petroleum ether/EtOAc (0 - 70% EtOAc). Yield: 105 mg (40%) of **8o** as a white solid. ^{1}H NMR (400 MHz, CDCl$_3$) δ 7.52 (s, 1H), 7.25 – 7.19 (m, 2H), 7.18 – 7.14 (m, 1H), 7.09 – 7.05 (m, 2H), 7.00 – 6.95 (m, 2H), 6.70 (d, *J* = 7.5 Hz, 1H), 6.45 (dd, *J* = 17.4, 9.8 Hz, 1H), 6.37 (dd, *J* = 17.4, 1.9 Hz, 1H), 5.89 (dd, *J* = 9.8, 1.9 Hz, 1H), 5.18 – 5.09 (m, 1H), 4.55 – 4.49 (m, 1H), 4.49 – 4.40 (m, 2H), 3.20 (dd, *J* = 14.1, 6.5 Hz, 1H), 3.04 (dd, *J* = 14.1, 5.7 Hz, 1H), 1.73 – 1.65 (m, 1H), 1.60 – 1.52 (m, 2H), 0.92 (d, *J* = 5.6 Hz, 3H),

43

0.91 (d, J = 5.7 Hz, 3H). ^{13}C NMR (101 MHz, CDCl$_3$) δ 196.96, 170.94, 166.77, 151.80, 135.54, 133.26, 131.85, 131.36, 130.85, 129.57 (2 x C), 128.62 (2 x C), 127.23, 126.27, 122.44, 115.73, 68.36, 57.11, 51.52, 41.15, 37.62, 24.95, 23.01, 22.17. ESI-MS [M + Na]$^+$ = 547.3. HPLC t$_R$ = 10.50 min.

(S)-2-(2-(3-Methoxyphenoxy)acetamido)-4-methyl-N-((S)-3-oxo-1-phenylpent-4-en-2-yl)pentanamide (8p). Obtained from the reaction of **5p** (243 mg, 0.5 mmol) and 1 M vinylmagnesium bromide in THF (3.2 mL, 0.5 mmol) following general procedure D. Flash purification with petroleum ether/EtOAc (0 - 70% EtOAc). Yield: 113 mg (55%) of **8p** as a white solid. ^{1}H NMR (400 MHz, CDCl$_3$) δ 7.25 – 7.19 (m, 3H), 7.19 – 7.14 (m, 1H), 7.10 – 7.05 (m, 2H), 6.80 (d, J = 8.3 Hz, 1H), 6.69 (d, J = 7.5 Hz, 1H), 6.62 – 6.57 (m, 1H), 6.52 – 6.49 (m, 2H), 6.45 (dd, J = 17.5, 9.7 Hz, 1H), 6.37 (dd, J = 17.4, 1.9 Hz, 1H), 5.88 (dd, J = 9.7, 1.9 Hz, 1H), 5.15 – 5.08 (m, 1H), 4.56 – 4.49 (m, 1H), 4.49 – 4.38 (m, 2H), 3.80 (s, 3H), 3.18 (dd, J = 14.1, 6.4 Hz, 1H), 2.99 (dd, J = 14.1, 6.1 Hz, 1H), 1.67 – 1.62 (m, 1H), 1.57 – 1.48 (m, 2H), 0.89 (d, J = 6.3 Hz, 3H), 0.88 (d, J = 6.3 Hz, 3H). ^{13}C NMR (101 MHz, CDCl$_3$) δ 197.01, 171.14, 168.32, 161.17, 158.38, 135.62, 133.28, 130.74, 130.43, 129.52 (2 x C), 128.63 (2 x C), 127.23, 107.99, 106.70, 101.50, 67.26, 57.13, 55.51, 51.29, 40.92, 37.61, 24.82, 22.95, 22.13. ESI-MS [M - H]$^-$ = 451.1. HPLC t$_R$ = 8.89 min.

(S)-2-(2-(3-(Dimethylamino)phenoxy)acetamido)-4-methyl-N-((S)-3-oxo-1-phenylpent-4-en-2-yl)pentanamide (8q). Obtained from the reaction of **5q** (249 mg, 0.5 mmol) and 1 M vinylmagnesium bromide in THF (3.2 mL, 0.5 mmol) following general procedure D. Flash purification with petroleum ether/EtOAc (0 - 70% EtOAc). Yield: 102 mg (44%) of **8q** as a white solid. ^{1}H NMR (400 MHz, CDCl$_3$) δ 7.25 – 7.19 (m,2H), 7.19 – 7.16 (m, H), 7.14 (d, J = 8.2 Hz, 1H), 7.09 – 7.04 (m, 2H), 6.82 (d, J = 8.4 Hz, 1H), 6.72 (d, J = 7.5 Hz, 1H), 6.44 (dd, J = 17.4, 9.8 Hz, 2H), 6.37 (dd, J = 17.4, 1.8 Hz, 1H), 6.31 – 6.28 (m, 1H), 6.26 (d, J = 8.0 Hz,

1H), 5.87 (dd, J = 9.8, 1.8 Hz, 1H), 5.16 – 5.06 (m, 1H), 4.55 – 4.50 (m, 1H), 4.49 – 4.40 (m,

2H), 3.17 (dd, J = 14.0, 6.4 Hz, 1H), 3.00 – 2.96 (m, 1H), 2.95 (s, 6H), 1.68 – 1.62 (m, 1H),

1.57 – 1.47 (m, 2H), 0.89 (d, J = 5.7 Hz, 3H), 0.87 (d, J = 5.8 Hz, 3H). ^{13}C NMR (101 MHz,

CDCl$_3$) δ 197.05, 171.21, 168.82, 158.47, 135.79, 133.38, 130.52, 130.25, 129.52 (3 x C),

128.63 (3 x C), 127.20, 107.16, 102.12, 99.79, 67.31, 57.14, 51.34, 40.88, 40.67, 37.61, 24.82,

22.96, 22.14. ESI-MS [M + Na]$^+$ = 488.5. HPLC t$_R$ = 8.74 min.

(S)-4-Methyl-N-((S)-3-oxo-1-phenylpent-4-en-2-yl)-2-(2-(phenylthio)acetamido)

*pentanamide (**8r**).* Obtained from the reaction of **5r** (236 mg, 0.5 mmol) and 1M

vinylmagnesium bromide in THF (3.2 mL, 0.5 mmol) following general procedure D. Flash

purification with petroleum ether/EtOAc (0 - 50% EtOAc). Yield: 110 mg (50%) of **8r** as a

white solid. ^{1}H NMR (400 MHz, CDCl$_3$) δ 7.28 – 7.26 (m, 1H), 7.26 – 7.25 (m, 1H), 7.25 –

7.22 (m, 2H), 7.22 – 7.17 (m, 3H), 7.17 – 7.13 (m, 1H), 7.03 – 6.99 (m, 2H), 6.95 (d, J = 8.1

Hz, 1H), 6.55 (d, J = 7.5 Hz, 1H), 6.38 (dd, J = 17.4, 9.6 Hz, 1H), 6.31 (dd, J = 17.4, 2.0 Hz,

1H), 5.82 (dd, J = 9.6, 2.0 Hz, 1H), 5.07 – 5.01 (m, 1H), 4.37 – 4.29 (m, 1H), 3.68 – 3.63 (m,

1H), 3.54 – 3.48 (m, 1H), 3.08 (dd, J = 14.0, 6.5 Hz, 1H), 2.92 (dd, J = 14.0, 6.0 Hz, 1H), 1.52

– 1.32 (m, 2H), 1.26 – 1.18 (m, 1H), 0.74 (d, J = 6.6 Hz, 3H), 0.72 (d, J = 6.5 Hz, 3H). [13]C

NMR (101 MHz, CDCl$_3$) δ 197.00, 171.20, 168.03, 135.69, 134.49, 133.31, 130.66, 129.56 (2

x C), 129.49 (2 x C), 128.66 (2 x C), 128.43 (2 x C), 127.23, 126.95, 57.12, 52.04, 40.92, 37.63,

37.35, 24.59, 23.02, 21.83. ESI-MS [M + Na]$^+$ = 461.1. HPLC t$_R$ = 8.54 min.

(S)-4-Methyl-2-(2-methyl-2-(phenylthio)propanamido)-N-((S)-3-oxo-1-phenylpent-4-en-2-

*yl)pentanamide (**8s**).* Obtained from the reaction of 5**s** (250 mg, 0.5 mmol) and 1 M

vinylmagnesium bromide in THF (3.2 mL, 0.5 mmol) following general procedure D. Flash

purification with petroleum ether/EtOAc (0 – 42% EtOAc). Yield: 170 mg (73%) of **8s** as a

white solid. ^{1}H NMR (400 MHz, CDCl$_3$) δ 7.45 – 7.36 (m, 2H), 7.30 – 7.27 (m, 2H), 7.27 –

45

7.24 (m, 3H), 7.24 – 7.20 (m, 2H), 7.10 – 7.01 (m, 2H), 6.63 (d, J = 7.3 Hz, 1H), 6.41 (dd, J =

17.4, 9.6 Hz, 1H), 6.34 (dd, J = 17.4, 2.0 Hz, 1H), 5.86 (dd, J = 9.6, 2.0 Hz, 1H), 5.14 – 5.06

(m, 1H), 4.42 – 4.34 (m, 1H), 3.14 (dd, J = 14.0, 6.7 Hz, 1H), 3.03 (dd, J = 14.0, 5.5 Hz, 1H),

1.68 – 1.61 (m, 1H), 1.60 – 1.51 (m, 2H), 1.51 (s, 3H), 1.47 (s, 3H), 0.91 (d, J = 4.9 Hz, 3H),

0.89 (d, J = 4.9 Hz, 3H). ^{13}C NMR (101 MHz, CDCl$_3$) δ 197.02, 174.71, 171.52, 135.58, 134.42

(2 x C), 133.30, 131.87, 130.70, 129.55 (2 x C), 129.09 (2 x C), 128.73, 128.70 (2 x C), 127.26,

57.28, 52.57, 52.43, 41.41, 37.76, 27.12, 26.97, 24.89, 23.06, 22.05. ESI-MS [M - H]$^-$ = 465.3.

HPLC t$_R$ = 9.53 min.

(S)-2-(2-((3-Methoxyphenyl)thio)acetamido)-4-methyl-N-((S)-3-oxo-1-phenylpent-4-en-2-

yl)pentanamide (8t). Obtained from the reaction of **5t** (251 mg, 0.5 mmol) and 1 M

vinylmagnesium bromide in THF (3.2 mL, 0.5 mmol) following general procedure D. Flash

purification with petroleum ether/EtOAc (0 - 50% EtOAc). Yield: 136 mg (58%) of **8t** as a

white solid. ^{1}H NMR (400 MHz, CDCl$_3$) δ 7.26 – 7.21 (m, 3H), 7.21 – 7.15 (m, 1H), 7.06 –

7.01 (m, 2H), 6.97 (d, J = 8.1 Hz, 1H), 6.88 – 6.82 (m, 2H), 6.75 – 6.69 (m, 1H), 6.59 (d, J =

7.5 Hz, 1H), 6.41 (dd, J = 17.4, 9.6 Hz, 1H), 6.34 (dd, J = 17.4, 2.1 Hz, 1H), 5.85 (dd, J = 9.6,

2.1 Hz, 1H), 5.10 – 5.03 (m, 1H), 4.40 – 4.33 (m, 1H), 3.76 (s, 3H), 3.73 – 3.65 (m, 1H), 3.56

– 3.50 (m, 1H), 3.12 (dd, J = 14.0, 6.6 Hz, 1H), 2.95 (dd, J = 14.0, 5.9 Hz, 1H), 1.55 – 1.34 (m,

2H), 1.29 – 1.21 (m, 1H), 0.77 (d, J = 6.6 Hz, 3H), 0.75 (d, J = 6.6 Hz, 3H). ^{13}C NMR (101

MHz, CDCl$_3$) δ 197.00, 171.19, 167.96, 160.26, 135.68, 135.66, 133.25, 130.71, 130.37, 129.54

(2 x C), 128.64 (2 x C), 127.21, 120.23, 113.74, 112.66, 57.11, 55.39, 51.95, 40.87, 37.57,

37.14, 24.53, 23.04, 21.77. ESI-MS [M - H]$^-$ = 467.3. HPLC t$_R$ = 9.08 min.

(R,S)-N-((S)-4-Methyl-1-oxo-1-(((S)-3-oxo-1-phenylpent-4-en-2-yl)amino)pentan-2-

yl)chromane-2-carboxamide (8u). Obtained from the reaction of **5u** (241 mg, 0.5 mmol) and 1

M vinylmagnesium bromide in THF (3.2 mL, 0.5 mmol) following general procedure D. Flash

46

purification with petroleum ether/EtOAc (0 - 70% EOAc). Yield: 88 mg (39%) of **8u** as a white solid. ^{1}H NMR (400 MHz, CDCl$_3$) δ 7.26 – 7.17 (m, 3H), 7.17 – 7.12 (m, 1H), 7.12 – 7.04 (m, 2H), 7.04 – 7.00 (m, 1H), 6.94 – 6.81 (m, 3H), 6.77 – 6.55 (m, 1H), 6.49 – 6.31 (m, 2H), 5.90 – 5.83 (m, 1H), 5.16 – 5.05 (m, 1H), 4.55 – 4.42 (m, 2H), 3.23 – 3.10 (m, 1H), 3.06 – 2.92 (m, 1H), 2.91 – 2.72 (m, 2H), 2.43 – 2.34 (m, 1H), 2.10 – 1.86 (m, 1H), 1.78 – 1.65 (m, 1H), 1.62 – 1.34 (m, 2H), 0.98 – 0.92 (m, 3H), 0.86 – 0.77 (m, 3H). ^{13}C NMR (101 MHz, CDCl$_3$) δ 197.00, 171.17, 171.05, 153.01, 135.65, 133.34, 130.65, 129.93, 129.52 (2 x C), 128.64 (2 x C), 127.73, 127.20, 122.17, 121.57, 116.91, 75.43, 57.09, 51.60, 40.84, 37.66, 25.11, 24.84, 24.08, 23.02, 22.08. ESI-MS [M + Na]$^+$ = 471.2. HPLC t$_R$ = 9.39 min.

N-((S)-4-Methyl-1-oxo-1-(((S)-3-oxo-1-phenylpent-4-en-2-yl)amino)pentan-2-yl)benzofuran-2-carboxamide (8v). Obtained from the reaction of **5v** (233 mg, 0.5 mmol) and 1 M vinylmagnesium bromide in THF (3.2 mL, 0.5 mmol) following general procedure D. Flash purification with petroleum ether/EtOAc (0 - 70% EOAc). Yield: 164 mg (76%) of **8v** as a white solid. ^{1}H NMR (400 MHz, CDCl$_3$) δ 7.69 (d, *J* = 7.5 Hz, 1H), 7.55 – 7.48 (m, 2H), 7.47 – 7.41 (m, 1H), 7.34 – 7.28 (m, 1H), 7.15 – 7.10 (m, 2H), 7.09 – 7.03 (m, 3H), 6.93 (d, *J* = 8.5 Hz, 1H), 6.77 (d, *J* = 7.6 Hz, 1H), 6.46 (dd, *J* = 17.4, 9.7 Hz, 1H), 6.38 (dd, *J* = 17.4, 1.9 Hz, 1H), 5.88 (dd, *J* = 9.7, 1.9 Hz, 1H), 5.18 – 5.11 (m, 1H), 4.72 – 4.64 (m, 1H), 3.19 (dd, *J* = 14.0, 6.4 Hz, 1H), 3.00 (dd, *J* = 14.0, 6.2 Hz, 1H), 1.76 – 1.67 (m, 2H), 1.67 – 1.63 (m, 1H), 0.95 (d, *J* = 5.1 Hz, 3H), 0.94 (d, *J* = 5.3 Hz, 3H). ^{13}C NMR (101 MHz, CDCl$_3$) δ 197.02, 171.22, 158.75, 154.97, 148.21, 135.54, 133.31, 130.77, 129.51 (2 x C), 128.59 (2 x C), 127.67, 127.29, 127.13, 123.94, 122.92, 112.03, 111.18, 57.24, 51.51, 41.36, 37.73, 24.93, 23.02, 22.26. ESI-MS [M + Na]$^+$ = 455.2. HPLC t$_R$ = 8.72 min.

N-((S)-4-Methyl-1-oxo-1-(((S)-3-oxo-1-phenylpent-4-en-2-yl)amino)pentan-2-yl)-5-phenylfuran-2-carboxamide (8w). Obtained from the reaction of **5w** (246 mg, 0.5 mmol) and 1

47

M vinylmagnesium bromide in THF (3.2 mL, 0.5 mmol) following general procedure D. Flash purification with petroleum ether/EtOAc (0 - 60% EOAc). Yield: 213 mg (93%) of **8w** as a white solid. ^{1}H NMR (400 MHz, CDCl$_3$) δ 7.74 – 7.71 (m, 2H), 7.47 – 7.42 (m, 2H), 7.39 – 7.34 (m, 1H), 7.23 (d, J = 3.6 Hz, 1H), 7.15 – 7.09 (m, 3H), 7.09 – 7.05 (m, 2H), 6.81 – 6.78 (m, 1H), 6.78 – 6.76 (m, 1H), 6.65 (d, J = 8.5 Hz, 1H), 6.46 (dd, J = 17.4, 9.8 Hz, 1H), 6.39 (dd, J = 17.4, 1.8 Hz, 1H), 5.88 (dd, J = 9.8, 1.8 Hz, 1H), 5.19 – 5.12 (m, 1H), 4.70 – 4.63 (m, 1H), 3.19 (dd, J = 14.0, 6.3 Hz, 1H), 2.99 (dd, J = 14.0, 6.4 Hz, 1H), 1.77 – 1.71 (m, 1H), 1.67 – 1.60 (m, 2H), 0.96 (d, J = 6.1 Hz, 3H), 0.94 (d, J = 6.1 Hz, 3H). ^{13}C NMR (101 MHz, CDCl$_3$) δ 197.07, 171.46, 158.24, 155.96, 146.52, 135.61, 133.34, 129.66, 129.51 (2 x C), 129.04 (2 x C), 128.97 (2 x C), 128.57 (2 x C), 127.13, 124.74 (2 x C), 117.24, 107.52, 57.20, 51.26, 41.28, 37.74, 24.94, 23.03, 22.32. ESI-MS [M + Na]$^+$ = 481.3. HPLC t$_R$ = 9.08 min.

N-((S)-4-Methyl-1-oxo-1-(((S)-3-oxo-1-phenylpent-4-en-2-yl)amino)pentan-2-yl)-1H-indole-2-carboxamide (8x). Obtained from the reaction of **5x** (232 mg, 0.5 mmol) and 1 M vinylmagnesium bromide in THF (3.2 mL, 0.5 mmol) following general procedure D. Flash purification with petroleum ether/EtOAc (0 - 70% EOAc). Yield: 17 mg (8%) of **8x** as a white solid. ^{1}H NMR (400 MHz, CDCl$_3$) δ 9.71 – 9.50 (m, 1H), 7.76 – 7.58 (m, 2H), 7.49 – 7.40 (m, 1H), 7.35 – 7.27 (m, 1H), 7.24 – 7.08 (m, 4H), 7.05 – 7.00 (m, 2H), 6.95 – 6.90 (m, 1H), 6.88 – 6.77 (m, 1H), 6.55 – 6.44 (m, 1H), 6.43 – 6.32 (m, 1H), 5.94 – 5.81 (m, 1H), 5.32 – 5.16 (m, 1H), 5.02 – 4.75 (m, 1H), 3.22 – 3.11 (m, 1H), 3.08 – 2.96 (m, 1H), 1.71 – 1.66 (m, 1H), 1.65 – 1.56 (m, 2H), 0.93 – 0.90 (m, 3H), 0.90 – 0.87 (m, J = 6.4 Hz, 3H). ^{13}C NMR (101 MHz, CDCl$_3$) δ 197.80, 171.96, 161.45, 136.67, 135.63, 133.42, 130.98, 130.18, 129.45 (2 x C), 128.57 (2 x C), 127.75, 127.16, 124.77, 122.21, 120.83, 112.14, 103.09, 57.11, 51.77, 41.99, 37.87, 25.03, 22.96, 22.48. ESI-MS [M + Na]$^+$ = 454.1. HPLC t$_R$ = 8.51 min.

1-Methyl-N-((S)-4-methyl-1-oxo-1-(((S)-3-oxo-1-phenylpent-4-en-2-yl)amino)pentan-2-yl)-

1H-indole-2-carboxamide (8y). Obtained from the reaction of **5y** (239 mg, 0.5 mmol) and 1 M vinylmagnesium bromide in THF (3.2 mL, 0.5 mmol) following general procedure D. Flash purification with petroleum ether/EtOAc (0 - 50% EtOAc). Yield: 116 mg (52%) of **8y** as a white solid. ^{1}H NMR (400 MHz, CDCl$_3$) δ 7.63 (d, J = 8.0 Hz, 1H), 7.40 – 7.37 (m, 1H), 7.36 – 7.31 (m, 1H), 7.18 – 7.13 (m, 2H), 7.13 – 7.10 (m, 2H), 7.08 – 7.06 (m, 1H), 7.06 – 7.04 (m, 1H), 6.89 (s, 1H), 6.82 (d, J = 7.4 Hz, 1H), 6.57 (d, J = 8.2 Hz, 1H), 6.47 (dd, J = 17.4, 9.9 Hz, 1H), 6.39 (dd, J = 17.4, 1.8 Hz, 1H), 5.89 (dd, J = 9.9, 1.8 Hz, 1H), 5.18 – 5.11 (m, 1H), 4.68 – 4.61 (m, 1H), 3.99 (s, 3H), 3.22 (dd, J = 14.0, 6.4 Hz, 1H), 3.04 (dd, J = 14.0, 5.7 Hz, 1H), 1.77 – 1.68 (m, 2H), 1.68 – 1.61 (m, 1H), 0.97 (d, J = 4.2 Hz, 3H), 0.95 (d, J = 4.0 Hz, 3H).^{13}C NMR (101 MHz, CDCl$_3$) δ 196.96, 171.67, 162.49, 139.28, 135.51, 133.26, 131.24, 130.81, 129.55 (2 x C), 128.59 (2 x C), 127.19, 126.09, 124.45, 122.08, 120.72, 110.28, 104.55, 57.28, 51.76, 41.27, 37.62, 31.69, 25.07, 23.06, 22.27. ESI-MS [M + Na]$^+$ = 468.3. HPLC t$_R$ = 9.05 min.

N-((S)-4-Methyl-1-oxo-1-(((S)-3-oxo-1-phenylpent-4-en-2-yl)amino)pentan-2-yl)benzo[b]thiophene-2-carboxamide (8z). Obtained from the reaction of **5z** (241 mg, 0.5 mmol) and 1 M vinylmagnesium bromide in THF (3.2 mL, 0.5 mmol) following general procedure D. Flash purification with petroleum ether/EtOAc (0 - 50% EtOAc). Yield: 85 mg (38%) of **8z** as a white solid. ^{1}H NMR (400 MHz, CDCl$_3$) δ 7.89 – 7.85 (m, 1H), 7.84 – 7.80 (m, 1H), 7.80 – 7.76 (m, 1H), 7.46 – 7.36 (m, 2H), 7.18 – 7.10 (m, 3H), 7.09 – 7.04 (m, 2H), 6.81 (d, J = 7.7 Hz, 1H), 6.64 (d, J = 8.3 Hz, 1H), 6.46 (dd, J = 17.4, 9.8 Hz, 1H), 6.38 (dd, J = 17.4, 1.9 Hz, 1H), 5.88 (dd, J = 9.8, 1.8 Hz, 1H), 5.18 – 5.11 (m, 1H), 4.73 – 4.65 (m, 1H), 3.18 (dd, J = 14.0, 6.3 Hz, 1H), 3.00 (dd, J = 14.0, 6.2 Hz, 1H), 1.74 – 1.68 (m, 2H), 1.67 – 1.61 (m, 1H), 0.95 (d, J = 5.7 Hz, 3H), 0.94 (d, J = 5.7 Hz, 3H).^{13}C NMR (101 MHz, CDCl3) δ 197.02, 171.49, 162.20, 141.20, 139.18, 137.97, 135.53, 133.31, 130.77, 129.53 (2 x C), 128.65 (2 x

49

C), 127.21, 126.63, 125.75, 125.29, 125.12, 122.87, 57.33, 52.23, 41.54, 37.75, 25.02, 22.99, 22.40. ESI-MS $[M + Na]^+ = $ 471.3. HPLC $t_R = 8.95$ min.

N-((S)-4-Methyl-1-oxo-1-(((S)-3-oxo-1-phenylpent-4-en-2-yl)amino)pentan-2-yl)-5-phenylthiophene-2-carboxamide (8aa). Obtained from the reaction of **5aa** (254 mg, 0.5 mmol) and 1 M vinylmagnesium bromide in THF (3.2 mL, 0.5 mmol) following general procedure D. Flash purification with petroleum ether/EtOAc (0 - 50% EtOAc). Yield: 85 mg (36%) of **8aa** as a white solid. ^{1}H NMR (400 MHz, CDCl$_3$) δ 7.63 – 7.58 (m, 2H), 7.48 (d, J = 3.9 Hz, 1H), 7.42 – 7.37 (m, 2H), 7.36 – 7.31 (m, 1H), 7.25 (s, 1H), 7.18 – 7.11 (m, 3H), 7.08 – 7.04 (m, 2H), 6.83 (d, J = 7.7 Hz, 1H), 6.51 (d, J = 8.3 Hz, 1H), 6.45 (dd, J = 17.4, 9.8 Hz, 1H), 6.37 (dd, J = 17.4, 1.8 Hz, 1H), 5.87 (dd, J = 9.8, 1.8 Hz, 1H), 5.15 – 5.09 (m, 1H), 4.69 – 4.61 (m, 1H), 3.17 (dd, J = 14.0, 6.3 Hz, 1H), 2.99 (dd, J = 14.0, 6.2 Hz, 1H), 1.70 – 1.64 (m, 2H), 1.64 – 1.57 (m, 1H), 0.93 (d, J = 6.0 Hz, 3H), 0.92 (d, J = 6.0 Hz, 3H). ^{13}C NMR (101 MHz, CDCl$_3$) δ 197.06, 171.74, 161.75, 149.64, 136.93, 135.60, 133.59, 133.33, 130.71, 129.55 (2 x C), 129.22 (2 x C), 128.75 (2 x C), 128.64 (2 x C), 127.19, 126.28 (2 x C), 123.62, 57.34, 52.06, 41.41, 37.73, 25.00, 23.01, 22.35. ESI-MS $[M + Na]^+ = $ 498.1. HPLC $t_R = 9.66$ min.

4-Methyl-N-((S)-4-methyl-1-oxo-1-(((S)-3-oxo-1-phenylpent-4-en-2-yl)amino)pentan-2-yl)-2-phenylthiazole-5-carboxamide (8ab). Obtained from the reaction of **5ab** (261 mg, 0.5 mmol) and 1 M vinylmagnesium bromide in THF (3.2 mL, 0.5 mmol) following general procedure D. Flash purification with petroleum ether/EtOAc (0 - 45% EtOAc). Yield: 122 mg (50%) of **8ab** as a white solid. ^{1}H NMR (400 MHz, CDCl$_3$) δ 7.99 – 7.88 (m, 2H), 7.50 – 7.40 (m, 3H), 7.24 – 7.13 (m, 3H), 7.10 – 7.04 (m, 2H), 6.74 (d, J = 7.6 Hz, 1H), 6.47 (dd, J = 17.4, 9.7 Hz, 1H), 6.39 (dd, J = 17.5, 1.9 Hz, 1H), 6.27 (d, J = 8.1 Hz, 1H), 5.90 (dd, J = 9.7, 1.9 Hz, 1H), 5.19 – 5.11 (m, 1H), 4.69 – 4.58 (m, 1H), 3.20 (dd, J = 14.0, 6.3 Hz, 1H), 3.02 (dd, J = 14.0, 6.0 Hz, 1H), 2.73 (s, 3H), 1.72 – 1.64 (m, 2H), 1.64 – 1.57 (m, 1H), 0.96 (d, J = 6.1 Hz, 3H), 0.94 (d, J

50

1019 = 6.1 Hz, 3H). ^{13}C NMR (101 MHz, CDCl$_3$) δ 196.83, 171.32, 167.70, 161.60, 156.65, 135.35,

1020 133.13, 132.82, 130.93, 130.76, 129.40 (2 x C), 129.10 (2 x C), 128.52 (2 x C), 127.14, 126.80

1021 (2 x C), 125.29, 57.15, 52.09, 41.49, 37.59, 24.91, 22.87, 22.26, 17.61. ESI-MS [M - H]$^-$ =

1022 488.3. HPLC t$_R$ = 9.66 min.

1023

1024 *N-((S)-4-Methyl-1-oxo-1-(((S)-3-oxo-1-phenylpent-4-en-2-yl)amino)pentan-2-yl)-2-*

1025 *phenylthiazole-4-carboxamide (8ac).* Obtained from the reaction of **5ac** (254 mg, 0.5 mmol)

1026 and 1 M vinylmagnesium bromide in THF (3.2 mL, 0.5 mmol) following general procedure D.

1027 Flash purification with petroleum ether/EtOAc (0 - 50% EtOAc). Yield: 71 mg (30%) of **8ac**

1028 as a white solid. ^{1}H NMR (400 MHz, CDCl$_3$) δ 8.11 (s, 1H), 8.02 – 7.93 (m, 2H), 7.66 (d, *J* =

1029 8.5 Hz, 1H), 7.54 – 7.43 (m, 3H), 7.14 – 7.07 (m, 3H), 7.07 – 7.03 (m, 2H), 6.93 (d, *J* = 7.4 Hz,

1030 1H), 6.46 (dd, *J* = 17.4, 9.9 Hz, 1H), 6.37 (dd, *J* = 16.3, 1.8 Hz, 1H), 5.86 (dd, *J* = 9.8, 1.8Hz,

1031 1H), 5.20 – 5.11 (m, 1H), 4.72 – 4.63 (m, 1H), 3.18 (dd, *J* = 14.0, 6.3 Hz, 1H), 3.00 (dd, *J* =

1032 14.0, 6.2 Hz, 1H), 1.80 – 1.75 (m, 1H), 1.73 – 1.63 (m, 2H), 0.96 (d, *J* = 6.1 Hz, 3H), 0.94 (d,

1033 *J* = 6.1 Hz, 6H).^{13}C NMR (101 MHz, CDCl$_3$) δ 197.15, 171.43, 168.46, 161.17, 150.18, 135.68,

1034 133.35, 132.85, 130.89, 130.63, 129.48 (2 x C), 129.23 (2 x C), 128.51 (2 x C), 127.02, 126.87

1035 (2 x C), 123.70, 57.16, 51.63, 40.86, 37.62, 24.95, 23.06, 22.22. ESI-MS [M + Na]$^+$ = 499.1.

1036 HPLC t$_R$ = 9.40 min.

1037

1038 *5-Methyl-N-((S)-4-methyl-1-oxo-1-(((S)-3-oxo-1-phenylpent-4-en-2-yl)amino)pentan-2-*

1039 *yl)isoxazole-3-carboxamide (8ad).* Obtained from the reaction of **5ad** (215 mg, 0.5 mmol) and

1040 1 M vinylmagnesium bromide in THF (3.2 mL, 0.5 mmol) following general procedure D.

1041 Flash purification with petroleum ether/EtOAc (0 - 50% EtOAc). Yield: 165 mg (83%) of **8ad**

1042 as a white solid. ^{1}H NMR (400 MHz, CDCl$_3$) δ 7.20 – 7.13 (m, 3H), 7.08 (d, *J* = 8.4 Hz, 1H),

1043 7.06 – 7.02 (m, 2H), 6.78 (d, *J* = 7.5 Hz, 1H), 6.43 (dd, *J* = 17.4, 9.7 Hz, 1H), 6.44 – 6.43 (m,

1044 1H), 5.87 (dd, *J* = 17.7, 1.9 Hz, 1H), 5.17 – 5.10 (m, 1H), 4.63 – 4.55 (m, 1H), 3.17 (dd, *J* =

51

14.0, 6.5 Hz, 1H), 3.00 (dd, *J* = 14.0, 5.8 Hz, 1H), 2.49 (s, 3H), 1.71 – 1.66 (m, 1H), 1.66 – 1.56 (m, 2H), 0.92 (d, *J* = 4.8 Hz, 3H), 0.91 (d, *J* = 4.6 Hz, 3H).^{13}C NMR (101 MHz, CDCl$_3$) δ 197.07, 171.46, 170.92, 159.21, 158.29, 135.55, 133.31, 130.77, 129.53 (2 x C), 128.58 (2 x C), 127.15, 101.59, 57.16, 51.78, 41.01, 37.68, 24.87, 22.99, 22.04, 12.47. ESI-MS [M + Na]$^+$ = 420.2. HPLC t$_R$ = 7.51 min.

3-(Tert-butyl)-1-methyl-N-((S)-4-methyl-1-oxo-1-(((S)-3-oxo-1-phenylpent-4-en-2-yl)amino)pentan-2-yl)-1H-pyrazole-5-carboxamide (8ae). Obtained from the reaction of **5ae** (243 mg, 0.5 mmol) and 1 M vinylmagnesium bromide in THF (3.2 mL, 0.5 mmol) following general procedure D. Flash purification with petroleum ether/EtOAc (0 - 50% EtOAc). Yield: 188 mg (83%) of **8ae** as a white solid. ^{1}H NMR (400 MHz, CDCl$_3$) δ 7.17 – 7.12 (m, 3H), 7.07 – 7.01 (m, 2H), 6.85 (d, *J* = 7.5 Hz, 1H), 6.52 – 6.47 (m, 1H), 6.47 – 6.41 (m, 1H), 6.40 (d, *J* = 1.6 Hz, 1H), 6.37 (s, 1H), 5.88 (dd, *J* = 9.7, 1.6 Hz, 1H), 5.18 – 5.11 (m, 1H), 4.66 – 4.58 (m, 1H), 4.07 (s, 3H), 3.17 (dd, *J* = 14.0, 6.4 Hz, 1H), 3.00 (dd, *J* = 14.0, 5.9 Hz, 1H), 1.67 – 1.61 (m, 2H), 1.61 – 1.55 (m, 1H), 1.29 (s, 9H), 0.92 (d, *J* = 4.2 Hz, 3H), 0.91 (d, *J* = 4.2 Hz, 3H).^{13}C NMR (101 MHz, CDCl$_3$) δ 197.04, 171.62, 160.36, 159.99, 135.45, 134.75, 133.30, 130.82, 129.49 (2 x C), 128.57 (2 x C), 127.18, 103.01, 57.24, 51.52, 41.43, 39.12, 37.65, 32.07, 30.62 (3 x C), 24.91, 22.94, 22.22. ESI-MS [M + Na]$^+$ = 475.3. HPLC t$_R$ = 9.54 min.

(S)-2-(2-(2,4-Dichlorophenoxy)acetamido)-N-((S)-1-(3-fluorophenyl)-3-oxopent-4-en-2-yl)-4-methylpentanamide (9a). Obtained from the reaction of **6a** (271 mg, 0.5 mmol) and 1 M vinylmagnesium bromide in THF (3.2 mL, 0.5 mmol) following general procedure D. Flash purification with petroleum ether/EtOAc (0 - 40% EtOAc). Yield: 104 mg (41%) of **9a** as a white solid. ^{1}H NMR (400 MHz, CDCl$_3$) δ 7.46 – 7.39 (m, 1H), 7.25 – 7.20 (m, 1H), 7.20 – 7.15 (m, 1H), 7.02 (d, *J* = 7.7 Hz, 1H), 6.90 – 6.82 (m, 3H), 6.81 – 6.76 (m, 2H), 6.46 (dd, *J* = 17.5, 9.6 Hz, 1H), 6.39 (dd, *J* = 17.3, 2.0 Hz, 1H), 5.96 – 5.89 (m, 1H), 5.18 – 5.07 (m, 1H),

52

4.52 – 4.49 (m, 2H), 4.49 – 4.44 (m, 1H), 3.21 (dd, J = 14.0, 6.2 Hz, 1H), 3.00 (dd, J = 14.1,

5.9 Hz, 1H), 1.75 – 1.67 (m, 1H), 1.62 – 1.51 (m, 2H), 0.92 (d, J = 6.6 Hz, 3H), 0.91 (d, J = 6.8

Hz, 3H). ^{13}C NMR (101 MHz, CDCl$_3$) δ 196.62, 171.01, 167.52, 162.77 (d, J = 246.2 Hz),

151.65, 138.17 (d, J = 7.4 Hz), 133.14, 131.13, 130.42, 130.08 (d, J = 8.3 Hz), 128.17, 127.77,

125.23 (d, J = 2.9 Hz), 124.11, 116.56 (d, J = 21.2 Hz), 114.89, 114.17 (d, J = 21.0 Hz), 68.27,

56.87, 51.61, 40.82, 37.26, 24.93, 22.99, 22.13. ESI-MS [M + Na]$^+$ = 531.0. HPLC t$_R$ = 9.74

min.

(S)-N-((S)-1-(3-Fluorophenyl)-3-oxopent-4-en-2-yl)-4-methyl-2-(2-

*(phenylthio)acetamido)pentanamide (**9b**).* Obtained from the reaction of **6b** (367 mg, 0.5 mmol)

and 1 M vinylmagnesium bromide in THF (3.2 mL, 0.5 mmol) following general procedure D.

Flash purification with petroleum ether/EtOAc (0 - 40% EtOAc). Yield: 168 mg (49%) of **9b**

as a white solid. ^{1}H NMR (400 MHz, CDCl$_3$) δ 7.30 – 7.25 (m, 2H), 7.25 – 7.20 (m, 2H), 7.18

– 7.11 (m, 2H), 7.10 (d, J = 8.3 Hz, 1H), 7.01 (d, J = 7.6 Hz, 1H), 6.88 – 6.82 (m, 1H), 6.80 (d,

J = 7.7 Hz, 1H), 6.73 (d, J = 9.6 Hz, 1H), 6.39 (dd, J = 17.4, 9.6 Hz, 1H), 6.32 (dd, J = 17.0,

2.0 Hz, 1H), 5.86 – 5.79 (m, 1H), 5.09 – 4.99 (m, 1H), 4.46 – 4.38 (m, 1H), 3.69 – 3.62 (m,

1H), 3.58 – 3.50 (m, 1H), 3.07 (dd, J = 14.0, 6.3 Hz, 1H), 2.87 (dd, J = 14.0, 6.2 Hz, 1H), 1.49

– 1.31 (m, 2H), 1.27 – 1.17 (m, 1H), 0.73 (d, J = 6.6 Hz, 3H), 0.71 (d, J = 6.5 Hz, 3H). ^{13}C

NMR (101 MHz, CDCl$_3$) δ 196.69, 171.39, 168.15, 162.66 (d, J = 246.0 Hz), 138.40 (d, J = 7.4

Hz), 134.52, 133.16, 130.81, 129.98 (d, J = 8.3 Hz), 129.33 (2 x C), 128.41 (2 x C), 126.78,

125.18 (d, J = 2.8 Hz), 116.39 (d, J = 21.2 Hz), 113.98 (d, J = 21.0 Hz), 56.78, 51.94, 40.87,

37.20, 37.07, 24.48, 22.89, 21.82. ESI-MS [M - H]$^-$ = 455.2. HPLC t$_R$ = 8.64 min.

(S)-N-((S)-1-(3-Chlorophenyl)-3-oxopent-4-en-2-yl)-2-(2-(2,4-dichlorophenoxy)acetamido)-4-

*methylpentanamide (**10a**).* Obtained from the reaction of **7a** (279 mg, 0.5 mmol) and 1 M

vinylmagnesium bromide in THF (3.2 mL, 0.5 mmol) following general procedure D. Flash

53

1097 purification with petroleum ether/EtOAc (0 - 40% EtOAc). Yield: 61 mg (23%) of **10a** as a

1098 white solid. ^{1}H NMR (400 MHz, CDCl$_3$) δ 7.45 – 7.39 (m, 1H), 7.25 – 7.20 (m, 1H), 7.19 –

1099 7.11 (m, 2H), 7.10 – 7.05 (m, 1H), 7.01 (d, J = 7.8 Hz, 1H), 6.97 (d, J = 6.6 Hz, 1H), 6.87 –

1100 6.79 (m, 2H), 6.46 (dd, J = 17.5, 9.6 Hz, 1H), 6.40 (dd, J = 17.5, 2,0 Hz, 1H), 5.97 – 5.88 (m,

1101 1H), 5.17 – 5.08 (m, 1H), 4.50 (s, 2H), 4.49 – 4.44 (m, 1H), 3.19 (dd, J = 14.1, 6.2 Hz, 1H),

1102 2.97 (dd, J = 14.1, 5.9 Hz, 1H), 1.74 – 1.67 (m, 1H), 1.65 – 1.54 (m, 2H), 0.93 (d, J = 6.4 Hz,

1103 3H), 0.91 (d, J = 6.4 Hz, 3H). ^{13}C NMR (101 MHz, CDCl$_3$) δ 196.41, 170.92, 167.32, 151.49,

1104 137.66, 134.23, 133.07, 130.78, 130.22, 129.73, 129.52, 128.17, 127.69, 127.42, 127.12,

1105 123.83, 114.89, 68.30, 56.66, 51.56, 40.69, 37.00, 24.76, 22.86, 21.96. ESI-MS [M + Na]$^+$ =

1106 547.8. HPLC t$_R$ = 10.07 min.

1107

1108 *(S)-N-((S)-1-(3-Chlorophenyl)-3-oxopent-4-en-2-yl)-4-methyl-2-(2-*

1109 *(phenylthio)acetamido)pentanamide (**10b**).* Obtained from the reaction of **7b** (253 mg, 0.5

1110 mmol) and 1M vinylmagnesium bromide in THF (3.2 mL, 0.5 mmol) following general

1111 procedure D. Flash purification with petroleum ether/EtOAc (0 - 40% EtOAc). Yield: 144 mg

1112 (61%) of **8b** as a white solid. ^{1}H NMR (400 MHz, CDCl$_3$) δ 7.29 – 7.21 (m, 4H), 7.19 – 7.12

1113 (m, 3H), 7.03 – 6.96 (m, 2H), 6.93 – 6.88 (m, 1H), 6.77 (d, J = 7.6 Hz, 1H), 6.40 (dd, J = 17.4,

1114 9.3 Hz, 1H), 6.33 (dd, J = 17.5, 2.3 Hz, 1H), 5.85 (dd, J = 9.3, 2.3 Hz, 1H), 5.05 – 4.98 (m,

1115 1H), 4.39 – 4.31 (m, 1H), 3.70 – 3.64 (m, 1H), 3.59 – 3.52 (m, 1H), 3.08 (dd, J = 14.1, 6.3 Hz,

1116 1H), 2.84 (dd, J = 14.1, 6.2 Hz, 1H), 1.52 – 1.32 (m, 2H), 1.25 – 1.20 (m, 1H), 0.75 (d, J = 6.6

1117 Hz, 3H), 0.71 (d, J = 6.5 Hz, 3H). ^{13}C NMR (101 MHz, CDCl$_3$) δ 196.59, 171.32, 168.20,

1118 137.91, 134.45, 134.24, 133.13, 131.02, 129.86, 129.64, 129.46 (2 x C), 128.31 (2 x C), 127.71,

1119 127.37, 126.88, 56.82, 52.09, 40.75, 37.20, 37.05, 24.55, 22.99, 21.76. ESI-MS [M + Na]$^+$ =

1120 495.2. HPLC t$_R$ = 9.33 min.

1121

(S)-N-((S)-1-(3-Chlorophenyl)-3-oxopent-4-en-2-yl)-2-(2-(3-methoxyphenoxy)acetamido)-

4-methylpentanamide (10c). Obtained from the reaction of **7c** (260 mg, 0.5 mmol) and 1 M

vinylmagnesium bromide in THF (3.2 mL, 0.5 mmol) following general procedure D. Flash

purification with petroleum ether/EtOAc (0 - 50% EtOAc). Yield: 76 mg (31%) of **10c** as a

colorless solid. ^{1}H NMR (400 MHz, CDCl$_3$) δ 7.24 – 7.18 (m, 1H), 7.16 – 7.12 (m, 2H), 7.08 –

7.03 (m, 1H), 7.00 – 6.94 (m, 1H), 6.86 (d, *J* = 7.6 Hz, 1H), 6.81 (d, *J* = 8.3 Hz, 1H), 6.60 –

6.56 (m, 1H), 6.53 – 6.49 (m, 2H), 6.45 (dd, *J* = 17.5, 9.4 Hz, 1H), 6.39 (dd, *J* = 17.4, 2.2 Hz,

1H), 5.90 (dd, *J* = 9.4, 2.2 Hz, 1H), 5.13 – 5.06 (m, 1H), 4.57 – 4.50 (m, 1H), 4.50 – 4.42 (m,

2H), 3.79 (s, 3H), 3.16 (dd, *J* = 14.1, 6.2 Hz, 1H), 2.92 (dd, *J* = 14.1, 6.3 Hz, 1H), 1.69 – 1.61

(m, 1H), 1.56 – 1.45 (m, 2H), 0.89 (d, *J* = 5.9 Hz, 3H), 0.88 (d, *J* = 5.4 Hz, 3H). ^{13}C NMR (101

MHz, CDCl$_3$) δ 196.63, 171.25, 168.50, 161.23, 158.44, 137.97, 134.36, 133.26, 130.91,

130.42, 129.85, 129.67, 127.68, 127.41, 108.08, 106.77, 101.60, 67.36, 56.84, 55.50, 51.49,

40.85, 37.17, 24.88, 22.93, 22.13. ESI-MS [M + Na]$^+$ = 509.9. HPLC t$_R$ = 9.07 min.

N-((S)-4-Methyl-1-oxo-1-(((S)-3-oxo-1-phenylbutan-2-yl)amino)pentan-2-yl)benzofuran-2-

carboxamide (11a). Obtained from the reaction of **5v** (232 mg, 0.5 mmol) and 3 M

methylmagnesium bromide in Et$_2$O (0.53 mL, 1.60 mmol) following general procedure E. Flash

purification with petroleum ether/EtOAc (0 - 40% EtOAc). Yield: 129 mg (61%) of **11a** as a

white solid. ^{1}H NMR (400 MHz, CDCl$_3$) δ 7.69 (d, *J* = 7.8 Hz, 1H), 7.55 – 7.50 (m, 1H), 7.50

– 7.47 (m, 1H), 7.47 – 7.42 (m, 1H), 7.36 – 7.29 (m, 1H), 7.16 – 7.12 (m, 2H), 7.11 – 7.07 (m,

3H), 6.90 (d, *J* = 8.3 Hz, 1H), 6.74 (d, *J* = 7.3 Hz, 1H), 4.87 – 4.79 (m, 1H), 4.71 – 4.61 (m,

1H), 3.14 (dd, *J* = 14.0, 6.5 Hz, 1H), 2.99 (dd, *J* = 14.1, 6.7 Hz, 1H), 2.16 (s, 3H), 1.77 – 1.69

(m, 2H), 1.69 – 1.64 (m, 1H), 0.96 (d, *J* = 6.0 Hz, 3H), 0.95 (d, *J* = 6.0 Hz, 3H). ESI-MS [M +

Na]$^+$ = 443.7. HPLC t$_R$ = 8.85 min.

N-((S)-4-Methyl-1-oxo-1-(((S)-3-oxo-1-phenylbutan-2-yl)amino)pentan-2-

yl)benzo[b]thiophene-2-carboxamide (11b). Obtained from the reaction of **5z** (224 mg, 0.5

mmol) and 3 M methylmagnesium bromide in Et$_2$O (0.50 mL, 1.49 mmol) following general

procedure E. Flash purification with petroleum ether/EtOAc (0 - 40% EtOAc). Yield: 135 mg

(66%) of **11b** as a white solid. ^{1}H NMR (400 MHz, CDCl$_3$) δ δ 7.88 – 7.84 (m, 1H), 7.84 – 7.81

(m, 1H), 7.76 (s, 1H), 7.48 – 7.37 (m, 2H), 7.20 – 7.14 (m, 2H), 7.14 – 7.08 (m, 3H), 6.79 (d, *J*

= 7.4 Hz, 1H), 6.62 (d, *J* = 8.2 Hz, 1H), 4.85 – 4.77 (m, 1H), 4.72 – 4.63 (m, 1H), 3.14 (dd, *J* =

14.0, 6.4 Hz, 1H), 2.98 (dd, *J* = 14.0, 6.7 Hz, 1H), 2.16 (s, 3H), 1.76 – 1.68 (m, 2H), 1.68 – 1.61

(m, 1H), 0.96 (d, *J* = 5.4 Hz, 3H), 0.95 (d, *J* = 5.4 Hz, 3H). ESI-MS [M + Na]$^+$ = 459.3. HPLC

t$_R$ = 8.73 min.

N-((S)-1-(((S)-5-(Dimethylamino)-3-oxo-1-phenylpent-4-en-2-yl)amino)-4-methyl-1-

oxopentan-2-yl)benzofuran-2-carboxamide (12a). Obtained from the reaction of **11a** (126 mg,

0.30 mmol) and *N,N*-dimethylformamide dimethyl acetal (80 µL, 0.60 mmol) following general

procedure F. Flash purification with CH$_2$Cl$_2$/MeOH (0 – 3.5% MeOH). Yield: 110 mg (77%)

of **12a** as a yellow solid. ^{1}H NMR (400 MHz, CDCl$_3$) δ 7.74 – 7.62 (m, 1H), 7.61 – 7.47 (m,

4H), 7.34 – 7.25 (m, 2H), 7.25 – 7.20 (m, 2H), 7.20 – 7.12 (m, 3H), 7.11 – 6.98 (m, 1H), 4.95

– 4.78 (m, 2H), 4.78 – 4.66 (m, 1H), 3.12 – 3.05 (m, 3H), 3.04 – 2.87 (m, 2H), 2.81 – 2.63 (m,

3H), 1.80 – 1.68 (m, 1H), 1.68 – 1.51 (m, 2H), 1.01 – 0.95 (m, 3H), 0.95 – 0.89 (m, 3H). ^{13}C

NMR (101 MHz, CDCl$_3$) δ 192.96, 171.04, 158.50, 154.99, 153.75, 148.64, 137.44, 129.78 (3

x C), 128.27 (2 x C), 127.72, 127.04, 126.63, 123.79, 122.78, 112.04, 110.77, 93.60, 57.86,

51.78, 42.47, 39.51, 37.08, 24.98, 23.06, 22.36. ESI-MS [M + Na]$^+$ = 498.9. HPLC t$_R$ = 8.67 &

8.90 min (E/Z-isomeric mixture).

N-((S)-1-(((S)-5-(Dimethylamino)-3-oxo-1-phenylpent-4-en-2-yl)amino)-4-methyl-1-

oxopentan-2-yl)benzo[b]thiophene-2-carboxamide (12b). Obtained from the reaction of **11b**

56

(132 mg, 0.30 mmol) and *N,N*-dimethylformamide dimethyl acetal (80 μL, 0.60 mmol) following general procedure F. Flash purification with CH_2Cl_2/MeOH (0 - 5% MeOH). Yield: 90 mg (61%) of **12b** as a light yellow solid. ^{1}H NMR (400 MHz, CDCl$_3$) δ 8.78 – 8.69 (m, 1H), 8.31 (d, *J* = 8.7 Hz, 1H), 8.25 – 8.21 (m, 1H), 8.06 – 7.99 (m, 1H), 7.98 – 7.91 (m, 1H), 7.57 – 7.48 (m, 1H), 7.48 – 7.40 (m, 2H), 7.24 – 7.20 (m, 1H), 7.20 – 7.17 (m, 2H), 7.17 – 7.14 (m, 1H), 7.14 – 7.07 (m, 1H), 5.34 – 5.08 (m, 1H), 4.54 – 4.37 (m, 2H), 3.11 – 3.00 (m, 3H), 2.90 – 2.79 (m, 2H), 2.79 – 2.65 (m, 3H), 1.68 – 1.39 (m, 2H), 1.32 – 1.19 (m, 1H), 0.92 – 0.84 (m, 3H), 0.84 – 0.76 (m, 3H). ^{13}C NMR (101 MHz, DMSO-d_6) δ 192.93, 171.42, 161.33, 153.34, 140.25, 139.60, 139.19, 138.57, 129.20 (2 x C), 127.87 (2 x C), 126.18 (2 x C), 125.93, 125.31, 125.18, 124.91, 122.78, 91.53, 52.17, 44.24, 40.30, 37.25, 35.76, 24.23, 22.89, 21.59. ESI-MS $[M + Na]^+$ = 514.4. HPLC t_R = 8.52 & 8.77 min (E/Z-isomeric mixture).

(S)-N-((S)-1-(Benzo[d]thiazol-2-yl)-1-oxo-3-phenylpropan-2-yl)-4-methyl-2-(2-(phenylthio)acetamido)pentanamide (13a). A flame-dried, two-necked flask equipped with a stir bar and purged with argon with 2-bromobenzo[*d*]thiazole (1017 mg, 4.75 mmol) and THF (10 mL) was cooled to 0 °C. To this mixture was added isopropyl magnesium chloride lithium chloride complex (3.65 mL, 4.75 mmol, 6.4 equiv.) dropwise to give a yellow solution. The reaction was stirred for 30 minutes and then added dropwise to a solution of **6r** (350 mg, 0.74 mmol, 1 equiv.) in Et$_2$O (dry) at -10 °C. After 4–6 hours of stirring at 0 °C, the reaction mixture was quenched with 1N HCl and extracted with EtOAc (3 x 20 mL). The combined organic layers were dried over Na$_2$SO$_4$, filtered, and concentrated under reduced pressure to afford the crude product. Flash purification with petroleum ether/EtOAc (0 - 25% EtOAc). Yield: 180 mg (45%) of **13a** as a light-yellow solid. ^{1}H NMR (400 MHz, CDCl$_3$) δ 8.23 – 8.18 (m, 1H), 8.00 – 7.95 (m, 1H), 7.61 – 7.56 (m, 1H), 7.56 – 7.51 (m, 1H), 7.26 – 7.24 (m, 3H), 7.23 – 7.22 (m, 1H), 7.22 – 7.13 (m, 4H), 7.04 – 6.99 (m, 2H), 6.97 (d, *J* = 8.2 Hz, 1H), 6.69 (d, *J* = 7.7 Hz, 1H), 6.04 – 5.97 (m, 1H), 4.41 – 4.34 (m, 1H), 3.66 (d, *J* = 16.9 Hz, 1H), 3.48 (d, *J* = 16.9 Hz,

1199　1H), 3.42 (dd, J = 14.1, 5.3 Hz, 1H), 3.21 (dd, J = 14.1, 6.9 Hz, 1H), 1.53 – 1.44 (m, 1H), 1.40

1200　– 1.31 (m, 1H), 1.23 – 1.17 (m, 1H), 0.72 (d, J = 5.3 Hz, 3H), 0.70 (d, J = 5.2 Hz, 3H). [13]C

1201　NMR (101 MHz, CDCl$_3$) δ 191.98, 171.06, 167.89, 163.67, 153.52, 137.26, 135.55, 134.32,

1202　129.48 (2 x C), 129.36 (2 x C), 128.56 (2 x C), 128.31 (2 x C), 128.16, 127.28, 127.15, 126.81,

1203　125.87, 122.45, 56.55, 51.79, 40.66, 38.24, 37.23, 24.39, 22.90, 21.73. ESI-MS [M + Na]$^+$ =

1204　567.6. HPLC t$_R$ = 9.77 min.

1205

1206　*(S)-N-((S)-1-(1H-Indol-3-yl)-3-oxopent-4-en-2-yl)-2-(2-(2,4-dichlorophenoxy)acetamido)-*

1207　*4-methylpentanamide (**10d**).* Obtained from the reaction of **16a** (282 mg, 0.5 mmol) and 1 M

1208　vinylmagnesium bromide in THF (3.2 mL, 0.5 mmol) following general procedure D. Flash

1209　purification with petroleum ether/EtOAc (0 - 50% EtOAc). Yield: 66 mg (25%) of **10d** as a

1210　white solid. ^{1}H NMR (400 MHz, CDCl$_3$) δ 8.17 (s, 1H), 7.53 – 7.49 (m, 1H), 7.41 (d, J = 2.5

1211　Hz, 1H), 7.25 – 7.22 (m, 1H), 7.20 – 7.16 (m, 1H), 7.08 – 7.02 (m, 2H), 7.00 – 6.92 (m, 3H),

1212　6.70 (d, J = 8.8 Hz, 1H), 6.47 (dd, J = 17.5, 10.3 Hz, 1H), 6.36 (dd, J = 17.4, 1.1 Hz, 1H), 5.87

1213　(dd, J = 10.3, 1.1 Hz, 1H), 5.26 – 5.20 (m, 1H), 4.60 – 4.53 (m, 1H), 4.40 – 4.34 (m, 1H), 4.13

1214　– 4.07 (m, 1H), 3.36 (dd, J = 15.0, 6.2 Hz, 1H), 3.23 (dd, J = 15.1, 5.4 Hz, 1H), 1.71 – 1.66 (m,

1215　1H), 1.60 – 1.53 (m, 2H), 0.91 (d, J = 6.4 Hz, 3H), 0.89 (d, J = 6.4 Hz, 3H).^{13}C NMR (101

1216　MHz, CDCl$_3$) δ 197.47, 171.64, 167.56, 151.54, 136.00, 133.40, 130.45, 130.23, 128.02,

1217　127.60, 127.45, 123.91, 123.30, 122.15, 119.59, 118.64, 114.74, 111.33, 109.40, 67.93, 56.78,

1218　51.34, 41.34, 27.34, 24.92, 23.08, 22.00. ESI-MS [M + Na]$^+$ = 552.4. HPLC t$_R$ = 9.41 min.

1219

1220　*(S)-2-(2-(2,4-Dichlorophenoxy)acetamido)-N-((S)-1-(2-fluorophenyl)-3-oxopent-4-en-2-*

1221　*yl)-4-methylpentanamide (**10e**).* Obtained from the reaction of **16b** (271 mg, 0.5 mmol) and 1

1222　M vinylmagnesium bromide in THF (3.2 mL, 0.5 mmol) following general procedure D. Flash

1223　purification with petroleum ether/EtOAc (0 - 40% EtOAc). Yield: 168 mg (66%) of **10e** as a

1224　white solid. ^{1}H NMR (400 MHz, CDCl$_3$) δ 7.46 – 7.40 (m, 1H), 7.25 – 7.19 (m, 1H), 7.20 –

58

7.13 (m, 1H), 7.12 – 7.06 (m, 1H), 7.03 – 6.92 (m, 3H), 6.83 (d, J = 8.8 Hz, 1H), 6.74 (d, J = 7.6 Hz, 1H), 6.48 (dd, J = 17.5, 9.8 Hz, 1H), 6.40 (dd, J = 17.5, 1.8 Hz, 1H), 5.93 (dd, J = 9.8, 1.1 Hz, 1H), 5.25 – 5.16 (m, 1H), 4.55 – 4.44 (m, 3H), 3.25 (dd, J = 14.1, 5.8 Hz, 1H), 2.98 (dd, J = 14.1, 6.7 Hz, 1H), 1.72 – 1.66 (m, 1H), 1.60 – 1.48 (m, 2H), 0.91 (d, J = 6.0 Hz, 3H), 0.90 (d, J = 6.2 Hz, 3H).^{13}C NMR (101 MHz, CDCl$_3$) δ 196.88, 170.99, 167.38, 161.44 (d, J = 245.4 Hz), 151.69, 133.33, 131.95 (d, J = 4.4 Hz), 130.80, 130.44, 129.18 (d, J = 8.2 Hz), 128.17, 127.78, 124.20, 124.16 (d, J = 2.4 Hz), 122.84 (d, J = 15.8 Hz), 115.47 (d, J = 22.1 Hz), 114.90, 68.36, 55.89, 51.50, 40.96, 31.40, 24.91, 23.02, 22.11. ESI-MS [M + Na]$^+$ = 531.0. HPLC t$_R$ = 10.13 min.

*(S)-4-Methyl-N-((S)-3-oxo-1-((S)-2-oxopyrrolidin-3-yl)pent-4-en-2-yl)-2-(2-(2,4,5-trichlorophenoxy)acetamido)pentanamide (**10f**).* Obtained from the reaction of **16c** (283 mg, 0.5 mmol) and 1 M vinylmagnesium bromide in THF (3.2 mL, 0.5 mmol) following general procedure D. Flash purification with CH$_2$Cl$_2$/MeOH (0 - 3% MeOH). Yield: 109 mg (41%) of **10f** as a white solid. ^{1}H NMR (400 MHz, CDCl$_3$) δ 8.15 (d, J = 6.3 Hz, 1H), 7.49 (s, 1H), 7.14 (d, J = 8.3 Hz, 1H), 7.00 (s, 1H), 6.54 (dd, J = 17.4, 10.4 Hz, 1H), 6.41 (dd, J = 17.4, 1.3 Hz, 1H), 6.13 (s, 1H), 5.85 (dd, J = 10.4, 1.3 Hz, 1H), 4.73 – 4.63 (m, 2H), 4.59 – 4.48 (m, 2H), 3.38 – 3.29 (m, 2H), 2.48 – 2.39 (m, 2H), 2.11 – 2.04 (m, 1H), 1.85 – 1.78 (m, 2H), 1.77 – 1.74 (m, 1H), 1.73 – 1.68 (m, 1H), 1.67 – 1.61 (m, 1H), 0.97 (d, J = 5.9 Hz, 3H), 0.95 (d, J = 5.9 Hz, 3H).^{13}C NMR (101 MHz, CDCl$_3$) δ 197.46, 179.84, 172.18, 166.78, 151.97, 132.41, 131.72, 131.27, 130.44, 126.08, 122.48, 115.76, 68.54, 56.45, 51.50, 42.01, 40.66, 38.65, 32.29, 28.97, 24.98, 23.06, 22.12. ESI-MS [M + Na]$^+$ = 553.5. HPLC t$_R$ = 9.36 min.

SARS-CoV-2 M^{pro} Inhibition Assays. The enzyme was expressed and purified as previously described.[27] The assay was performed at 37 °C with an excitation wavelength of 360 nm and an emission wavelength of 460 nm. The total volume per well was 50 μL. The assay buffer was

50 mM MOPS, pH 7.2 containing 10 mM NaCl, 1 mM EDTA, and 0.01% Triton X-100. The substrate Boc-Abu-Tle-Leu-Gln-AMC was prepared as a 10 mM stock solution in DMSO. The substrate stock solution was diluted with assay buffer and pipetted into a well containing 15 μL of inhibitor solution. This mixture was kept at 37 °C for 5 min. A volume of 1 μL of an enzyme-containing solution was diluted with assay buffer and added to start the reaction, which was monitored for 60 min. The final substrate concentration was 50 μM (= 1.03 K_m), and the final DMSO content was 4% (v/v).

Cathepsin L Inhibition Assay

The assay was performed as described.[39,40] The enzyme stock solution (20 mM malonate buffer pH 5.5, 400 mM NaCl, and 1 mM EDTA) was diluted 1:100 with assay buffer (100 mM sodium phosphate buffer pH 6.0, 100 mM NaCl, 5 mM EDTA, and 0.01% (w/v) Brij 35) containing 5 mM DTT, incubated at 37 °C for 30 min, and then stored on ice. A 10 mM solution of the substrate Z-Phe-Arg-pNA was prepared in DMSO. In a cuvette containing 940 μL of assay buffer, the chromogenic substrate (10 μL) and DMSO and/or inhibitor solution (10 μL) was piped. Upon addition of CatL (40 μL), the measurement was started and followed at 37 °C for 60 min at 405 nm. The final substrate concentration was 100 μM (= 5.88 × K_m), and the final DMSO concentration was 2% (v/v).

Inhibition Assays against Recombinant SARS-CoV M^{pro} and MERS-CoV M^{pro}. Recombinant SARS-CoV-1 M^{pro} and MERS-CoV M^{pro} were purchased from R&D Systems (E720 and E719, respectively). Proteolytic activity was determined as previously described.[29] Briefly, assays were performed at 25 °C, in a final volume of 30 μL of 50 mM HEPES pH 7.5, 150 mM sodium chloride, 1 mM EDTA, 0.01% Tween 20 in the presence of 50 nM enzyme and 10 μM of Ac-Abu-Tle-Leu-Gln-ACC substrate for both enzymes.[56-58] Fluorescence was monitored in a Synergy HTX (Biotek) plate reader for up to 2 hours, with 360/460 nm

wavelength (excitation/emission). All assays were performed in 384-well black microplates, with a 15 min pre-incubation of the compounds with the enzyme. The initial screening was performed with 10 μM of compounds and those that inhibited 50% or more of the enzyme activity progressed to eight-point (0.01 - 40 μM) concentration-response assays. The half-maximal inhibitory concentration (IC_{50}) was calculated by nonlinear regression ($r^2 > 0.9$), and the deviation of each data point from the calculated nonlinear regression was < 10%. For each compound, two independent experiments were performed, each in triplicate (n = 6 data points). The percentage of inhibition was calculated in comparison to the DMSO controls (up to 0.2%). Protease inhibitor nirmatrelvir was used as a positive control. Data were analyzed using GraphPad Prism 9.0 (GraphPad Software, San Diego, California, USA).

Cytotoxicity. *Cell Cultures.* Calu-3 cells (human lung, ATCC Cat# HTB-55) were maintained in Dulbecco's modified Eagle medium (DMEM)/F-12 supplemented with 10% FCS and 10 mM sodium pyruvate. Cells were incubated at 37 °C and 5% CO_2 in a humidified atmosphere. *Cell Viability Assays.* To determine the cell viability of Calu-3 cells treated with inhibitors, the CellTiter-Glo Luminescent Cell Viability Assay Kit (Promega) was used. Cells were grown in 96-well microplates until reaching 50–60% confluency before they were incubated with DMSO (a solvent control) or test compounds at a concentration of 10 μM in DMEM with 5% FCS for 24 h. Next, cell culture supernatants were removed, and 50 μL of the CellTiter-Glo substrate was added to each well and incubated for 30 min on a rocking platform. Finally, samples were transferred into white 96-well microplates, and luminescence was measured using a Hidex Sense plate luminometer (Hidex).

Antiviral Activity. SARS-CoV-2 were performed in a BSL-3 laboratory at the German Primate Centre, Göttingen/Germany. Calu-3 cells were grown in 48-well microplates until reaching approx. 70% confluency. Cells were incubated with 10-fold serial dilutions (10 – 0.001 μM) of

1303   M^{pro} inhibitors in DMEM for 1 h at 37 °C prior to infection. Next, media was removed, and

1304   cells were infected with the SARS-CoV-2 isolate NK, lineage B.1.513 (Pango classification),

1305   at MOI of 0.01 in 400 μL of fresh DMEM without FCS for 1 h at 37 °C. At 1 h post-infection

1306   (*h.p.i.*), the inoculum was removed, and cells were washed with PBS three times and further

1307   incubated in DMEM with 5% FCS containing the respective inhibitors. Virus-containing

1308   supernatants were collected 24 *h.p.i.* and stored at −80 °C until titration. To determine viral

1309   titers, confluently grown Vero E6 cells in DMEM supplemented with 5% FCS were inoculated

1310   for 1 h at 37 °C with 10-fold serial dilutions of virus-containing supernatants as described.[29]

1311   Next, the inoculum was removed, and cells were washed once with PBS before they were

1312   overlaid with 1% plaque agarose (Biozym) dissolved in Eagle's minimal essential medium

1313   (MEM) without phenol red (Lonza) and further incubated. At 48 h post-infection, virus-induced

1314   plaques were counted, and viral titters were determined as PFU/mL.

1315

1316   **Pharmacokinetic studies *in vitro*.** Plasma stability assay, Metabolic stability assay, and

1317   Plasma protein binding assay were conducted as described previously.[59, 60] For the HPLC-MS

1318   measurements, samples were analyzed using an Agilent 1290 Infinity II HPLC system coupled

1319   to an AB Sciex QTrap 6500plus or an AB Sciex Qtrap7500 mass spectrometer. LC conditions

1320   were as described previously.[36] MS/MS transitions can be found in Tables S2 and S3.

1321

1322   **Co-crystal structure determination**

1323   SARS-CoV-2 M^{pro} was expressed and purified in analogy to described procedures.[36] M^{pro}

1324   containing an *N*-terminal autocleavage site and a C-terminal human rhinovirus (HRV) 3C

1325   cleavage site was expressed in E. coli (BL21(DE3)) utilizing the pGEX-6P-1 vector. Bacterial

1326   cells were sonicated, and M^{pro} was purified by metal affinity chromatography. After HRV 3C

1327   cleavage followed by dialysis, the full-length enzyme with original N- and C-termini was

1328   obtained, and stored in buffer consisting of 20 mM 2-[4-(2-hydroxyethyl)piperazin-1-

62

1329 yl]ethane-1-sulfonic acid (HEPES) and 1 mM Tris(2-carboxyethyl)phosphin (TCEP), pH 7.4.

1330 Freshly prepared protein (15 mg/mL, ca. 500 μM) was incubated with inhibitor (dissolved in

1331 DMSO) at a molar ratio of 1 : 1.25. Sitting-drop crystallization experiments were performed as

1332 previously described.[30] Crystals started appearing after 8 days under the following condition:

1333 0.1M MMT (sodium malonate, imidazole, and boric acid in the molar ratios 2:3:3), pH 5.0,

1334 25% w/v polyethylene glycol (PEG)1500.

1335 X-ray diffraction data were collected at 100 K at EMBL beamlines P13 at the DESY

1336 synchrotron in Hamburg, Germany (Table S1). The diffraction data were indexed, integrated

1337 and scaled with XDS[61] and STARANISO[62] as implemented in ISPyB[63] at DESY. The structure

1338 7lkd[64] was used as a starting model for refinement. The inhibitor was refined at full occupancy.

1339 Phenix[65] was used for refinement and Coot[66] for model building. Stereochemical restraints for

1340 ligand refinement were generated using grade2 (https://grade.globalphasing.org). The

1341 molecular figure was generated using PyMOL (https://pymol.org).

1342

1343 **ASSOCIATED CONTENT**

1344 **Supporting Information**

1345 The Supporting Information is available free of charge at https://

1346 Antiviral activity in Calu-3 cells (Figure S1); concentration-dependent curves of selected

1347 SARS-CoV-1 M^{pro} inhibitors (Figure S2); concentration-dependent curves of selected MERS-

1348 CoV M^{pro} inhibitors (Figure S3); diffraction data and refinement statistics of **8p** (Table S1);

1349 crystal structure of the SARS-CoV-2 M^{pro} catalytic site bound to **8p** depicting its binding mode

1350 and interactions (Figure S4); SARS-CoV-2 M^{pro} dimer structure and the active site

1351 conformation (Figure S5); synthesis of chemical intermediates; ^1H and ^{13}C NMR spectra of all

1352 tested compounds; HPLC traces of all tested compounds at 254 and 230 nm.

1353 Molecular formula strings and biological data of final compounds (CSV).

1354 M^{pro}-**8p** (PDB code 9GV2).

1355 CCDC file for **8p** (PDF).

The pdb file for **8p** (pdb)

The binary file for **8p** (mtz)

Trajectories and interaction data are available on the Zenodo repository (under the code: 10.5281/zenodo.10722085, 10.5281/zenodo.10837432, and 10.5281/zenodo.10836982).

AUTHOR INFORMATION

Corresponding Authors

Thanigaimalai Pillaiyar − *Institute of Pharmacy, Pharmaceutical/Medicinal Chemistry and Tübingen Center for Academic Drug Discovery, Eberhard Karls University Tübingen, Auf der Morgenstelle 8, 72076 Tübingen, Germany;* https://orcid.org/0000-0001-5575-8896; E-mail: thanigaimalai.pillaiyar@uni-tuebingen.de

Authors

Philipp Flury − *Institute of Pharmacy, Pharmaceutical/Medicinal Chemistry and Tübingen Center for Academic Drug Discovery, Eberhard Karls University Tübingen, Auf der Morgenstelle 8, 72076 Tübingen, Germany.*

Nadine Krüger − *Platform Infection Models, German Primate Center, Leibniz Institute for Primate Research Göttingen, Göttingen 37077, Germany.*

Katharina Sylvester − *PharmaCenter Bonn, Pharmaceutical Institute, Pharmaceutical & Medicinal Chemistry, University of Bonn, Bonn D-53121, Germany.*

Julian Breidenbach − *PharmaCenter Bonn, Pharmaceutical Institute, Pharmaceutical & Medicinal Chemistry, University of Bonn, Bonn D-53121, Germany.*

Ghazl Al Hamwi − *PharmaCenter Bonn, Pharmaceutical Institute, Pharmaceutical & Medicinal Chemistry, University of Bonn, Bonn D-53121, Germany.*

1381 **Jingxin Qiao** − *Department of Biotherapy, Cancer Center and State Key Laboratory of*

1382 *Biotherapy, West China Hospital, Sichuan University, Chengdu, Sichuan, 610041, China.*

1383 **Yan Chen** − *Department of Biotherapy, Cancer Center and State Key Laboratory of*

1384 *Biotherapy, West China Hospital, Sichuan University, Chengdu, Sichuan, 610041, China.*

1385 **Cheila Rocha** − *Infection Biology Unit, German Primate Center, Leibniz Institute for Primate*

1386 *Research Göttingen, Göttingen 37077, Germany.*

1387 **Mateus Sá–Magalhães Serafim** - *Department of Microbiology, Institute of Biological*

1388 *Sciences, Federal University of Minas Gerais, Belo Horizonte, 31270-901, Minas Gerais,*

1389 *Brazil; Center for Discovery and Innovation in Parasitic Diseases, Skaggs School of Pharmacy*

1390 *and Pharmaceutical Sciences, University of California San Diego, 9500 Gilman Drive, La*

1391 *Jolla, CA 92093-0657, USA;* orcid.org/0000-0002-7505-8659.

1392 **Elan– Barbosa da Silva** - *Center for Discovery and Innovation in Parasitic Diseases, Skaggs*

1393 *School of Pharmacy and Pharmaceutical Sciences, University of California San Diego, 9500*

1394 *Gilman Drive, La Jolla, CA 92093-0657, USA; orcid.org/0000-0002-1926-3500.*

1395 **Stefan Pöhlmann** − *Infection Biology Unit, German Primate Center, Leibniz Institute for*

1396 *Primate Research Göttingen, Kellnerweg 4, 37077 Göttingen, Germany: Faculty of Biology*

1397 *and Psychology, University Göttingen, Göttingen 37073, Germany.*

1398 *https://orcid.org/0000-0001-6086-9136*

1399 **Antti Poso -** *Institute of Pharmacy, Pharmaceutical/ Medicinal Chemistry and Tübingen*

1400 *Center for Academic Drug Discovery, Eberhard Karls University Tübingen, Auf der*

1401 *Morgenstelle 8, 72076 Tübingen, Germany. https://orcid.org/0000-0003-4196-4204*

1402 **Thales Kronenberger -** German Center for Infection Research (DZIF), partner-site Tübingen,

1403 Tübingen, Germany. *Institute of Pharmacy, Pharmaceutical/ Medicinal Chemistry and*

1404 *Tübingen Center for Academic Drug Discovery, Eberhard Karls University Tübingen, Auf der*

1405 *Morgenstelle 8, 72076 Tübingen, Germany. https://orcid.org/0000-0001-6933-7590*

Katharina Rox − *Department of Chemical Biology, Helmholtz Centre for Infection Research (HZI) and German Center for Infection Research (DZIF), Inhoffenstraße 7, 38124 Braunschweig, Germany;* orcid.org/0000-0002-8020-1384.

Anthony J. O'Donoghue - *Center for Discovery and Innovation in Parasitic Diseases, Skaggs School of Pharmacy and Pharmaceutical Sciences, University of California San Diego, 9500 Gilman Drive, La Jolla, CA 92093-0657, USA;* orcid.org/0000-0001-5695-0409.

Shengyong Yang − *Department of Biotherapy, Cancer Center and State Key Laboratory of Biotherapy, West China Hospital, Sichuan University, Chengdu, Sichuan, 610041, China. https://orcid.org/0000-0001-5147-3746*

Norbert Sträter − *Center for Biotechnology and Biomedicine, Leipzig University, Deutscher Platz 5, 04103 Leipzig, Germany.* https://orcid.org/0000-0002-2001-0500.

Michael Gütschow − *PharmaCenter Bonn, Pharmaceutical Institute, Pharmaceutical & Medicinal Chemistry, University of Bonn, An der Immenburg 4, D-53121 Bonn, Germany;* https://orcid.org/0000-0002-9376-7897.

Stefan A. Laufer − *Institute of Pharmacy, Pharmaceutical/ Medicinal Chemistry and Tübingen Center for Academic Drug Discovery, Eberhard Karls University Tübingen, Auf der Morgenstelle 8, 72076 Tübingen, Germany. Germany;* orcid.org/0000-0001-6952- 1486.

Christa E. Müller − *PharmaCenter Bonn, Pharmaceutical Institute, Pharmaceutical&Medicinal Chemistry, University of Bonn, Bonn D-53121, Germany;* https://orcid.org/0000-0002-0013-6624.

Complete contact information is available at:

Author Contributions

¥These authors contributed equally.

Notes

The authors declare no competing financial interest.

ABBREVIATIONS

ADME, absorption, distribution, metabolism and excretion; AUC, area under the curve; CatL, human cathepsin L; COVID-19, coronavirus disease 2019; CoV, coronavirus; DIPEA, diisopropylethylamine; EDTA, 2,2′,2″,2‴-(ethane-1,2-diyldinitrilo)tetraacetic acid; GSH, glutathione; HPLC, high-pressure liquid chromatography; MOPS, 3-(morpholin-4-yl)propane-1-sulfonic acid; M^{pro}, main protease; NMR, nuclear magnetic resonance; PBC, periodic boundary condition; PFU, plaque forming units; PL^{pro}, papain-like protease; PME, Particle Mesh Ewald; PPB, plasma protein binding; RdRp, RNA-dependent RNA polymerase; RMSD, root-mean-square deviation; S, spike glycoprotein; SAR, structure-activity relationship; SARS, severe acute respiratory syndrome; SARS-CoV, severe acute respiratory syndrome-related coronavirus; TLC, thin layer chromatography; TMPRSS2, transmembrane protease serine subtype 2; TüKIC, Tübingen Kinase Inhibitor Collection.

References

1. Gorbalenya, A. E.; Baker, S. C.; Baric, R. S.; de Groot, R. J.; Drosten, C.; Gulyaeva, A. A.; Haagmans, B. L.; Lauber, C.; Leontovich, A. M.; Neuman, B. W.; Penzar, D.; Perlman, S.; Poon, L. L. M.; Samborskiy, D. V.; Sidorov, I. A.; Sola, I.; Ziebuhr, J. The species Severe acute respiratory syndrome-related coronavirus: classifying 2019-nCoV and naming it SARS-CoV-2. *Nat. Microbiol.* **2020**, *5* (4), 536-544. DOI: 10.1038/s41564-020-0695-z.
2. *World Health Organization 2023 data.who.int, WHO Coronavirus (COVID-19) dashboard > Deaths [Dashboard].* https://data.who.int/dashboards/covid19/deaths (accessed 01.09.2024).
3. Li, G.; Hilgenfeld, R.; Whitley, R.; De Clercq, E. Therapeutic strategies for COVID-19: progress and lessons learned. *Nat. Rev. Drug Discov.* **2023**, *449–475*. DOI: 10.1038/s41573-023-00672-y.
4. Andrews, N.; Stowe, J.; Kirsebom, F.; Toffa, S.; Rickeard, T.; Gallagher, E.; Gower, C.; Kall, M.; Groves, N.; O'Connell, A.-M.; Simons, D.; Blomquist, P. B.; Zaidi, A.; Nash, S.; Iwani Binti Abdul Aziz, N.; Thelwall, S.; Dabrera, G.; Myers, R.; Amirthalingam, G.; Gharbia, S.; Barrett, J. C.; Elson, R.; Ladhani, S. N.; Ferguson, N.; Zambon, M.; Campbell, C. N. J.; Brown, K.; Hopkins, S.; Chand, M.; Ramsay, M.; Lopez Bernal, J. Covid-19 Vaccine Effectiveness against the Omicron (B.1.1.529) Variant. *N. Engl. J. Med.* **2022**, *386* (16), 1532-1546. DOI: 10.1056/NEJMoa2119451.
5. Tuekprakhon, A.; Nutalai, R.; Dijokaite-Guraliuc, A.; Zhou, D.; Ginn, H. M.; Selvaraj, M.; Liu, C.; Mentzer, A. J.; Supasa, P.; Duyvesteyn, H. M. E.; Das, R.; Skelly, D.; Ritter, T. G.; Amini, A.; Bibi, S.; Adele, S.; Johnson, S. A.; Constantinides, B.; Webster, H.; Temperton, N.; Klenerman, P.; Barnes, E.; Dunachie, S. J.; Crook, D.; Pollard, A. J.; Lambe, T.; Goulder, P.; Paterson, N. G.; Williams, M. A.; Hall, D. R.; Fry, E. E.; Huo, J.; Mongkolsapaya, J.; Ren, J.; Stuart, D. I.; Screaton, G. R. Antibody escape of SARS-CoV-2 Omicron BA.4 and BA.5 from vaccine and BA.1 serum. *Cell* **2022**, *185* (14), 2422-2433.e2413. DOI: 10.1016/j.cell.2022.06.005.
6. Nagu, P.; Parashar, A.; Behl, T.; Mehta, V. CNS implications of COVID-19: a comprehensive review. *Nat. Rev. Neurosci.* **2021**, *32* (2), 219-234. DOI: 10.1515/revneuro-2020-0070.

1495 7.   Ip, J. D.; Wing-Ho Chu, A.; Chan, W.-M.; Cheuk-Ying Leung, R.; Umer Abdullah, S. M.; Sun, Y.; To, K.
1496 K.-W. Global prevalence of SARS-CoV-2 3CL protease mutations associated with nirmatrelvir or
1497 ensitrelvir resistance. *eBioMedicine* **2023**, *91*, 104559. DOI: 10.1016/j.ebiom.2023.104559.
1498 8.   Kiso, M.; Yamayoshi, S.; Iida, S.; Furusawa, Y.; Hirata, Y.; Uraki, R.; Imai, M.; Suzuki, T.; Kawaoka, Y.
1499 In vitro and in vivo characterization of SARS-CoV-2 resistance to ensitrelvir. *Nat. Commun.* **2023**, *14*
1500 (1), 4231. DOI: 10.1038/s41467-023-40018-1.
1501 9.   Iketani, S.; Mohri, H.; Culbertson, B.; Hong, S. J.; Duan, Y.; Luck, M. I.; Annavajhala, M. K.; Guo, Y.;
1502 Sheng, Z.; Uhlemann, A.-C.; Goff, S. P.; Sabo, Y.; Yang, H.; Chavez, A.; Ho, D. D. Multiple pathways for
1503 SARS-CoV-2 resistance to nirmatrelvir. *Nature* **2023**, *613* (7944), 558-564. DOI: 10.1038/s41586-022-
1504 05514-2.
1505 10.   Hu, B.; Guo, H.; Zhou, P.; Shi, Z.-L. Characteristics of SARS-CoV-2 and COVID-19. *Nat. Rev.*
1506 *Microbiol.* **2021**, *19* (3), 141-154. DOI: 10.1038/s41579-020-00459-7.
1507 11.   Jin, Z.; Du, X.; Xu, Y.; Deng, Y.; Liu, M.; Zhao, Y.; Zhang, B.; Li, X.; Zhang, L.; Peng, C.; Duan, Y.; Yu,
1508 J.; Wang, L.; Yang, K.; Liu, F.; Jiang, R.; Yang, X.; You, T.; Liu, X.; Yang, X.; Bai, F.; Liu, H.; Liu, X.; Guddat,
1509 L. W.; Xu, W.; Xiao, G.; Qin, C.; Shi, Z.; Jiang, H.; Rao, Z.; Yang, H. Structure of Mpro from SARS-CoV-2
1510 and discovery of its inhibitors. *Nature* **2020**, *582* (7811), 289-293. DOI: 10.1038/s41586-020-2223-y.
1511 12.   Lee, J.; Kenward, C.; Worrall, L. J.; Vuckovic, M.; Gentile, F.; Ton, A.-T.; Ng, M.; Cherkasov, A.;
1512 Strynadka, N. C. J.; Paetzel, M. X-ray crystallographic characterization of the SARS-CoV-2 main protease
1513 polyprotein cleavage sites essential for viral processing and maturation. *Nat. Commun.* **2022**, *13* (1),
1514 5196. DOI: 10.1038/s41467-022-32854-4.
1515 13.   Zhao, Y.; Zhu, Y.; Liu, X.; Jin, Z.; Duan, Y.; Zhang, Q.; Wu, C.; Feng, L.; Du, X.; Zhao, J.; Shao, M.;
1516 Zhang, B.; Yang, X.; Wu, L.; Ji, X.; Guddat, L. W.; Yang, K.; Rao, Z.; Yang, H. Structural basis for replicase
1517 polyprotein cleavage and substrate specificity of main protease from SARS-CoV-2. *Proc. Natl. Acad. Sci.*
1518 *USA* **2022**, *119* (16), e2117142119. DOI: 10.1073/pnas.2117142119.
1519 14.   Zhang, Y. Z.; Holmes, E. C. A Genomic Perspective on the Origin and Emergence of SARS-CoV-2.
1520 *Cell* **2020**, *181* (2), 223-227. DOI: 10.1016/j.cell.2020.03.035.
1521 15.   Dai, W.; Zhang, B.; Jiang, X.-M.; Su, H.; Li, J.; Zhao, Y.; Xie, X.; Jin, Z.; Peng, J.; Liu, F. Structure-
1522 based design of antiviral drug candidates targeting the SARS-CoV-2 main protease. *Science* **2020**, *368*
1523 (6497), 1331-1335. DOI: 10.1126/science.abb4489.
1524 16.   Ma, C.; Sacco, M. D.; Hurst, B.; Townsend, J. A.; Hu, Y.; Szeto, T.; Zhang, X.; Tarbet, B.; Marty, M.
1525 T.; Chen, Y. Boceprevir, GC-376, and calpain inhibitors II, XII inhibit SARS-CoV-2 viral replication by
1526 targeting the viral main protease. *Cell Res.* **2020**, *30* (8), 678-692. DOI: 10.1038/s41422-020-0356-z.
1527 17.   Pillaiyar, T.; Sho, K.; Takehito, Y.; Yuji, K.; Akihiro, T.; Kentaro, T.; Fumika, Y.; Kenichi, A.; Yoshiaki,
1528 K.; Yuko, K. Design, synthesis, and biological evaluation of novel dipeptide-type SARS-CoV 3CL protease
1529 inhibitors: Structure–activity relationship study. *Eur. J. Med. Chem.* **2013**, *65*, 436-447. DOI:
1530 10.1016/j.ejmech.2013.05.005.
1531 18.   Konno, S.; Kobayashi, K.; Senda, M.; Funai, Y.; Seki, Y.; Tamai, I.; Schäkel, L.; Sakata, K.; Pillaiyar,
1532 T.; Taguchi, A.; Taniguchi, A.; Güzschow, M.; Müller, C. E.; Takeuchi, K.; Hirohama, M.; Kawaguchi, A.;
1533 Kojima, M.; Senda, T.; Shirasaka, Y.; Kamitani, W.; Hayashi, Y. 3CL protease inhibitors with an
1534 electrophilic arylketone moiety as anti-SARS-CoV-2 agents. *J. Med. Chem.* **2021**, *65* (4), 2926-2939. DOI:
1535 10.1021/acs.jmedchem.1c00665.
1536 19.   Owen, D. R.; Allerton, C. M. N.; Anderson, A. S.; Aschenbrenner, L.; Avery, M.; Berritt, S.; Boras,
1537 B.; Cardin, R. D.; Carlo, A.; Coffman, K. J.; Dantonio, A.; Di, L.; Eng, H.; Ferre, R.; Gajiwala, K. S.; Gibson,
1538 S. A.; Greasley, S. E.; Hurst, B. L.; Kadar, E. P.; Kalgutkar, A. S.; Lee, J. C.; Lee, J.; Liu, W.; Mason, S. W.;
1539 Noell, S.; Novak, J. J.; Obach, R. S.; Ogilvie, K.; Patel, N. C.; Pettersson, M.; Rai, D. K.; Reese, M. R.;
1540 Sammons, M. F.; Sathish, J. G.; Singh, R. S. P.; Steppan, C. M.; Stewart, A. E.; Tuttle, J. B.; Updyke, L.;
1541 Verhoest, P. R.; Wei, L.; Yang, Q.; Zhu, Y. An oral SARS-CoV-2 Mpro inhibitor clinical candidate for the
1542 treatment of COVID-19. *Science* **2021**, *374* (6575), 1586-1593. DOI: 10.1126/science.abl4784.
1543 20.   Arman, B. Y.; Brun, J.; Hill, M. L.; Zitzmann, N.; von Delft, A. An Update on SARS-CoV-2 Clinical
1544 Trial Results—What We Can Learn for the Next Pandemic. *Int. J. Mol. Sci* **2024**, *25* (1), 354. DOI:
1545 10.3390/ijms25010354.

21.   Allerton, C. M. N.; Arcari, J. T.; Aschenbrenner, L. M.; Avery, M.; Bechle, B. M.; Behzadi, M. A.; Boras, B.; Buzon, L. M.; Cardin, R. D.; Catlin, N. R.; Carlo, A. A.; Coffman, K. J.; Dantonio, A.; Di, L.; Eng, H.; Farley, K. A.; Ferre, R.; Gernhardt, S. S.; Gibson, S. A.; Greasley, S. E.; Greenfield, S. R.; Hurst, B. L.; Kalgutkar, A. S.; Kimito, E.; Lanyon, L. F.; Lovett, G. H.; Lian, Y.; Liu, W.; Martínez Alsina, L. A.; Noell, S.; Obach, R. S.; Owen, D. R.; Patel, N. C.; Rai, D. K.; Reese, M. R.; Rothan, H. A.; Sakata, S.; Sammons, M. F.; Sathish, J. G.; Sharma, R.; Steppan, C. M.; Tuttle, J. B.; Verhoest, P. R.; Wei, L.; Yang, Q.; Yurgelonis, I.; Zhu, Y. A Second-Generation Oral SARS-CoV-2 Main Protease Inhibitor Clinical Candidate for the Treatment of COVID-19. *J. Med. Chem.* **2024**, *67* (16), 13550-13571. DOI: 10.1021/acs.jmedchem.3c02469.

22.   *Discovery of PF-07817883: A next generation oral protease inhibitor for the treatment of COVID-19.* https://acs.digitellinc.com/p/s/discovery-of-pf-07817883-a-next-generation-oral-protease-inhibitor-for-the-treatment-of-covid-19-585045 (accessed 02.05.2024).

23.   Jiang, X.; Su, H.; Shang, W.; Zhou, F.; Zhang, Y.; Zhao, W.; Zhang, Q.; Xie, H.; Jiang, L.; Nie, T.; Yang, F.; Xiong, M.; Huang, X.; Li, M.; Chen, P.; Peng, S.; Xiao, G.; Jiang, H.; Tang, R.; Zhang, L.; Shen, J.; Xu, Y. Structure-based development and preclinical evaluation of the SARS-CoV-2 3C-like protease inhibitor simnotrelvir. *Nat. Commun.* **2023**, *14* (1), 6463. DOI: 10.1038/s41467-023-42102-y.

24.   Chen, M.; Jiang, Y.; Ding, Y. Recent progress in unraveling the biosynthesis of natural sunscreens mycosporine-like amino acids. *J. ind. microbiol. biotech.* **2023**, kuad038. DOI: 10.1093/jimb/kuad038.

25.   Hattori, S. I.; Higashi-Kuwata, N.; Hayashi, H.; Allu, S. R.; Raghavaiah, J.; Bulut, H.; Das, D.; Anson, B. J.; Lendy, E. K.; Takamatsu, Y.; Takamune, N.; Kishimoto, N.; Murayama, K.; Hasegawa, K.; Li, M.; Davis, D. A.; Kodama, E. N.; Yarchoan, R.; Wlodawer, A.; Misumi, S.; Mesecar, A. D.; Ghosh, A. K.; Mitsuya, H. A small molecule compound with an indole moiety inhibits the main protease of SARS-CoV-2 and blocks virus replication. *Nat. Commun.* **2021**, *12* (1), 668. DOI: 10.1038/s41467-021-20900-6.

26.   Ghosh, A. K.; Raghavaiah, J.; Shahabi, D.; Yadav, M.; Anson, B. J.; Lendy, E. K.; Hattori, S. I.; Higashi-Kuwata, N.; Mitsuya, H.; Mesecar, A. D. Indole Chloropyridinyl Ester-Derived SARS-CoV-2 3CLpro Inhibitors: Enzyme Inhibition, Antiviral Efficacy, Structure-Activity Relationship, and X-ray Structural Studies. *J. Med. Chem.* **2021**, *64* (19), 14702-14714. DOI: 10.1021/acs.jmedchem.1c01214.

27.   Breidenbach, J.; Lemke, C.; Pillaiyar, T.; Schäkel, L.; Al Hamwi, G.; Diett, M.; Gedschold, R.; Geiger, N.; Lopez, V.; Mirza, S.; Namasivayam, V.; Schiedel, A. C.; Sylvester, K.; Thimm, D.; Vielmuth, C.; Phuong Vu, L.; Zyulina, M.; Bodem, J.; Gütschow, M.; Müller, C. E. Targeting the Main Protease of SARS-CoV-2: From the Establishment of High Throughput Screening to the Design of Tailored Inhibitors. *Angew. Chem. Int. Ed.* **2021**, *60* (18), 10423-10429. DOI: 10.1002/anie.202016961.

28.   Oneto, A.; Hamwi, G. A.; Schäkel, L.; Krüger, N.; Sylvester, K.; Petry, M.; Shamleh, R. A.; Pillaiyar, T.; Claff, T.; Schiedel, A. C.; Sträter, N.; Gütschow, M.; Müller, C. E. Nonpeptidic Irreversible Inhibitors of SARS-CoV-2 Main Protease with Potent Antiviral Activity. *J. Med. Chem.* **2024**, *67* (17), 14986-15011. DOI: 10.1021/acs.jmedchem.4c00535.

29.   Pillaiyar, T.; Flury, P.; Krüger, N.; Su, H.; Schäkel, L.; Barbosa Da Silva, E.; Eppler, O.; Kronenberger, T.; Nie, T.; Luedtke, S.; Rocha, C.; Sylvester, K.; Petry, M. R. I.; McKerrow, J. H.; Poso, A.; Pöhlmann, S.; Gütschow, M.; O'Donoghue, A. J.; Xu, Y.; Müller, C. E.; Laufer, S. A. Small-Molecule Thioesters as SARS-CoV-2 Main Protease Inhibitors: Enzyme Inhibition, Structure–Activity Relationships, Antiviral Activity, and X-ray Structure Determination. *J. Med. Chem.* **2022**, *65* (13), 9376-9395. DOI: 10.1021/acs.jmedchem.2c00636.

30.   Gao, S.; Song, L.; Sylvester, K.; Mercorelli, B.; Loregian, A.; Toth, K.; Weiße, R. H.; Useini, A.; Sträter, N.; Yang, M.; Ye, B.; Tollefson, A. E.; Müller, C. E.; Liu, X.; Zhan, P. Design, Synthesis, and Biological Evaluation of Trisubstituted Piperazine Derivatives as Noncovalent Severe Acute Respiratory Syndrome Coronavirus 2 Main Protease Inhibitors with Improved Antiviral Activity and Favorable Druggability. *J. Med. Chem.* **2023**, *66* (13), 16426-16440. DOI: 10.1021/acs.jmedchem.3c01876.

31.   Unoh, Y.; Uehara, S.; Nakahara, K.; Nobori, H.; Yamatsu, Y.; Yamamoto, S.; Maruyama, Y.; Taoda, Y.; Kasamatsu, K.; Suto, T.; Kouki, K.; Nakahashi, A.; Kawashima, S.; Sanaki, T.; Toba, S.; Uemura, K.; Mizutare, T.; Ando, S.; Sasaki, M.; Orba, Y.; Sawa, H.; Sato, A.; Sato, T.; Kato, T.; Tachibana, Y. Discovery of S-217622, a Noncovalent Oral SARS-CoV-2 3CL Protease Inhibitor Clinical Candidate for Treating COVID-19. *J. Med. Chem.* **2022**, *65* (9), 6499-6512. DOI: 10.1021/acs.jmedchem.2c00117.

32. Telenti, A.; Hodcroft, E. B.; Robertson, D. L. The Evolution and Biology of SARS-CoV-2 Variants. *old Spring Harb. Perspect. Med.* **2022**, *12* (5). DOI: 10.1101/cshperspect.a041390.

33. Moghadasi, S. A.; Esler, M. A.; Otsuka, Y.; Becker, J. T.; Moraes, S. N.; Anderson, C. B.; Chamakuri, S.; Belica, C.; Wick, C.; Harki, D. A.; Young, D. W.; Scampavia, L.; Spicer, T. P.; Shi, K.; Aihara, H.; Brown, W. L.; Harris, R. S. Gain-of-Signal Assays for Probing Inhibition of SARS-CoV-2 Mpro/3CL in Living Cells. *mBio* **2022**, *13* (3), e00784-00722. DOI: doi:10.1128/mbio.00784-22.

34. Abdelnabi, R.; Jochmans, D.; Donckers, K.; Trüeb, B.; Ebert, N.; Weynand, B.; Thiel, V.; Neyts, J. Nirmatrelvir-resistant SARS-CoV-2 is efficiently transmitted in female Syrian hamsters and retains partial susceptibility to treatment. *Nat. Commun.* **2023**, *14* (1), 2124. DOI: 10.1038/s41467-023-37773-6.

35. Sato, K.; Sinclair, J. E.; Sadeghirad, H.; Fraser, J. F.; Short, K. R.; Kulasinghe, A. Cardiovascular disease in SARS-CoV-2 infection. *Clin. Transl. Immunol.* **2021**, *10* (9), e1343. DOI: 10.1002/cti2.1343.

36. Flury, P.; Breidenbach, J.; Krüger, N.; Voget, R.; Schäkel, L.; Si, Y.; Krasniqi, V.; Calistri, S.; Olfert, M.; Sylvester, K.; Rocha, C.; Ditzinger, R.; Rasch, A.; Pöhlmann, S.; Kronenberger, T.; Poso, A.; Rox, K.; Laufer, S. A.; Müller, C. E.; Gütschow, M.; Pillaiyar, T. Cathepsin-Targeting SARS-CoV-2 Inhibitors: Design, Synthesis, and Biological Activity. *ACS Pharmacol. Transl. Sci.* **2024**, *7* (2), 493-514. DOI: 10.1021/acsptsci.3c00313.

37. Masyeni, S.; Iqhrammullah, M.; Frediansyah, A.; Nainu, F.; Tallei, T.; Emran, T. B.; Ophinni, Y.; Dhama, K.; Harapan, H. Molnupiravir: A lethal mutagenic drug against rapidly mutating severe acute respiratory syndrome coronavirus 2—A narrative review. *J. Med. Virol.* **2022**, *94* (7), 3006-3016. DOI: 10.1002/jmv.27730.

38. Vuong, W.; Khan, M. B.; Fischer, C.; Arutyunova, E.; Lamer, T.; Shields, J.; Saffran, H. A.; McKay, R. T.; van Belkum, M. J.; Joyce, M. A.; Young, H. S.; Tyrrell, D. L.; Vederas, J. C.; Lemieux, M. J. Feline coronavirus drug inhibits the main protease of SARS-CoV-2 and blocks virus replication. *Nat. Commun.* **2020**, *11* (1), 4282. DOI: 10.1038/s41467-020-18096-2.

39. Frizler, M.; Lohr, F.; Lülsdorff, M.; Gütschow, M. Facing the gem-Dialkyl Effect in Enzyme Inhibitor Design: Preparation of Homocycloleucine-Based Azadipeptide Nitriles. *Chem. Eur. J.* **2011**, *17* (41), 11419-11423. DOI: 10.1002/chem.201101350.

40. Lemke, C.; Benýšek, J.; Brajtenbach, D.; Breuer, C.; Jílková, A.; Horn, M.; Buša, M.; Ulrychová, L.; Illies, A.; Kubatzky, K. F.; Bartz, U.; Mareš, M.; Gütschow, M. An activity-based probe for cathepsin K imaging with excellent potency and selectivity. *J. Med. Chem.* **2021**, *64* (18), 13793-13806. DOI: 10.1021/acs.jmedchem.1c01178.

41. Ou, X.; Liu, Y.; Lei, X.; Li, P.; Mi, D.; Ren, L.; Guo, L.; Guo, R.; Chen, T.; Hu, J.; Xiang, Z.; Mu, Z.; Chen, X.; Chen, J.; Hu, K.; Jin, Q.; Wang, J.; Qian, Z. Characterization of spike glycoprotein of SARS-CoV-2 on virus entry and its immune cross-reactivity with SARS-CoV. *Nat. Commun.* **2020**, *11* (1), 1620. DOI: 10.1038/s41467-020-15562-9.

42. Pišlar, A.; Mitrović, A.; Sabotič, J.; Pečar Fonović, U.; Perišić Nanut, M.; Jakoš, T.; Senjor, E.; Kos, J. The role of cysteine peptidases in coronavirus cell entry and replication: The therapeutic potential of cathepsin inhibitors. *PLOS Pathog.* **2020**, *16* (11), e1009013. DOI: 10.1371/journal.ppat.1009013.

43. Mellott, D. M.; Tseng, C.-T.; Drelich, A.; Fajtová, P.; Chenna, B. C.; Kostomiris, D. H.; Hsu, J.; Zhu, J.; Taylor, Z. W.; Kocurek, K. I. A clinical-stage cysteine protease inhibitor blocks SARS-CoV-2 infection of human and monkey cells. *ACS Chem. Biol.* **2021**, *16* (4), 642-650. DOI: 10.1021/acschembio.0c00875.

44. Mondal, S.; Chen, Y.; Lockbaum, G. J.; Sen, S.; Chaudhuri, S.; Reyes, A. C.; Lee, J. M.; Kaur, A. N.; Sultana, N.; Cameron, M. D.; Shaffer, S. A.; Schiffer, C. A.; Fitzgerald, K. A.; Thompson, P. R. Dual Inhibitors of Main Protease (MPro) and Cathepsin L as Potent Antivirals against SARS-CoV2. *J. Med. Chem.* **2022**, *144* (46), 21035-21045. DOI: 10.1021/jacs.2c04626.

45. Heilmann, E.; Costacurta, F.; Moghadasi, S. A.; Ye, C.; Pavan, M.; Bassani, D.; Volland, A.; Ascher, C.; Weiss, A. K. H.; Bante, D. SARS-CoV-2 3CLpro mutations selected in a VSV-based system confer resistance to nirmatrelvir, ensitrelvir, and GC376. *Sci. Transl. Med.* **2022**, *15* (678), eabq7360. DOI: 10.1126/scitranslmed.abq7360.

46. Noske, G. D.; de Souza Silva, E.; de Godoy, M. O.; Dolci, I.; Fernandes, R. S.; Guido, R. V. C.; Sjö, P.; Oliva, G.; Godoy, A. S. Structural basis of nirmatrelvir and ensitrelvir activity against naturally occurring

1650 polymorphisms of the SARS-CoV-2 main protease. *J. Biol. Chem.* **2023**, *299* (3), 103004. DOI:
1651 10.1016/j.jbc.2023.103004.

1652 47. Zhou, Y.; Gammeltoft, K. A.; Ryberg, L. A.; Pham, L. V.; Tjørnelund, H. D.; Binderup, A.; Duarte
1653 Hernandez, C. R.; Fernandez-Antunez, C.; Offersgaard, A.; Fahnøe, U. Nirmatrelvir-resistant SARS-CoV-
1654 2 variants with high fitness in an infectious cell culture system. *Sci. Adv.* **2022**, *8* (51), eadd7197. DOI:
1655 10.1126/sciadv.add7197.

1656 48. Jochmans, D.; Liu, C.; Donckers, K.; Stoycheva, A.; Boland, S.; Stevens, S. K.; De Vita, C.;
1657 Vanmechelen, B.; Maes, P.; Trüeb, B. The substitutions L50F, E166A, and L167F in SARS-CoV-2 3CLpro
1658 are selected by a protease inhibitor in vitro and confer resistance to nirmatrelvir. *MBio* **2023**, *14* (1),
1659 e02815-02822. DOI: 10.1128/mbio.02815-22.

1660 49. Hu, Y.; Lewandowski, E. M.; Tan, H.; Zhang, X.; Morgan, R. T.; Zhang, X.; Jacobs, L. M. C.; Butler,
1661 S. G.; Gongora, M. V.; Choy, J. Naturally occurring mutations of SARS-CoV-2 main protease confer drug
1662 resistance to nirmatrelvir. *ACS Cent. Sci.* **2023**, *9* (8), 1658-1669. DOI: 10.1021/acscentsci.3c00538.

1663 50. Iketani, S.; Mohri, H.; Culbertson, B.; Hong, S. J.; Duan, Y.; Luck, M. I.; Annavajhala, M. K.; Guo, Y.;
1664 Sheng, Z.; Uhlemann, A.-C. Multiple pathways for SARS-CoV-2 resistance to nirmatrelvir. *Nature* **2023**,
1665 *613* (7944), 558-564. DOI: 10.1038/s41586-022-05514-2.

1666 51. Moghadasi, S. A.; Heilmann, E.; Khalil, A. M.; Nnabuife, C.; Kearns, F. L.; Ye, C.; Moraes, S. N.;
1667 Costacurta, F.; Esler, M. A.; Aihara, H. Transmissible SARS-CoV-2 variants with resistance to clinical
1668 protease inhibitors. *Sci. Adv.* **2023**, *9* (13), eade8778. DOI: 10.1126/sciadv.ade8778.

1669 52. Huang, C.; Shuai, H.; Qiao, J.; Hou, Y.; Zeng, R.; Xia, A.; Xie, L.; Fang, Z.; Li, Y.; Yoon, C.; Huang, Q.;
1670 Hu, B.; You, J.; Quan, B.; Zhao, X.; Guo, N.; Zhang, S.; Ma, R.; Zhang, J.; Wang, Y.; Yang, R.; Zhang, S.;
1671 Nan, J.; Xu, H.; Wang, F.; Lei, J.; Chu, H.; Yang, S. A new generation Mpro inhibitor with potent activity
1672 against SARS-CoV-2 Omicron variants. *Signal Transduct. Target. Ther.* **2023**, *8* (1), 128. DOI:
1673 10.1038/s41392-023-01392-w.

1674 53. Cheng, S. C.; Chang, G. G.; Chou, C. Y. Mutation of Glu-166 blocks the substrate-induced
1675 dimerization of SARS coronavirus main protease. *Biophys. J.* **2010**, *98* (7), 1327-1336. DOI:
1676 10.1016/j.bpj.2009.12.4272.

1677 54. Fan, K.; Wei, P.; Feng, Q.; Chen, S.; Huang, C.; Ma, L.; Lai, B.; Pei, J.; Liu, Y.; Chen, J.; Lai, L.
1678 Biosynthesis, purification, and substrate specificity of severe acute respiratory syndrome coronavirus
1679 3C-like proteinase. *J. Biol. Chem.* **2004**, *279* (3), 1637-1642. DOI: 10.1074/jbc.M310875200.

1680 55. Duan, Y.; Zhou, H.; Liu, X.; Iketani, S.; Lin, M.; Zhang, X.; Bian, Q.; Wang, H.; Sun, H.; Hong, S. J.;
1681 Culbertson, B.; Mohri, H.; Luck, M. I.; Zhu, Y.; Liu, X.; Lu, Y.; Yang, X.; Yang, K.; Sabo, Y.; Chavez, A.; Goff,
1682 S. P.; Rao, Z.; Ho, D. D.; Yang, H. Molecular mechanisms of SARS-CoV-2 resistance to nirmatrelvir.
1683 *Nature* **2023**, *622* (7982), 376-382. DOI: 10.1038/s41586-023-06609-0.

1684 56. Tomar, S.; Johnston, M. L.; St John, S. E.; Osswald, H. L.; Nyalapatla, P. R.; Paul, L. N.; Ghosh, A. K.;
1685 Denison, M. R.; Mesecar, A. D. Ligand-induced Dimerization of Middle East Respiratory Syndrome
1686 (MERS) Coronavirus nsp5 Protease (3CLpro): IMPLICATIONS FOR nsp5 REGULATION AND THE
1687 DEVELOPMENT OF ANTIVIRALS. *J. Biol. Chem.* **2015**, *290* (32), 19403-19422. DOI:
1688 10.1074/jbc.M115.651463.

1689 57. Wu, A.; Wang, Y.; Zeng, C.; Huang, X.; Xu, S.; Su, C.; Wang, M.; Chen, Y.; Guo, D. Prediction and
1690 biochemical analysis of putative cleavage sites of the 3C-like protease of Middle East respiratory
1691 syndrome coronavirus. *Virus Res.* **2015**, *208*, 56-65. DOI: 10.1016/j.virusres.2015.05.018.

1692 58. Chen, Y. W.; Yiu, C. B.; Wong, K. Y. Prediction of the SARS-CoV-2 (2019-nCoV) 3C-like protease
1693 (3CL (pro)) structure: virtual screening reveals velpatasvir, ledipasvir, and other drug repurposing
1694 candidates. *F1000Res* **2020**, *9*, 129. DOI: 10.12688/f1000research.22457.2.

1695 59. Mała, P.; Siebs, E.; Meiers, J.; Rox, K.; Varrot, A.; Imberty, A.; Titz, A. Discovery of N-β-l-Fucosyl
1696 Amides as High-Affinity Ligands for the Pseudomonas aeruginosa Lectin LecB. *J. Med. Chem.* **2022**, *65*
1697 (20), 14180-14200. DOI: 10.1021/acs.jmedchem.2c01373.

1698 60. Rox, K.; Heyner, M.; Krull, J.; Harmrolfs, K.; Rinne, V.; Hokkanen, J.; Perez Vilaro, G.; Díez, J.; Müller,
1699 R.; Kröger, A.; Sugiyama, Y.; Brönstrup, M. Physiologically Based Pharmacokinetic/Pharmacodynamic
1700 Model for the Treatment of Dengue Infections Applied to the Broad Spectrum Antiviral Soraphen A.
1701 *ACS Pharmacol. Transl. Sci.* **2021**, *4* (5), 1499-1513. DOI: 10.1021/acsptsci.1c00078.

1702   61.   Kabsch, W. XDS. *Acta Crystallogr. D Biol. Crystallogr.* **2010**, *66* (Pt 2), 125-132. DOI:
1703   10.1107/s0907444909047337.

1704   62.   Vonrhein, C.; Tickle, I. J.; Flensburg, C.; Keller, P.; Paciorek, W.; Sharff, A.; Bricogne, G. Advances
1705   in automated data analysis and processing within autoPROC, combined with improved
1706   characterisation, mitigation and visualisation of the anisotropy of diffraction limits using STARANISO.
1707   *Acta Crystallogr. A.* **2018**, *74*, A360-A360.

1708   63.   Delagenière, S.; Brenchereau, P.; Launer, L.; Ashton, A. W.; Leal, R.; Veyrier, S.; Gabadinho, J.;
1709   Gordon, E. J.; Jones, S. D.; Levik, K. E.; McSweeney, S. M.; Monaco, S.; Nanao, M.; Spruce, D.; Svensson,
1710   O.; Walsh, M. A.; Leonard, G. A. ISPyB: an information management system for synchrotron
1711   macromolecular crystallography. *Bioinformatics* **2011**, *27* (22), 3186-3192. DOI:
1712   10.1093/bioinformatics/btr535 PubMed.

1713   64.   Narayanan, A.; Narwal, M.; Majowicz, S. A.; Varricchio, C.; Toner, S. A.; Ballatore, C.; Brancale, A.;
1714   Murakami, K. S.; Jose, J. Identification of SARS-CoV-2 inhibitors targeting Mpro and PLpro using in-cell-
1715   protease assay. *Commun. Biol.* **2022**, *5* (1), 169. DOI: 10.1038/s42003-022-03090-9.

1716   65.   Liebschner, D.; Afonine, P. V.; Baker, M. L.; Bunkóczi, G.; Chen, V. B.; Croll, T. I.; Hintze, B.; Hung,
1717   L. W.; Jain, S.; McCoy, A. J.; Moriarty, N. W.; Oeffner, R. D.; Poon, B. K.; Prisant, M. G.; Read, R. J.;
1718   Richardson, J. S.; Richardson, D. C.; Sammito, M. D.; Sobolev, O. V.; Stockwell, D. H.; Terwilliger, T. C.;
1719   Urzhumtsev, A. G.; Videau, L. L.; Williams, C. J.; Adams, P. D. Macromolecular structure determination
1720   using X-rays, neutrons and electrons: recent developments in Phenix. *Acta Crystallogr. D. Struct. Biol.*
1721   **2019**, *75* (Pt 10), 861-877. DOI: 10.1107/s2059798319011471.

1722   66.   Emsley, P.; Lohkamp, B.; Scott, W. G.; Cowtan, K. Features and development of Coot. *Acta*
1723   *Crystallogr D Biol Crystallogr* **2010**, *66* (Pt 4), 486-501. DOI: 10.1107/s0907444910007493.

1724

1725

1726

Table of Content

8r
SARS-CoV-2 M^{pro} IC$_{50}$ = 0.0199 µM
SARS-CoV-2 EC$_{50}$ = 10.6 nM

8p
SARS-CoV-2 M^{pro} IC$_{50}$ = 0.0887 µM
SARS-CoV-2 EC$_{50}$ = 557 nM

M^{pro}- 8p

74